

Bifurcation theory of the L-H transition in fusion plasmas

Weymiens, W.

DOI:
[10.6100/IR773252](https://doi.org/10.6100/IR773252)

Published: 01/01/2014

Document Version

Publisher's PDF, also known as Version of Record (includes final page, issue and volume numbers)

Please check the document version of this publication:

- A submitted manuscript is the author's version of the article upon submission and before peer-review. There can be important differences between the submitted version and the official published version of record. People interested in the research are advised to contact the author for the final version of the publication, or visit the DOI to the publisher's website.
- The final author version and the galley proof are versions of the publication after peer review.
- The final published version features the final layout of the paper including the volume, issue and page numbers.

[Link to publication](#)

Citation for published version (APA):

Weymiens, W. (2014). Bifurcation theory of the L-H transition in fusion plasmas Eindhoven: Technische Universiteit Eindhoven DOI: [10.6100/IR773252](https://doi.org/10.6100/IR773252)

General rights

Copyright and moral rights for the publications made accessible in the public portal are retained by the authors and/or other copyright owners and it is a condition of accessing publications that users recognise and abide by the legal requirements associated with these rights.

- Users may download and print one copy of any publication from the public portal for the purpose of private study or research.
- You may not further distribute the material or use it for any profit-making activity or commercial gain
- You may freely distribute the URL identifying the publication in the public portal ?

Take down policy

If you believe that this document breaches copyright please contact us providing details, and we will remove access to the work immediately and investigate your claim.

Bifurcation theory of the L-H transition in fusion plasmas

PROEFSCHRIFT

ter verkrijging van de graad van doctor aan de
Technische Universiteit Eindhoven, op gezag van
de rector magnificus, prof.dr.ir. C.J. van Duijn,
voor een commissie aangewezen door het College
voor Promoties in het openbaar te verdedigen op
donderdag 17 april 2014 om 16:00 uur

door

Wolf Weymiens

geboren te Leiderdorp

Dit proefschrift is goedgekeurd door de promotor en de samenstelling van de promotiecommissie is als volgt:

voorzitter: prof.dr.ir. G.M.W. Kroesen
promotor: prof.dr. A.J.H. Donné
copromotoren: dr. H.J. de Blank (FOM-Instituut DIFFER)
dr. G.M.D. Hogeweij (FOM-Instituut DIFFER)
leden: dr. G.D. Conway (Max-Planck-Institut für Plasmaphysik, Garching)
prof.dr. Y. Kuznetsov (Universiteit Utrecht)
prof.dr.ir. B. Koren
prof.dr. U.M. Ebert

Bifurcation theory of the L-H transition in fusion plasmas

A catalogue record is available from the Eindhoven University of Technology Library

Weymiens, Wolf

Bifurcation theory of the L-H transition in fusion plasmas

ISBN: 978-94-6259-106-6

NUR: 925

© Copyright 2014 Wolf Weymiens



The work described in this dissertation, supported by the European Communities under the Contract of Association between EURATOM/FOM, was carried out within the framework of the European Fusion Programme with financial support of the ' Nederlandse Organisatie voor Wetenschappelijk Onderzoek' (NWO). The views and opinions expressed herein do not necessarily reflect those of the European Commission. The research was carried out at the FOM Institute DIFFER - Dutch Institute for Fundamental Energy Research, in Nieuwegein, the Netherlands

Contents

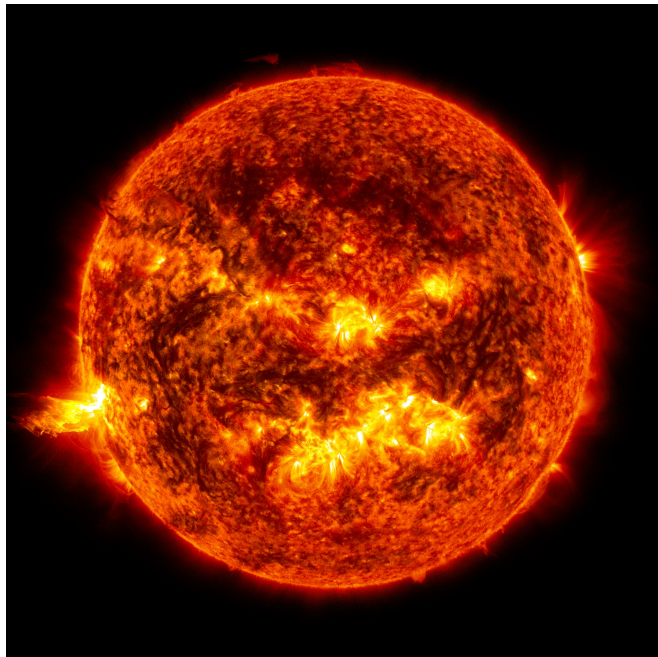
1	Introduction	1
1.1	Fusion on earth	2
1.2	L-H transition	3
1.3	Research questions	5
1.4	Publications	8
	References	10
2	L-H transitions in magnetically confined plasmas	11
2.1	Experimental observations	11
2.2	Related physical mechanisms	14
	References	17
3	Bifurcation theory	19
3.1	Introduction	19
3.2	Bifurcations vs L-H transition dynamics	23
4	Bifurcation theory for the L-H transition in magnetically confined fusion plasmas	27
	Abstract	27
4.1	Introduction	28
4.2	Generalized bifurcation theory	31
4.3	Finite dimensional case	34
4.4	Transport model for the L-H transition	38
4.5	Conclusion and discussion	48
	References	50
5	Bifurcation theory of a one-dimensional transport model for the L-H transition	53
	Abstract	53
5.1	Introduction	54
5.2	Transport model for the L-H transition	55
5.3	Bifurcation analysis	58

Contents

5.4 The transport barrier: space and time consistently	62
5.5 Two different regimes in transport barrier sizes	65
5.6 Conclusion and discussion	68
References	70
6 Comparison of bifurcation dynamics of turbulent transport models for the L-H transition	73
Abstract	73
6.1 Introduction	74
6.2 Turbulent transport models for the L-H transition	75
6.3 Bifurcation analysis	78
6.4 Bifurcator	84
6.5 Numerical bifurcation analysis	85
6.6 Conclusion and discussion	90
6.A Appendix: Radial currents	91
References	94
7 Evaluation and future prospects	99
7.1 Conclusions and discussion	99
7.2 Outlook	103
References	106
Summary	107
Samenvatting	109
Acknowledgement	113
Curriculum vitae	117

1

Introduction



*The most intense source of energy daily appreciated by all that live on earth is the sun. The energy production of the sun is gigantic. In just a single second the sun produces enough energy to supply the entire world for more than 7.9 trillion years. Such massive power can only be produced by the simple reaction known as **nuclear fusion**. During a fusion reaction two small atoms are colliding so vigorously that they merge together into a single bigger atom, releasing lots of energy. If we could only reproduce just a tiny fraction of what the sun can do, the energy problems of today would be solved.*

1.1 Fusion on earth

For fusion reactions to occur there is a limited amount of collision energy required. This can be accomplished by heating a gas to enormous temperatures. At these temperatures the gas becomes a plasma, which means that the atoms of the gas have fallen apart into their atom core and loose electrons. To keep such a plasma in place here on earth magnetic fields are used because the charged particles of a plasma follow the magnetic field lines. For this reason the magnetic field lines are closed onto themselves in the shape of a torus, see Fig. 1.1. In the core of the sun the density is very large, such that fusion collisions occur frequently. However, in the magnetically confined fusion plasmas these densities can never be reached. To compensate this in acquiring a high fusion reaction rate, the temperatures in earth's fusion devices need to be ten times as high as the temperature in the core of the sun. The 150 million degrees Celsius in the core of a fusion reactor makes it the hottest place in our entire solar system. Note that no existing material can withstand these kind of temperatures, and therefore the magnetic field configuration is very important to keep the plasma from touching the wall. The magnetic field is configured such that its field lines lay on nested tori, meaning that field lines that start on a surface in the core of the plasma go around the torus and stay in the core, while field lines starting more outward stay on that surface, as is depicted in Fig. 1.1. All particles that are confined on the same surface are in thermal equilibrium, such that every surface has its own temperature, decreasing from the hot core towards the colder edge of the plasma; therefore it can effectively be described as a one-dimensional system. All physical quantities can therefore be projected onto this direction, i.e., the minor radius of the toroidal plasma, and expressed as radial profiles as shown in Fig. 1.2. Outside the last closed surface the magnetic fields lines are diverted into an exhaust. The thin layer of plasma that is diverted is called the scrape-off layer.

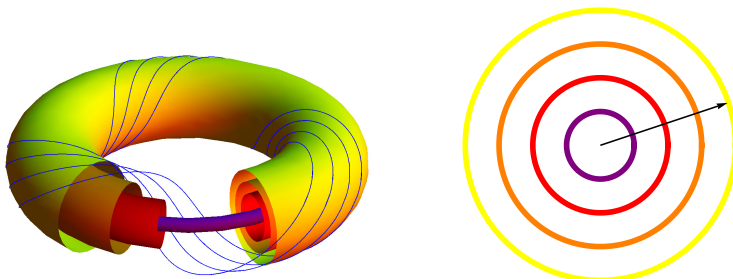


Figure 1.1: Magnetic geometry of a fusion device: nested tori

Although this magnetic configuration confines the toroidal plasma very well, there will always be transport of particles and heat from one surface to the next in the radial direction outwards toward the scrape-off layer. This one-dimensional transport is partly due to collisional processes but mainly driven by turbulence. These transport effects limit the energy confinement and therewith the steepness of the density and temperature profiles.

1.2 L-H transition

The generation of turbulence enhances the radial transport such that the confinement is limited, and is therefore called the ‘low-confinement mode’ or L-mode. However, there is a state of the plasma in which the turbulent transport is locally reduced such that the confinement is enhanced, which is called the ‘high-confinement mode’ or H-mode. This H-mode is recognized by the existence of a small radial domain at the edge of the plasma near the scrape-off layer where the turbulent transport is reduced and the gradients of energy and density are locally increased. This domain is therefore called the ‘edge transport barrier’. An example of such an H-mode compared to an L-mode is shown in Fig. 1.2, where the temperature and pressure in the central part of the plasma are much larger in H-mode than in L-mode. This better confinement results in an increase in core temperature and therewith an increase in fusion energy production.

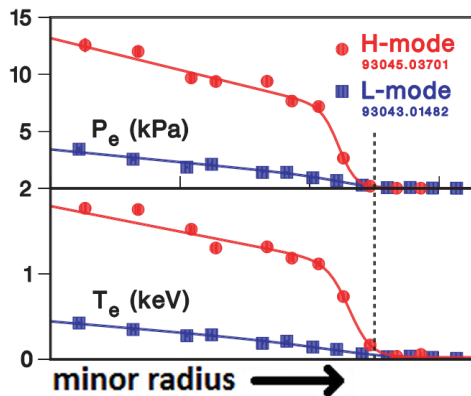


Figure 1.2: L-mode versus H-mode profiles for the temperature and pressure along the minor radius of the plasma (machine: DIII-D), showing the existence of an edge transport barrier near the last closed magnetic surface (indicated with the dashed line). [1]

The H-mode was first observed by the ASDEX-team[2] in 1982 when sufficient heating power was applied to the plasma and nowadays almost all magnetic confinement devices have observed this spontaneous plasma phenomenon. However, after more than three decades of H-mode research there is still no consensus on which plasma physics mechanism causes this spontaneous transition from the L-mode to the H-mode. Since earlier attempts to unravel the L-H transition were unsuccessful, in this thesis a different approach is introduced to tackle the mystery of the H-mode. It is realised that distinctions could be made in the type of dynamics during the transition from L-mode to H-mode. Usually, the dynamics during the L-H transition is observed as a sudden sharp transition from a stationary L-mode state to a stationary H-mode state when the heating power is increased above some threshold value. Moreover, under some conditions it is observed that for increasing heating power the plasma first exhibits oscillatory behaviour before it settles into the H-mode. This is dynamically different from the sharp transitions. A third type of transition is the smooth transition, during which the plasma gradually changes with increasing heating power from an L-mode stationary state to an H-mode. Thus, three types of dynamics are observed, sharp, oscillatory and smooth. Furthermore, it is noted that the sharp transitions exhibit hysteresis between the L-H and the H-L transition.

There are not many models capable of describing multiple types of transitions, therefore the quality of a proposed L-H transition model can additionally be judged, besides their physical viability, on its capability of describing the very characteristic transition dynamics observed in fusion plasmas. In this respect bifurcation theory is used in this thesis. Bifurcation theory is the mathematical study of qualitative changes in the solutions of dynamical systems. Many dynamic models have stationary states that are qualitatively similar for large parts of their parameter space, only when a bifurcation is encountered the system directly changes to a qualitatively different state. Bifurcation theory additionally describes the dynamics during such a qualitative change, which is therefore very useful to analyse the dynamics during transitions between the qualitatively different states of the fusion plasma, i.e., the L-H transition.

1.3 Research questions

Since there are many similarities between bifurcation dynamics and the dynamics observed during L-H transitions, the main purpose of the research described in this thesis is concentrated at the following question:

How can we employ bifurcation theory to unravel the L-H transition mechanism?

To this aim, firstly the mathematics of bifurcation theory is investigated and extended. Once the proper mathematical framework is put in place, the investigation of the physics is performed. This subdivision between mathematics and physics can therefore be noted in the specific research questions addressed in this thesis.

The mathematical field of bifurcation theory is very extensive, however the number of bifurcations that could be identified in physical systems is limited. Thus, first of all it is necessary to identify which bifurcations are relevant for the description of L-H transition dynamics. Therefore, the following question will be addressed,

What bifurcation structure can be recognized in L-H transition dynamics?

It will be shown in chapter 3 that a certain '*co-dimension 3 bifurcation*' organizes the observed transition dynamics. Bifurcation theory tools are well developed for systems of ordinary differential equations, however as was argued in chapter 1.2 the L-H transition should be described as a 1-dimensional problem. Unfortunately, it is not at all straightforward how to identify such a co-dimension 3 bifurcation in systems of partial differential equations. Therefore, we ask the question:

How can we identify the co-dimension 3 bifurcation in 1-dimensional models?

During the transition from the L-mode to the H-mode a transport barrier is formed near the edge of the plasma. Since the investigated bifurcating models are 1-dimensional, they should be able to describe this formation and final width of the transport barrier. This radial propagation of bifurcating dynamic solutions are, in part, similar to spatial propagation of flame fronts, or propagation of neural signals and other types of front propagations. Thus in a broad sense it is interesting, and from an L-H transition point of view it is essential, to investigate the following question,

How do these 1-dimensional bifurcating models combine transitions in time and in space?

With this mathematical framework in place we can start searching for the characteristic transition behaviour of the *co-dimension 3 bifurcation* in physics models of the L-H transition.

Two directions in L-H transition model investigation could be taken. Either, (all) existing models are investigated and compared on their bifurcating behaviour, or a certain bifurcating model is extended with different physical mechanisms and it is analysed how the bifurcation structure changes due to this additional physics. Since the second approach is the most constructive towards an advanced model for the L-H transition, that approach is followed in this thesis.

Since the H-mode shows a local reduction in the transport of energy and particles, the basic model should at least contain the continuity equations of energy and density to describe the H-mode properly. The generation of a transport barrier could then be caused by a local reduction of the transport coefficients. A certain model that uses this approach was described by Zohm in 1994[3]. This was an extension of the model initiated by Itoh et al. in 1991[4] that only considered the evolution of the density and not the energy. However, they both used the reduction of the transport coefficients as function of the radial electric field in the same manner, and self-consistently evolved the radial electric field temporally. Since simulations of these models in the considered papers showed bifurcating transition dynamics, it is first of all necessary to map out the possible types of transitions with the use of bifurcation analysis.

What is the bifurcation structure of the model proposed by Zohm?

The next step is to find out how this model can be improved in the physically most relevant way, and analyse how that changes the bifurcation structure, because on that basis, the models can properly be compared. In Zohm's model the reduction of the transport was due to the poloidal flow generated by the radial electric field, i.e., the $\mathbf{E} \times \mathbf{B}$ -flow. This is explained by the fact that the radial transport in fusion plasmas is dominated by turbulence, and that turbulence can be reduced by $\mathbf{E} \times \mathbf{B}$ -flows, as will be elaborated in chapter 2. However, it is more probable that not the magnitude of the $\mathbf{E} \times \mathbf{B}$ -flow but the shear of the $\mathbf{E} \times \mathbf{B}$ -flow can reduce the turbulent transport. Therefore, the comparison of both descriptions of the transport coefficients depending either on the gradient of the radial electric field or on its magnitude, is addressed in the following question,

How does the bifurcation structure change when changing the transport reduction mechanism?

These reduction mechanisms of the transport coefficients are instantaneous functions of the radial electric field. However, several models are introduced

in literature that describe the dynamic evolution of the turbulence, and show that its interactions could lead to additional oscillatory dynamics. Therefore, it is interesting to introduce an additional dynamical equation for the turbulence level, and see how that changes the dynamics of the model. The transport coefficients will then directly depend on the turbulence level, which in turn is reduced by the $E \times B$ -flow shear dynamically.

How does the bifurcation structure change when adding an extra dynamical equation for the turbulence?

However, there are multiple possibilities for this additional dynamical equation for the turbulence, leading to a question that needs to be answered simultaneously:

What is the best dynamical description of the turbulence reduction by sheared $E \times B$ -flows?

The two most fundamental possibilities are investigated and compared based on their bifurcation structure, such that conclusions can be drawn with respect to which of them is better, at least in terms of robustness.

Summarizing the questions addressed in this thesis, in chapter 3 the fundamental bifurcation responsible for the organisation of observed L-H transition dynamics is identified as the '*co-dimension 3 bifurcation*'. In chapter 4 the 1-dimensional bifurcation analysis of this bifurcation is introduced. In chapter 5 the '*generalized equal area rule*' is introduced to describe the spatiotemporal evolution of these 1-dimensional bifurcating models. The bifurcation analysis of Zohm's model is done in chapter 4, and its comparison to a different transport reduction mechanism is done in chapter 5. The two different fundamental possibilities of the turbulence reduction are introduced, analysed and discussed in chapter 6.

1.4 Publications

Refereed journal papers

- **Bifurcation theory for the L-H transition in magnetically confined fusion plasmas**
W. Weymiens, H.J. de Blank, G.M.D. Hogeweij and J.C. de Valen  a.
Physics of Plasmas **19** 072309 (2012)
- **Bifurcation theory of a 1-dimensional transport model for the L-H transition**
W. Weymiens, H.J. de Blank and G.M.D. Hogeweij.
Physics of Plasmas **20** 082306 (2013)
- **Comparison of bifurcation dynamics of turbulent transport models for the L-H transition**
W. Weymiens, S. Paquay, H.J. de Blank and G.M.D. Hogeweij.
Accepted by: *Physics of Plasmas* (2014)

Conference proceedings

- **Bifurcation theory for the L-H transition**
W. Weymiens, H.J. de Blank and G.M.D. Hogeweij.
38th EPS Conference on Plasma Physics, Strasbourg, France (2011)

Conference/workshop oral contributions

- **Bifurcation theory for the L-H transition**
W. Weymiens, H.J. de Blank and G.M.D. Hogeweij.
23th NNV-Symposium on Plasma Physics and Radiation Technology, Lunteren, The Netherlands (2011)
- **Bifurcation theory for the L-H transition**
W. Weymiens, H.J. de Blank and G.M.D. Hogeweij.
Lorentz workshop: Control of Burning Plasmas, Leiden, The Netherlands (2011)
- **Bifurcation theory: L-H transition dynamics unraveled**
W. Weymiens, S. Paquay, H.J. de Blank and G.M.D. Hogeweij.
Physics@FOM, Veldhoven, The Netherlands (2014)

Seminars

- **L-H transitions and Bifurcations**
W. Weymiens, H.J. de Blank and G.M.D. Hogeweij.
Max-Planck-Institut f  r Plasmaphysik, Garching, Germany (2013)

Posters

- **Bifurcation theory for the dynamics of H-mode transitions in fusion plasmas**
W. Weymiens, H.J. de Blank, G.M.D. Hogeweij and J.C. de Valen  a.
47th Culham Plasma Physics Summer School, Culham, UK (2010)
- **A bifurcation model for the L-H transition**
W. Weymiens, H.J. de Blank, G.M.D. Hogeweij and J.C. de Valen  a.
Physics@FOM, Veldhoven, The Netherlands (2011)
- **Bifurcation theory for the L-H transition**
W. Weymiens, H.J. de Blank and G.M.D. Hogeweij.
Lorentz workshop: Control of Burning Plasmas, Leiden, The Netherlands (2011)
- **Bifurcation theory for the L-H transition**
W. Weymiens, H.J. de Blank and G.M.D. Hogeweij.
38th EPS Conference on Plasma Physics, Strasbourg, France (2011)
- **Bifurcation theory for the L-H transition**
W. Weymiens, H.J. de Blank and G.M.D. Hogeweij.
13th H-mode workshop, Oxford, UK (2011)
- **Bifurcation theory for L-H transition dynamics in fusion plasmas**
W. Weymiens, H.J. de Blank and G.M.D. Hogeweij.
Physics@FOM, Veldhoven, The Netherlands (2012)
- **Bifurcation theory for L-H transition dynamics in fusion plasmas**
W. Weymiens, H.J. de Blank, G.M.D. Hogeweij and D. Zhelyazov.
24th NNV-Symposium on Plasma Physics and Radiation Technology, Lunteren, The Netherlands (2012)
- **Bifurcation theory of a 1-dimensional transport model for the L-H transition**
W. Weymiens, H.J. de Blank, G.M.D. Hogeweij and S. Paquay.
Theory of Fusion Plasmas, Joint Varenna-Lausanne International Workshop, Varenna, Italy (2012)
- **Bifurcation analysis of L-H transition models for fusion plasmas**
W. Weymiens, H.J. de Blank and G.M.D. Hogeweij.
25th NNV-Symposium on Plasma Physics and Radiation Technology, Lunteren, The Netherlands (2013)

References

- [1] A. W. Leonard, *EU/US-TFF, Copenhagen, Pedestal physics and models comparison with experiment.*
- [2] F. Wagner et al., *Physical Review Letters* **49** (1982) 1408
- [3] H. Zohm, *Physical Review Letters* **72** (1994) 222
- [4] S.-I. Itoh, K. Itoh, A. Fukuyama and Y. Miura, *Physical Review Letters* **67** (1991) 2485

2

L-H transitions in magnetically confined plasmas

The most successful present-day fusion devices are the tokamaks. The world record of fusion power production is achieved by the JET tokamak in 1997[1], the fusion reactions produced more than 16 MW. This world record was only possible due to the formation of the H-mode transport barrier. Therefore, this H-mode state of the plasma will be the standard scenario for operating future fusion devices. This chapter elaborates on the characteristics of the H-mode and the observed transition dynamics. Furthermore, the current understanding of the underlying mechanism and some possible models are discussed.

2.1 Experimental observations

The tokamak plasmas start out in the L-mode, and are additionally heated by either electromagnetic waves that resonate with plasma particles, or the injection of neutral beams. If the heating increases above a certain threshold value then spontaneously the plasma can reorganise itself into an H-mode. The physical mechanism initiating this transition is still not fully understood. The complex nonlinear behaviour of the plasma and the very fast timescales of the transition makes it very hard to discriminate the cause and effect relations between the many evolving physical quantities. Moreover, many diagnostics are not capable of capturing the very fast dynamics, such that only differences between the initial L-mode and the final H-mode can be characterised. The main observation is that after the transition the energy confinement is typically twice as good. However, the radial transport of energy outward stays the same in almost the whole tokamak plasma; it is only the transport in the last few centimeters that is affected. In this transport barrier apparently the turbulence that drives the transport in L-mode is quenched in H-mode. This change results in several other observations. First of all the reduction in turbulent transport of particles and heat allows the profiles of density, temperature and pressure to steepen locally inside the transport barrier. Therefore,

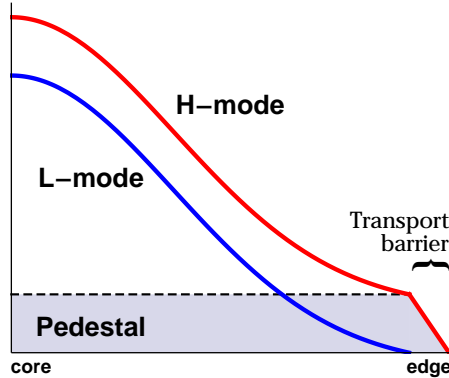


Figure 2.1: L-mode + pedestal = H-mode.

it appears that the L-mode profiles are lifted onto a pedestal, as is shown in Fig. 2.1. During the formation of this pedestal, less heat leaks out of the plasma, such that less neutrals that are present just outside the plasma get excited. This is apparent in a sudden temporary reduction of the line radiation of those neutrals. Afterwards, in the steady state H-mode these neutrals cannot penetrate as deeply into the plasma anymore as they could in L-mode due to the steep gradients. Therefore, the layer that emits line radiation is thinner in H-mode, as is shown in Fig. 2.2.

All these observations are understood as consequences of the reduced turbulent transport, however it is unclear what causes this reduction of turbulence. There are some separate observations that may help to understand what causes this change of turbulence during the L-H transition. The most promising observation is the acceleration of flows during the L-H transition. In fusion plasma physics many different types of flows are discussed and used

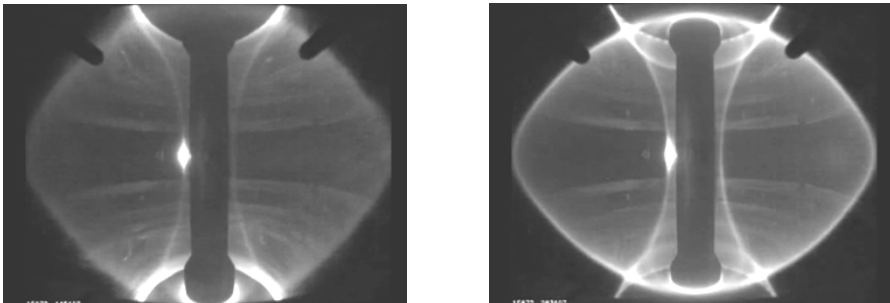


Figure 2.2: MAST: L-mode vs H-mode[2]

in sometimes confusing ways. Nonetheless, they are all influenced during the L-H transition, and probably hold the key in explaining the physical mechanism behind the L-H transition. Therefore, these flows and their relationship are elaborated in the next section. Additionally, the fact that this complex transition is seen in almost all present day magnetic confinement devices implies that the physical mechanism responsible for this effect must be very generic and robust.

However, there is more to learn about the L-H transition than simply looking at the differences between the L-mode and the H-mode, because additionally the different transition dynamics are very characteristic. Not always is the transition from L-mode to H-mode so sudden as described above, as was properly noted by Carlstrom in his review paper[3] from 1996. Throughout this paper, and many more, three different types of dynamics are observed during a transition from L-mode to H-mode.

- (i) **Sharp transitions.** This type of transition is most commonly observed. When the heating power is slowly increased, the plasma stays in L-mode until a certain threshold value is reached, then suddenly and quickly the plasma transits towards the H-mode, as shown in Fig. 2.3(a). An even more remarkable feature is that the plasma stays in H-mode even when the heating power is decreased again below this threshold value. Only when the heating power is decreased below another lower threshold value the system transits back to the L-mode. Thus, sharp transitions are accompanied by hysteresis characteristics.
- (ii) **Smooth transitions.** Carlstrom points out that for low-density discharges at JT-60U[4] and DIII-D so-called ‘transitionless H-modes’ are observed. In these cases the heating power was slowly increased and accordingly the density and temperature profiles evolved slowly from an L-mode state into an H-mode state. These smooth transitions from L-mode to H-mode without clear bifurcation are also seen in very low-density discharges at JET[5–7], see Fig. 2.3(c), and also at ASDEX Upgrade[8] some kind of ‘smoother’ transitions are observed.
- (iii) **Oscillatory transitions.** Recently, these type of transitions attracts more and more attention. Carlstrom noted the ‘dithering’ transitions observed at ASDEX Upgrade[9], where the early dithers are mostly L-mode with brief transitions to H-mode, while the late dithers are mostly H-mode with brief back transitions to L-mode. However, nowadays there are many investigations into all types of oscillatory transitions, at DIII-D[10], ASDEX Upgrade[11, 12], EAST[13, 14], JET[15], TJ-II[16] and HL-2A[17]. Often different names are given to this oscillatory behaviour in different machines, such as: I-phase, I-mode, transition-ELMs,

IM-mode, dithering (see Fig. 2.3(b)), limit cycle oscillations, predator-prey oscillations and geodesic acoustic modes. Most probably some of these observed oscillations are caused by the same mechanism, but there could also be multiple mechanisms at play leading to different kinds of oscillatory behaviour around the L-H transition.

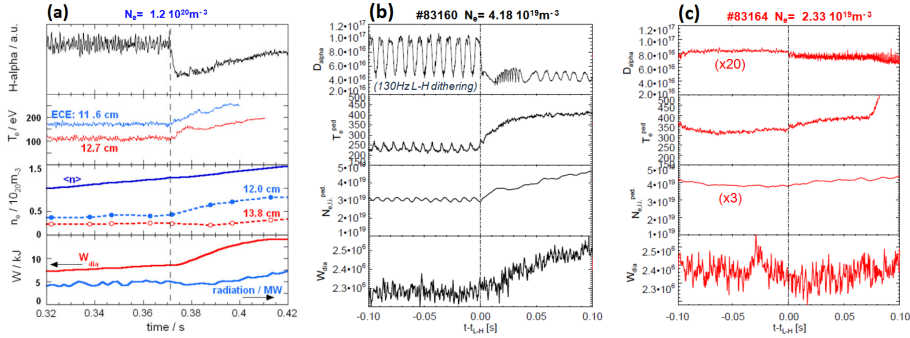


Figure 2.3: (a) A time trace of several quantities during a W7-AS high density L-H transition (dashed line), showing a sharp transition from an L-mode to an H-mode.[18] (b) A time trace of several quantities during a JET medium density L-H transition (dash-dotted line), showing a transition from a dithering phase to an H-mode.[19] (c) A time trace of several quantities during a JET low density L-H transition (dash-dotted line) experimentally identified as a smooth transition from an L-mode to an H-mode.[19]

Thus, many things are known about the H-mode and the transition to it. However, there is no consensus yet about what physical mechanism is underlying this spontaneous plasma behaviour.

2.2 Related physical mechanisms

Many proposed physical mechanisms for the L-H transition mainly fall apart into two categories, one focussing on the trigger mechanism of the transition, and the other focussing on the possibilities to sustain the H-mode. Since the H-mode is seen in many different devices and operating regimes these two points of view should be incorporated into a very generic and robust L-H transition mechanism.

One such general mechanism for the sustainment of the H-mode is the reduction of turbulence by sheared flows. The shearing of turbulent eddies until they break up into smaller eddies, and therewith reducing their spatial

extend, is a well known effect in fluid dynamics[18]. However, in plasmas there are different types of flows, sometimes confusingly mixed up, that may affect the turbulence. First of all, every particle species in the plasma has its own mass flow. Per species these flows can be decomposed in two orthogonal directions (there are no radial flows). At desire one can either decompose in poloidal and toroidal directions, or in directions parallel and perpendicular to the magnetic field lines. These two different decompositions are sometimes confusingly mixed up, because the magnetic fields are mainly toroidal such that the perpendicular direction is almost poloidal. Furthermore, these mass flows are driven by different effects, so the flows can additionally be decomposed into their driving terms, such as the diamagnetic flow (driven by a pressure gradient) and the $\mathbf{E} \times \mathbf{B}$ -flow (driven by an electric field), which in turn can be decomposed in the above discussed directions. Usually the plasma particles follow the magnetic field lines, but they do that equally in both directions such that no average mass flow occurs. On top of that, due to several effects, the plasma particles can drift away from their field lines. These collective particle drifts do add to the mass flows and can be different depending on the mass and charge of the plasma species. There is one plasma drift that is special, since it is the same for all plasma species independent of their mass or charge, and is named the $\mathbf{E} \times \mathbf{B}$ -drift:

$$V_{\mathbf{E} \times \mathbf{B}} = \frac{\mathbf{E} \times \mathbf{B}}{B^2} \quad (2-1)$$

As is clearly summarised in the appendix of Burrell's paper of 1994[20], it is this part of the flow that is capable of reducing the turbulence. He specifically refers to the microscopic analysis of a certain type of turbulence, i.e., ion temperature driven turbulence, by Kim et al.[21] that showed that the turbulent eddies, specifically the electrostatic flute-like modes, could only be convected by this $\mathbf{E} \times \mathbf{B}$ -flow and not by other parts of the mass flow. Therefore, only this $\mathbf{E} \times \mathbf{B}$ -flow can tear apart turbulent eddies, and therewith reduce the transport. This $\mathbf{E} \times \mathbf{B}$ -effect also resulted from the analysis by Biglari et al.[22]. Burrell additionally notes that because the $\mathbf{E} \times \mathbf{B}$ -flow is the same for all plasma species it can therefore stabilise all possible modes. This makes it a very universal mechanism for stabilizing turbulence, as is needed for the description of the L-H transition.

Nowadays, there is consensus about the turbulence reducing effect of sheared $\mathbf{E} \times \mathbf{B}$ -flows. This along with the observation of a radial electric field well near the edge of an H-mode plasma, makes it a viable mechanism for the sustainment of the H-mode. However, the question remains: what triggers the formation of this stable electric field near the plasma edge? The main experimental parameter used to trigger the L-H transition is the input power into the plasma. However, part of this power is radiated away by the core of

the plasma and can not affect the edge plasma where the transport barrier is formed. Thus, the physically more relevant parameter is the heat flux through the last few centimeters of the confined plasma. Evidence has recently[12] been found that it is mainly the heat flux of the ions that contributes, since at low densities the energy exchange between electrons and ions is very limited, and lots of electron heating (leading to a normal magnitude of ion heat flux) is needed for the plasma to go into H-mode. However, for practical and financial reasons the L-H transition thresholds are almost always given in terms of input power, since that is the basic control knob. Thus, to characterise what happens near the edge of the plasma at the L-H transition, it is necessary to investigate the threshold values in terms of the ion heat flux. Still, the mechanism which is triggered by this heat flux and forms the edge radial electric field is not yet known.

In the literature about possible L-H transition models yet another decomposition of flows is encountered. Namely, the division between mean flows and zonal flows, and is mostly applied to the $\mathbf{E} \times \mathbf{B}$ -part of the flow. The zonal flows are defined as driven by the turbulence itself, and result in small fluctuations of the radial electric field on top of the mean radial electric field that causes the mean $\mathbf{E} \times \mathbf{B}$ -flow. There is, however, no clear separation in length scales between a mean flow and a zonal flow. It is claimed[23] that the zonal flow scale length is somewhere in between the mean flow and the small scale turbulence. However, it could also be possible that the electric field well causing the mean flow is just a large zonal flow, because it is not clear yet where this electric field well comes from, and how it is triggered. How this and other flow generation effects either cooperate or compete to reduce the turbulent transport could be analysed with the use of bifurcation theory.

References

- [1] M. Keilhacker *et al.*, *Nuclear Fusion* **39** (1999) 209
- [2] *Mega Ampere Spherical Tokamak*, <http://www.ccf.ac.uk/MAST.aspx>
- [3] T. N. Carlstrom, *Plasma Physics and Controlled Fusion* **38** (1996) 1149
- [4] M. Mori, *Plasma Physics and Controlled Fusion* **36** (1994) A39
- [5] L. D. Horton *et al.*, *26th EPS Conf. on Plasma Physics* **23J** (1999) 193
- [6] Y. Andrew *et al.*, *Plasma Physics and Controlled Fusion* **48** (2006) 479
- [7] C. Maggi *et al.*, *Nuclear Fusion* **54** (2014) 023007
- [8] F. Ryter *et al.*, *Plasma Physics and Controlled Fusion* **40** (1998) 725
- [9] H. Zohm *et al.*, *Plasma Physics and Controlled Fusion* **37** (1995) 437
- [10] L. Schmitz *et al.*, *Physical Review Letters* **108** (2012) 155002
- [11] G. D. Conway, C. Angioni, F. Ryter, P. Sauter and J. Vicente, *Physical Review Letters* **106** (2011) 065001
- [12] F. Ryter *et al.*, *Nuclear Fusion* **53** (2013) 113003
- [13] G. S. Xu *et al.*, *Physical Review Letters* **107** (2011) 125001
- [14] H. Wang *et al.*, *Nuclear Fusion* **52** (2012) 123011
- [15] A. Loarte, R. D. Monk, A. S. Kukushkin, E. Righi, D. J. Campbell, G. D. Conway and C. F. Maggi, *Physical Review Letters* **83** (1999) 3657
- [16] T. Estrada, C. Hidalgo, T. Happel and P. H. Diamond, *Physical Review Letters* **107** (2011) 245004
- [17] J. Cheng *et al.*, *Physical Review Letters* **110** (2013) 265002
- [18] F. Wagner, *Plasma Physics and Controlled Fusion* **49** (2007) B1
- [19] E. Delabie, *private communication*
- [20] K. H. Burrell *et al.*, *Physics of Plasmas* **1** (1994) 1536
- [21] Y. B. Kim, P. H. Diamond, H. Biglari and J. D. Callen, *Physics of Fluids B: Plasma Physics* **3** (1991) 384
- [22] H. Biglari, P. H. Diamond and P. W. Terry, *Physics of Fluids B* **2** (1990) 1
- [23] K. Miki, P. H. Diamond, O. D. Gürcan, G. R. Tynan, T. Estrada, L. Schmitz and G. S. Xu, *Physics of Plasmas* **19** (2012) 092306

3

Bifurcation theory

Nonlinear dynamical systems can exhibit all kinds of rich behaviour. Depending on the parameter settings of the model the temporal evolution of dynamical systems can be completely different. However, small changes of the parameters do not always qualitatively change the dynamics, such that there could be entire regions in parameter space that show qualitatively similar behaviour. Only when crossing the boundaries of these regions in parameter space the topological structure of the dynamic solutions changes; these boundaries are called bifurcations. Thus, the bifurcation boundaries divide the entire parameter space of a certain model in regions with qualitatively the same type of solutions. Since the L-mode and H-mode are qualitatively distinct they are most likely separated by a bifurcation; especially the different characteristic types of transitions between them are indications of typical bifurcations. Bifurcation analysis of L-H transition models can directly determine if these different types of dynamics are present in those models, and in which part of its parameter space they will occur. With this technique physical mechanisms can be combined to get a more complete picture of the physics generating the different types of transitions, and to find which parameters can be used to go from one regime to another.

3.1 Introduction

The field of bifurcation theory is a well developed mathematical field of research, in which all types of complex dynamical behaviour is unraveled into their bare essentials, i.e., the bifurcations. A bifurcation is a topological change in the dynamical solution when a small and smooth change of a parameter is made. This means that in any model many parameters can be changed, however as long as no bifurcation is encountered every solution is qualitatively the same as the solution before the parameter change. Dynamical systems are described in terms of differential equations of the form,

$$\dot{x} = f(x), \quad (3-1)$$

where x is a dynamic variable, and $f(x)$ is an arbitrary function of that variable and probably depending on some parameters. One of the most fundamental bifurcations is encountered when f is a quadratic function of x ,

$$\dot{x} = a + x^2, \quad (3-2)$$

where a is a control parameter. As long as a is negative, there are two steady state solutions of this dynamical system, $x_0 = \pm\sqrt{-a}$, as is shown in Fig. 3.1. When changing a the exact value of the steady state solution, x_0 , will adapt to it, but two solutions remain. If, and only if, a crosses zero the system changes drastically. At this specific point in parameter space two steady state solutions merge and disappear, and the only possibility that is left is that x starts out toward infinity. This drastic change is known as the *fold bifurcation*.

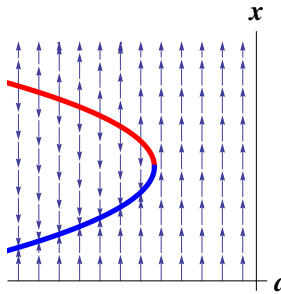


Figure 3.1: The fold bifurcation; two stationary states, one stable (blue) and one unstable (red), merge and disappear for the critical value a_{fold} .

The beauty of bifurcation theory is that any system where stationary states can appear or disappear due to a fold bifurcation can locally be described by this simple quadratic ordinary differential equation. Such a local description is possible for *all* bifurcations not only the fold bifurcation. That makes bifurcation theory so powerful. The simplest form to which any bifurcating system can be reduced is called the *topological normal form*. In case of the fold bifurcation, Eq. (3-2) is its topological normal form. The least number of parameters needed to construct this topological normal form is called the *co-dimension*, and is used to classify the bifurcations. Obviously, the fold bifurcation is a co-dimension 1 bifurcation. This additionally implies that in a multi-dimensional parameter space, the fold bifurcation spans a (multi-1)-dimensional subspace.

Bifurcation theory does not only describe the existence of stationary states it also contains the analysis of the stability of these stationary states. If the

steady state solutions is perturbed by a small ($x_1 \ll x_0$) exponential perturbation,

$$x \rightarrow x_0 + x_1 e^{\lambda t}, \quad (3-3)$$

then the eigenvalue λ determines if this perturbation will grow or shrink in time. For the fold bifurcation example, the steady state $x_0 = \sqrt{-a}$ has a positive eigenvalue, $\lambda = 2\sqrt{-a} > 0$, such that the perturbation will grow in time, making the steady state a repellor. The other steady state, $x_0 = -\sqrt{-a}$ has a negative eigenvalue, $\lambda = -2\sqrt{-a} < 0$, such that the perturbation will shrink in time, making this steady state an attractor. In Fig. 3.1 the stability of these stationary states is indicated with red and blue, and the corresponding time evolution of the system is depicted by the arrows. For systems of N equations, the eigenvalues become N -dimensional complex vectors. The signs of the real parts of the eigenvector determine if the corresponding directions are attracting or repelling. At the fold bifurcation both the real part and the imaginary part of one of the eigenvalues of two different steady states vanishes simultaneously.

Another co-dimension 1 bifurcation is the *Hopf bifurcation*. At this bifurcation the real part of a pair of complex conjugated eigenvalues vanishes. This means that the considered steady state changes from stable to unstable or vice versa. So if a stable steady state turns unstable (and infinity is repelling as in all physical systems) a stable limit cycle will emerge, surrounding the steady state, as is shown when going from Fig. 3.2a to b, this is called the *supercritical Hopf bifurcation*. The other way around (from Fig. 3.2b to a) the stable limit cycle will shrink in size until it merges with the unstable steady state and vanishes, leaving only a stable steady state. However, going from an unstable to a stable steady state can also occur due to the generation of an unstable (repelling) limit cycle surrounding the stable steady state, this is known as the *subcritical Hopf bifurcation*, as is shown when going from Fig. 3.2b to c. When this unstable limit cycle grows, see Fig. 3.2c to d, and touches the stable limit cycle they both vanish, see Fig. 3.2d to a. This is a special bifurcation since it not a local bifurcation (in a point) but a global bifurcation occurring around the whole limit cycle simultaneously. This is sometimes called a *global fold bifurcation*, because it corresponds to a fold bifurcation of limit cycles.

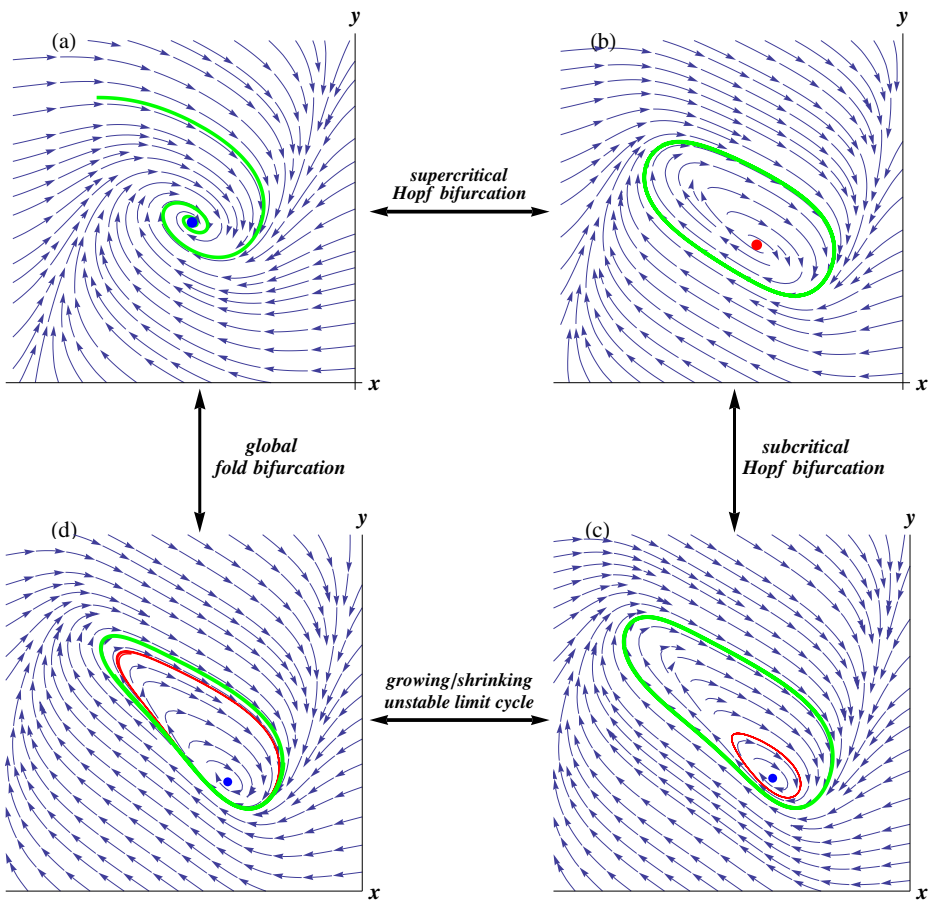


Figure 3.2: Different bifurcations of stable (blue) and unstable (red) steady states and stable (green) and unstable (red) limit cycles. (a)↔(b) supercritical Hopf bifurcation, (b)↔(c) subcritical Hopf bifurcation, (c)↔(d) a growing unstable limit cycle until it intersects with the stable limit cycle: (d)↔(a) and a global fold bifurcation will occur.

3.2 Bifurcations vs L-H transition dynamics

The different types of observed transition dynamics listed in chapter 2.1 can be recognised as certain types of bifurcations. For instance, slowly varying a control parameter across a fold bifurcation will cause a stationary state to disappear. If the system was in that steady state at the moment of the bifurcation, afterwards the system suddenly needs to evolve to a new stationary state. Thus, fold bifurcations are the natural way to describe sharp transitions as function of a control parameter, such as the L-H transition.

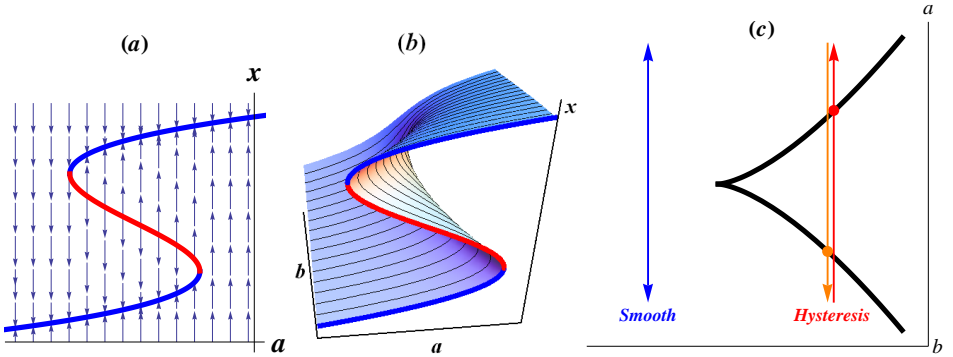


Figure 3.3: (a) Two fold bifurcations, causing hysteresis in the forward and backward transition as function of increasing and decreasing a . (b) Another control parameter, b , determines the size of the hysteresis, until the two fold bifurcations merge into a cusp bifurcation. (c) The (a, b) -parameter space where the black lines indicate the fold bifurcations. The point where the two fold bifurcations coincide is the cusp bifurcation, this point separates the parameter space into two regimes of transition types, as is indicated.

Additionally, it is observed that in this regime of sharp L-H transitions also the H-L back transitions are sharp, implying that also these are generated by a fold bifurcation. The natural way to combine two fold bifurcations is shown in Fig. 3.3a. This automatically shows the two different critical values for a , one for the forward transition and one for the backward transition. This hysteresis behaviour is characteristic of two co-dimension 1 fold bifurcations branching of an underlying co-dimension 2 *cusp bifurcation*. The topological normal form of this cusp bifurcation is,

$$\dot{x} = a - bx - x^3, \quad (3-4)$$

where b determines the size of the hysteresis, as is shown in Fig. 3.3b. At the point where the hysteresis disappears, the two fold bifurcations merge and disappear. This special point from which two fold bifurcations can arise is the cusp bifurcation. Indeed, two parameters, a and b , are needed to pinpoint this co-dimension 2 bifurcation. The cusp bifurcation separates the parameter space into two regimes, as is shown in Fig. 3.3c, one with sharp transitions with hysteresis encountering the fold bifurcations, and one with smooth transitions not encountering fold bifurcations, as function of increasing and decreasing parameter a .

Thus, the cusp bifurcation organises two types of L-H transition dynamics as is discussed in chapter 2.1, the smooth transitions and the sharp transitions exhibiting hysteresis. As is described in chapter 3.1 oscillatory behaviour can arise due to a Hopf bifurcation. There is a fundamental way in which the Hopf bifurcation can be combined with the cusp bifurcation, which can be viewed as a *degenerate Bogdanov-Takens bifurcation*. This underlying bifurcation organises the three co-dimension 1 bifurcations (two fold and one Hopf), and is called in this thesis the *co-dimension 3 bifurcation*. Be aware that there are also other bifurcations of co-dimension 3, however in this thesis always this specific one is meant. There are several equivalent unfoldings of this co-dimension 3 bifurcation, one of which, known as the FitzHugh-Nagumo model, is most closely related to the reaction-diffusion system of equations describing the plasma, as will be shown in the next chapter,

$$\dot{x} = a - bx - x^3 + cy, \quad (3-5a)$$

$$\dot{y} = -y - x. \quad (3-5b)$$

Note that the original cusp bifurcation equation is simply coupled to a damped variable. However, as long as the coupling constant, c , is less than some finite value c_{crit} , the parameter space is the same as indicated in Fig. 3.3c. This shows the robustness of the cusp bifurcation. If some small additional coupling would change the bifurcation structure of the model, then it would be a very sensitive model to perturbations and therefore very unlikely to be correct for a very robust phenomenon as the L-H transition. At the critical value c_{crit} the co-dimension 3 bifurcation is encountered at the position of the cusp bifurcation. Due to this co-dimension 3 bifurcation a regime of limit cycle solutions opens up, covering the original cusp-bifurcation point. These limit cycle solutions are produced by the Hopf bifurcations that make the originally stable steady states unstable. If both steady states are unstable the system will oscillate according to this limit cycle. However, if the steady state turns unstable while the other steady state is stable, the system will directly transit towards this stable steady state. Therefore, the oscillatory solutions will only occur in the region surrounding the cusp bifurcation point where there are no

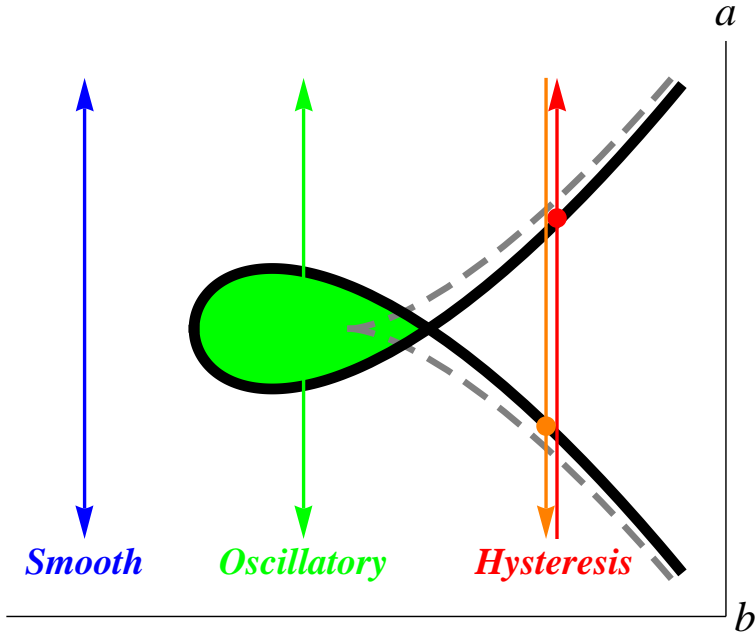


Figure 3.4: codimension 3 parameter space structure

stable steady states, as is shown in Fig. 3.4. This parameter space structure is characteristic for the underlying co-dimension 3 bifurcation. The specific arrangement of smooth transitions and sharp transitions separated by the oscillatory transitions, is therefore very generic and robust. If a model contains such a co-dimension 3 bifurcation then it is automatically proven that the model contains all the types of transition dynamics described above. Therefore, the quality of an H-mode model can be judged by the existence of the co-dimension 3 bifurcation. If the model does not contain this bifurcation, it can not describe all different types of L-H transitions in the specific order indicated in Fig. 3.4. If a model does describe all the types of transitions without having this co-dimension 3 bifurcation, then there is a parameter in that model that could pull, e.g., the oscillations towards a region in parameter space that is far away from the L-H transition point. Therefore, these models are not robust and need to be fine-tuned.

4

Bifurcation theory for the L-H transition in magnetically confined fusion plasmas

W. Weymiens, H.J. de Blank, G.M.D. Hogeweij and J.C. de Valen  a

FOM Institute DIFFER - Dutch Institute for Fundamental Energy Research,
Association EURATOM/FOM, Nieuwegein, the Netherlands

Abstract

The mathematical field of bifurcation theory is extended to be applicable to 1-dimensionally resolved systems of nonlinear partial differential equations, aimed at the determination of a certain specific bifurcation. This extension is needed to be able to properly analyze the bifurcations of the radial transport in magnetically confined fusion plasmas. This is of special interest when describing the transition from the low-energy-confinement state to the high-energy-confinement state of the radial transport in fusion plasmas (i.e. the L-H transition), because the nonlinear dynamical behavior during the transition corresponds to the dynamical behavior of a system containing such a specific bifurcation. This bifurcation determines how the three types (sharp, smooth and oscillating) of observed L-H transitions are organized as function of all the parameters contained in the model.

published in:
Physics of Plasmas **19**, 072309 (2012)

4.1 Introduction

The transport from the hot core to the cold edge of magnetically confined fusion plasmas, like the tokamak, determines the energy confinement and therewith the performance of the fusion reactor. This radial transport is dominated by turbulence which greatly limits the pressure build up in the core. However, under certain circumstances the plasma reorganizes to a self-sustained state in which locally the turbulence is suppressed. This bifurcation in the radial transport arises when, for instance, the heating power exceeds a threshold value. The resulting state of the plasma is called the high-confinement-mode, or H-mode, and was first discovered by the ASDEX team in 1982 [1]. The physical mechanism causing this transition from the L-mode (low-confinement-mode) to the H-mode is not yet fully identified[2]; however, the nonlinear dynamics observed during the L-H transition can be identified as certain fundamental bifurcations, which give directions to the possible underlying dynamical equations. Bifurcation theory categorizes all topological changes of the solutions of dynamical systems as function of a corresponding control parameter. The L-H and H-L transitions are quite naturally characterized as fold bifurcations, which describe the creation and disappearance of stationary solutions by slight changes of the relevant parameters. This fold bifurcation then describes the sudden disappearance of the L-mode stationary state by increasing the heating power slightly above a threshold value, therefore forcing the system to sharply transit to the only stationary state left, i.e., the H-mode. Because the back transition from the H-mode to the L-mode occurs at a different value of the heating power, there must be a separate fold bifurcation causing the disappearance of the H-mode. Thus, two separate fold bifurcations are needed to describe hysteresis like behavior. With bifurcation theory, it is proven that the existence and magnitude of the hysteresis between L-H and H-L transitions can be controlled by two types of parameters. By varying the first type of parameter, the disappearance of hysteresis occurs when the two fold bifurcations meet in a so-called cusp bifurcation. Varying the second type of parameter can cause the hysteresis (two stable solutions) to be replaced by limit cycle oscillations (no stable solutions) due to a Hopf bifurcation of the system. These two different regimes where the hysteresis has disappeared are also observed in tokamak plasmas. The first one results in smooth transitions[3] for both the L-H and H-L transitions without any bifurcations. The second one results in oscillatory behavior corresponding to a phase of dithering H-mode[2, 4] before the system settles into the final H-mode. How these different types of L-H transition phenomena are ordered relative to each other as function of the parameters of the model is determined by the underlying bifurcations. Indeed, hysteresis behavior in a dynamical system is governed by two separate fold bifurcations. As noted

before, there are two ways of destroying this hysteresis behavior according to bifurcation theory. Correspondingly, there are two types of parameters which will do this. One leading to the cusp bifurcation at which the magnitude of the hysteresis has shrunk to zero, and the other leading to a Hopf bifurcation due to which the hysteresis is replaced by oscillations. These two separate directions in parameter space branch off out of the underlying *co-dimension 3 bifurcation*. With the analysis of this bifurcation, it is possible to find with which parameter or combination of parameters the system evolves towards the different transition regimes [sharp (i), smooth (ii) and oscillating (iii)], and simultaneously to determine the threshold values of these parameters or combination of parameters.

The lowest order dynamical system containing this co-dimension 3 bifurcation is the FitzHugh-Nagumo model[5, 6]

$$\begin{aligned}\dot{x} &= -a - bx - x^3 + cy, \\ \dot{y} &= -x - y,\end{aligned}\tag{4-1}$$

which allows a clear visualization of the different types of directions for the different bifurcations and therewith the fundamental structure of the ordering for the different types of L-H transition phenomena around a co-dimension 3 bifurcation. For $c = 0$, the steady state solutions obviously can have one or multiple possibilities depending on the parameters a and b . The number of fixed points can only be changed at the fold bifurcations of the system which determine the characteristic cusp-shaped curve plotted in Fig. 4.1(a) bounding the region with multiple solutions. This directly indicates that the b -parameter is the one which can shrink the hysteresis to vanishing size by merging the two fold bifurcations at the origin of the graph, i.e., the cusp bifurcation. For $c \neq 0$, the bifurcation structure of the system stays actually exactly the same, only until c is increased above some threshold value $c_{crit} = 1$ a region of limit cycle solutions will appear, i.e., the shaded region in Fig. 4.1(b), which covers the cusp bifurcation and its fold bifurcations branching off of it. Passing through this region of oscillations (iii), indeed, no hysteresis will be present.

Thus, knowing that this co-dimension 3 bifurcation is present in a dynamical system, it is automatically proven that this system contains sharp transitions between different stationary states which exhibit hysteresis, that there are also smooth transitions between the different states, and that there are oscillatory transitions (see Fig. 4.2). If a detailed model for the edge transport barrier dynamics contains such a co-dimension 3 bifurcation, it is clear that the regions of parameter space with L-mode, H-mode, hysteresis, and dithering are organized in the same way as the (a, b, c) parameter space of system Eq. (4-1). The determination of these bifurcations is straightforwardly possible in coupled systems of ordinary differential equations (ODEs)[7] as given

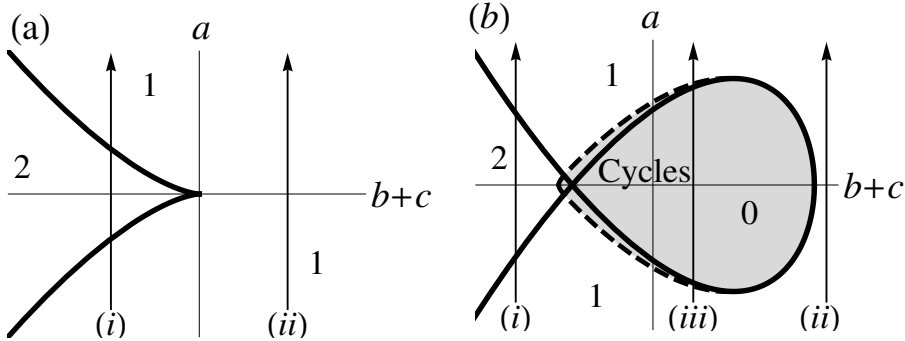


Figure 4.1: (a) The fold bifurcations surrounding the region with multiple stable stationary states (which are indicated by the numbers) that merge at the cusp bifurcation at the origin of the graph. The cusp bifurcation divides the parameter space in a region ($b + c < 0$), where sharp transition with hysteresis occur [trajectory (i)], and a region ($b + c > 0$) with smooth transitions without bifurcations [trajectory (ii)]. This structure is valid for all $c < c_{crit}$ in the FitzHugh-Nagumo model. (b) If $c > c_{crit}$ the cusp bifurcation gets covered with a region of limit cycle solutions, indicated by the shaded area, where the solid curve corresponds to the Hopf bifurcation and the dashed curve to a nonlocal bifurcation (described in Sec. 4.3) both generating the limit cycles. Thus, the region to the left [containing trajectory (i) describing a sharp transition] and the region to the right [containing trajectory (ii) describing a smooth transition] are now separated by a region with oscillatory transitions [the shaded region containing trajectory (iii)].

above. However, for the determination of bifurcations in radially resolved systems described with partial differential equations (PDEs), the bifurcation theory is strongly lacking. In Sec. 4.2, a new analysis method is developed especially aimed at determining this co-dimension 3 bifurcation in systems of PDEs, which is, however, also applicable on the ODE cases as is shown in Sec. 4.3. In Sec. 4.4, the new method is applied onto a 1-dimensional transport model for the L-H transition introduced by Zohm[8]. It then becomes clear how to use this new method on radially extended dynamical models, leading to clear criteria for different types of transition behavior and the corresponding threshold values.

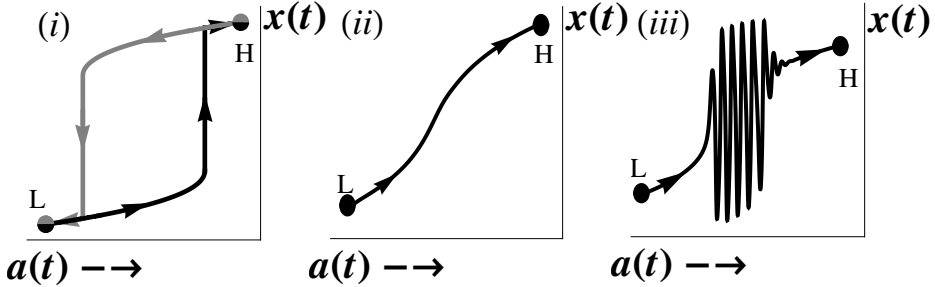


Figure 4.2: The three qualitatively different transition solutions of the FitzHugh-Nagumo model for $c = 3$, corresponding to the trajectories of Fig. 4.1. (i) $b = -5$, the black curve is the solution of the forward transition indicated by trajectory (i). The grey curve corresponds to the inverse trajectory describing the back transition, clearly showing hysteresis. (ii) $b = 0$, the solution of the evolution during a smooth transition. (iii) $b = -2.5$, with increasing control parameter $a(t)$, the system enters a regime of oscillatory solutions (limit cycles) until a second threshold is reached, after which the system settles into the other stationary state.

4.2 Generalized bifurcation theory

In this section, a general method is introduced to find a co-dimension 3 bifurcation in dynamical systems specified both by PDEs and by ODEs. This is possible by realizing that one can view a system of PDEs as an infinite system of ODEs. Where one of these ODEs describes the evolution of a single point along the spatial direction coupled to its neighboring points which are separately described by their own ODE. So an infinite set of these coupled ODEs construct the entire spatial direction

$$\dot{\mathbf{v}} = \mathbf{f}(\mathbf{v}), \quad (4-2)$$

so \mathbf{v} will be a finite dimensional vector for a set of ODEs and an infinite-dimensional vector for a set of PDEs, and \mathbf{f} can be any (nonlinear) operator not incorporating spatial derivatives. The steady states of such a system are simply defined as

$$\mathbf{f}(\mathbf{v}_0) = 0. \quad (4-3)$$

For the co-dimension 3 bifurcation of our interest, it is sufficient to Taylor expand the system up to second order around the fixed points

$$\dot{\mathbf{v}} \simeq \mathbf{f}(\mathbf{v}_0) + M_1(\mathbf{v} - \mathbf{v}_0) + \frac{1}{2} \left(M_2(\mathbf{v} - \mathbf{v}_0) \right) (\mathbf{v} - \mathbf{v}_0), \quad (4-4)$$

where the linear operator $M_1 = \partial \mathbf{f} / \partial \mathbf{v}$ (i.e., 2-tensor) and the operator $M_2 = \partial^2 \mathbf{f} / \partial \mathbf{v} \partial \mathbf{v}$ (i.e., 3-tensor); note that in the finite dimensional cases, the matrix multiplications are implied. If the parameters of the system are chosen such that the system is at the fold bifurcation, the linear operator M_1 becomes singular, implying a single vanishing eigenvalue with eigenvector \mathbf{v}_1 . This is also true in the adjoint picture: the image space of M_1 has co-dimension 1. Thus, at the fold bifurcation, there are vectors \mathbf{v}_1 and \mathbf{u}_1 which satisfy

$$\begin{aligned} M_1 \mathbf{v}_1 &= 0, \\ \mathbf{u}_1^T M_1 &= 0, \end{aligned} \quad (4-5)$$

The two different possibilities of destroying the hysteresis behavior, as described in Sec. 4.1, are caused by two different types of bifurcations: the cusp bifurcation and the Hopf bifurcation. The Hopf bifurcation arises from an underlying bifurcation, namely, the Bogdanov-Takens bifurcation[7] at which the Hopf bifurcation coincides with one of the fold bifurcations. At the cusp bifurcation, both the fold bifurcations coincide; if all three bifurcations coincide (i.e., the two fold bifurcation and the Hopf bifurcation) the system is at the co-dimension 3 bifurcation. At this point, in parameter space, the system is both at the cusp bifurcation and the Bogdanov-Takens bifurcation at the same time, so combining the two restrictions for the cusp bifurcation and the Bogdanov-Takens bifurcation leads to the subspace of parameter space at which the co-dimension 3 bifurcation occurs. First of all, the cusp bifurcation is given by the point where the two fold bifurcations meet tangentially, so when the vectors \mathbf{v}_1 and \mathbf{u}_1 can be found (at the fold bifurcation) additionally the second term in the Taylor expansion [Eq. (4-4)] evaluated in the same direction as the fold condition must vanish,

$$\mathbf{u}_1^T (M_2 \mathbf{v}_1) \mathbf{v}_1 = 0. \quad (4-6)$$

Second, for the Bogdanov-Takens bifurcation, we need to combine the Hopf bifurcation together with the fold bifurcation. At the Hopf bifurcation, the real part of a pair of complex conjugated eigenvalues vanishes. At the fold bifurcation, the imaginary and real part of an eigenvalue vanishes. Thus, at the Bogdanov-Takens bifurcation, a pair of eigenvalues must become zero simultaneously (i.e., $\lambda^2 = 0$). Then, according to the Cayley-Hamilton theorem[9], there must be some generalized eigenvector, \mathbf{v}_2 , and a generalized co-eigenvector, \mathbf{u}_2 , satisfying

$$M_1^2 \mathbf{v}_2 = 0, \quad \mathbf{u}_2^T M_1^2 = 0. \quad (4-7)$$

At this Bogdanov-Takens bifurcation point, these generalized eigenvectors can be related to the eigenvectors which have a vanishing eigenvalue at this point, leading to

$$M_1 \mathbf{v}_2 = \mathbf{v}_1, \quad \mathbf{u}_2^T M_1 = \mathbf{u}_1^T. \quad (4-8)$$

These conditions imply

$$\mathbf{u}_2^T \cdot \mathbf{v}_1 = \mathbf{u}_1^T \cdot \mathbf{v}_2. \quad (4-9)$$

The Bogdanov-Takens bifurcation will be given by the fold condition [Eq. (4-5)] combined with the condition

$$\mathbf{u}_1^T \cdot \mathbf{v}_1 = 0. \quad (4-10)$$

Summarizing, if in a general dynamical system, two vectors, \mathbf{v}_1 and \mathbf{u}_1 , can be found which simultaneously satisfy

$$\begin{aligned} M_1 \mathbf{v}_1 &= 0, \\ \mathbf{u}_1^T M_1 &= 0, \\ \mathbf{u}_1^T (M_2 \mathbf{v}_1) \mathbf{v}_1 &= 0, \\ \mathbf{u}_1^T \cdot \mathbf{v}_1 &= 0, \end{aligned} \quad (4-11)$$

then the system contains the co-dimension 3 bifurcation.

This analysis by itself is sufficient to conclude that the considered system has multiple steady states between which sharp transitions, smooth transitions, and oscillating transitions can occur and, moreover, that the sharp transitions exhibit hysteresis between the forward and backward transitions. However, a bit more extended bifurcation analysis might also specify for which parameter values these different types of transition take place and what the threshold values will be. For this, it is necessary to get a condition for the fold bifurcation and for the Hopf bifurcation separately. The fold bifurcation can be found quite straightforwardly by qualitatively analyzing the steady state conditions, as will become clear in Secs. 4.3 and 4.4 where an example of a set of coupled ordinary and partial differential equations are considered, respectively. The Hopf bifurcation, however, needs some further investigation. It is already noted that the Hopf bifurcation arises out of a Bogdanov-Takens bifurcation at which there are two simultaneously vanishing eigenvalues. The Hopf bifurcation can be found by unfolding the Bogdanov-Takens bifurcation in all its parameters and by identifying the specific direction which keeps the eigenvalues purely imaginary, i.e., the Hopf condition

$$M(\mathbf{v} - \mathbf{v}_{new}) = i\omega(\mathbf{v} - \mathbf{v}_{new}), \quad (4-12)$$

where $M = M_1 + \delta M$ is the linear operator of the system with the perturbed parameters. Additionally, it must be noted that the steady state solution, $\mathbf{v}_0 \rightarrow \mathbf{v}_{new}$, is also shifted. The complex solution can be decomposed in factors

of $i\omega$ where the real frequency ω is the small parameter which reduces to zero at the Bogdanov-Takens bifurcation,

$$\mathbf{v} = \mathbf{v}_{new} + (\mathbf{v}_1 + i\omega\mathbf{v}_2 - \omega^2\mathbf{v}_3 - i\omega^3\mathbf{v}_4)e^{i\omega t}. \quad (4-13)$$

Consistent ordering requires that $\delta M = \omega^2 M_3$, combining the same orders of $i\omega$ in the eigenvalue equation [Eq. (4-12)] then leads to

$$\begin{aligned} M_1\mathbf{v}_1 &= 0, \\ M_1\mathbf{v}_2 &= \mathbf{v}_1, \\ M_3\mathbf{v}_1 - M_1\mathbf{v}_3 &= -\mathbf{v}_2, \\ M_3\mathbf{v}_2 - M_1\mathbf{v}_4 &= -\mathbf{v}_3, \end{aligned} \quad (4-14)$$

where the first two orders give the Bogdanov-Takens point and the last two orders give the change of stability of the stationary states in the neighborhood of the Bogdanov-Takens point for small ω , i.e., the Hopf bifurcation. To avoid determining the vectors \mathbf{v}_3 and \mathbf{v}_4 , these equations can be dotted into the adjoint vectors \mathbf{u}_1^T and \mathbf{u}_2^T , while using the Bogdanov-Takens properties of M_1 , and smartly combining them leaves us with a single condition for the Hopf bifurcation that is invariant under renormalizations of the perturbation operator M_3 ,

$$\mathbf{u}_1^T \cdot \mathbf{v}_2(\mathbf{u}_1^T M_3 \mathbf{v}_2 + \mathbf{u}_2^T M_3 \mathbf{v}_1) = \mathbf{u}_2^T \cdot \mathbf{v}_2(\mathbf{u}_1^T M_3 \mathbf{v}_1). \quad (4-15)$$

Note that all expressions, including this result, are invariant under transformations,

$$\begin{aligned} \mathbf{u}_2 &\rightarrow \mathbf{u}_2 + \lambda_u \mathbf{u}_1, & (\mathbf{u}_1, \mathbf{u}_2) &\rightarrow \kappa_u(\mathbf{u}_1, \mathbf{u}_2), \\ \mathbf{v}_2 &\rightarrow \mathbf{v}_2 + \lambda_v \mathbf{v}_1, & (\mathbf{v}_1, \mathbf{v}_2) &\rightarrow \kappa_v(\mathbf{v}_1, \mathbf{v}_2). \end{aligned} \quad (4-16)$$

In Sec. 4.3, this new analysis is proved to work properly for the already known bifurcations of a set of ordinary differential equations which contain the co-dimension 3 bifurcation. Thereafter, the method can reliably be used for the bifurcation analysis of a 1-dimensional transport model proposed in 1994 by Zohm[8] to explain the dithering behavior during L-H transitions.

4.3 Finite dimensional case

To test the new general method for finding the co-dimension 3 bifurcation in a set of coupled dynamical equations, it will now be applied on an already known finite dimensional example of a system containing this bifurcation. Moreover, it helps to get a feeling for the abstract machinery developed in Sec. 4.2. As introduced in Sec. 4.1, the FitzHugh-Nagumo model [Eq. (4-1)] is such a finite dimensional model which contains the co-dimension 3 bifurcation. The steady states are straightforwardly found to be satisfying $y_0 = -x_0$

and $x_0^3 + (b+c)x_0 + a = 0$. Taylor expanding this system up to second order around these stationary state solutions leads to a linear operator

$$M_1 = \begin{pmatrix} -3x_0^2 - b & c \\ -1 & -1 \end{pmatrix}. \quad (4-17)$$

The corresponding eigenvector with vanishing eigenvalue and its adjoint can be given by

$$\mathbf{v}_1 = \begin{pmatrix} 1 \\ -1 \end{pmatrix} \quad \text{and} \quad \mathbf{u}_1 = \begin{pmatrix} 1 \\ c \end{pmatrix}, \quad (4-18)$$

as long as the fold condition is satisfied,

$$\det M_1 = 3x_0^2 + b + c = 0, \quad (4-19)$$

which corresponds to a surface in the 3-dimensional parameter space given by

$$a^2 = -\frac{4}{27}(b+c)^3. \quad (4-20)$$

This indeed leads to the characteristic cusp shaped curves which are plotted in Fig. 4.3 with the long dashed lines. For the cusp bifurcation, where the fold bifurcations come together, it is necessary to consider the second order term consisting of the 3-tensor M_2 ; in this case, however, seven of the eight components are zero and only the δx^2 -component is nonzero, leading to a simple restriction for the cusp bifurcation,

$$\mathbf{u}_1^T (M_2 \mathbf{v}_1) \mathbf{v}_1 = -6x_0 = 0. \quad (4-21)$$

Combining this with the fold condition leads to a line in parameter space given by

$$b_{cusp} = -c_{cusp} \quad \text{and} \quad a_{cusp} = 0. \quad (4-22)$$

The Bogdanov-Takens bifurcation can straightforwardly be found to be

$$\mathbf{u}_1^T \cdot \mathbf{v}_1 = 1 - c = 0, \quad (4-23)$$

leading to the Bogdanov-Takens curve in parameter space given by

$$c_{BT} = 1 \quad \text{and} \quad a_{BT}^2 = -\frac{4}{27}(b_{BT} + 1)^3. \quad (4-24)$$

The intersection of these two lines gives the point in parameter space at which the co-dimension 3 bifurcation occurs,

$$(a, b, c) = (0, -1, 1). \quad (4-25)$$

In conclusion, this model indeed has the dynamical behavior corresponding to a co-dimension 3 bifurcation, which is ordered according to the description in

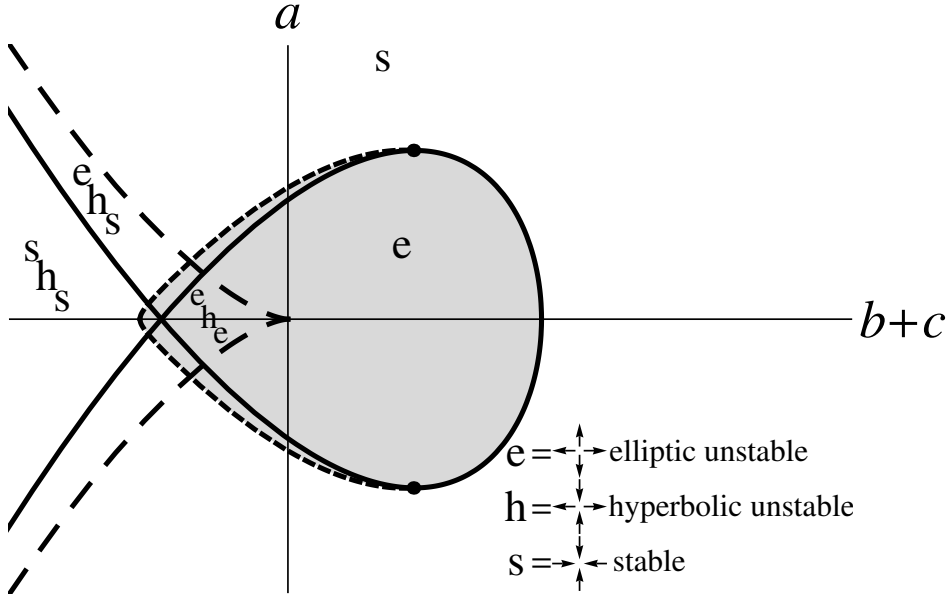


Figure 4.3: 2D parameter space for fixed $c > 1$ with two fold bifurcations (long-dashed curves) merging into a cusp bifurcation at $a = b + c = 0$, and a Hopf bifurcation indicated by the solid curve. The short-dashed curve, corresponding to a nonlocal bifurcation, ends at Bautin bifurcations[7] (black dots). The shaded area corresponds to the parameter range where stable limit cycle solutions of the system exist.

Sec. 4.1. The fold bifurcations are already found to have their characteristic shape. However, it would be nice if this match can also be done for the Hopf bifurcation. For the determination of the Hopf bifurcation, it is necessary to unfold the parameters around the Bogdanov-Takens bifurcation in the direction which keeps the eigenvalues purely imaginary, this leads to the following perturbed linear operator:

$$M = M_1 + \delta M = \begin{pmatrix} -3x_{new}^2 - b_{BT} - \delta b & c_{BT} + \delta c \\ -1 & -1 \end{pmatrix}. \quad (4-26)$$

Subtracting the linear operator evaluated at the Bogdanov-Takens point, M_1 , leaves the perturbation of the linear operator to be

$$\omega^2 M_3 = \delta M = \begin{pmatrix} -3x_{new}^2 - (b_{BT} + \delta b) - 1 & \delta c \\ -1 & -1 \end{pmatrix}. \quad (4-27)$$

And x_{new} is the new shifted fixed point, satisfying

$$-(a_{BT} + \delta a) - (b_{BT} + \delta b + c_{BT} + \delta c)x_{new} - x_{new}^3 = 0. \quad (4-28)$$

This only leaves the determination of the generalized eigenvectors, \mathbf{v}_2 and \mathbf{u}_2 , before the general Hopf criterium [Eq. (4-15)] can be used. Choose them to be

$$\mathbf{v}_2 = \begin{pmatrix} 2 \\ -1 \end{pmatrix} \quad \text{and} \quad \mathbf{u}_2 = \begin{pmatrix} 2 \\ 1 \end{pmatrix}, \quad (4-29)$$

such that the Hopf bifurcation restriction becomes

$$-3x_{new}^2 - (b_{BT} + \delta b) - 1 = 0, \quad (4-30)$$

which leads to a surface in parameter space directly in terms of the Bogdanov-Takens values plus their perturbation. Since, this analysis is true for an arbitrarily sized perturbation, it is allowed to redefine the shifted parameters as the original parameters (e.g., $a_{BT} + \delta a = a$) such that the Hopf bifurcation is described by the following expression:

$$a^2 = -\frac{4}{27}(b+1) \left(b + \frac{3}{2}c - \frac{1}{2} \right)^2, \quad (4-31)$$

which is shown as a solid curve in Fig. 4.3. In the region of parameter space surrounded by the Hopf bifurcation, there are no stable fixed points and there is one stable limit cycle causing the oscillatory behavior. Such a region only exists for $c > c_{crit} = 1$ and its size increases with c . This indeed corresponds to the co-dimension 3 bifurcation from which this Hopf bifurcation must branch off, as was expected.

Further bifurcation analysis reveals a tiny region of parameter space outside the Hopf bifurcation curve where there are still stable limit cycle solutions (i.e., in the shaded region) of the system surrounded by the short-dashed curve in Fig. 4.3. These cannot be found by the local analysis described in Secs. 4.1-4.3, where a Taylor expansion around the fixed points is used. This global bifurcation appears when a pair of limit cycles gets created (one stable and one unstable) and separate from each other. This does not happen locally around a fixed point, but globally along the entire contour of both limit cycles simultaneously. Importantly is to note that also this bifurcation is a characteristic of the co-dimension 3 bifurcation, so even though the exact boundary of this global bifurcation is probably impossible to determine in an infinite dimensional system of equations, it will still enlarge the region of stable limit cycles in that case.

4.4 Transport model for the L-H transition

The radial transport in a fully ionized fusion plasma from the hot core towards the cold edge can effectively be described by a continuity equation for the density and the energy

$$\frac{\partial n}{\partial t} = -\frac{\partial \Gamma}{\partial r}, \quad (4-32a)$$

$$\frac{\partial}{\partial t} \left(\frac{nT}{\gamma - 1} \right) = -\frac{\partial q}{\partial r}, \quad (4-32b)$$

for this it is assumed that the transport barrier occurs in a thin layer at the edge such that a slab geometry description is allowed. Furthermore, a single temperature description is used, $T_i = T_e = T$, and it is assumed that all the particle and energy deposition into the plasma is somewhere in the core outside our modeled domain, such that there are no sources inside the domain and all the particles and energy enter as a flux which is fixed by the boundary conditions. Inside the domain, the particle and heat flux are described by

$$\begin{aligned} \Gamma &= -D \frac{\partial n}{\partial r}, \\ q &= -\chi n \frac{\partial T}{\partial r} + \frac{\Gamma T}{\gamma - 1}. \end{aligned} \quad (4-33)$$

The particle flux, Γ , is governed by some effective particle diffusion due to the anomalous transport of electrons and ions. The heat flux, q , is a combination of some effective heat diffusion and heat advection due to the net flow described by the particle flux, with γ the adiabatic index. A change from low confinement to high confinement can, therefore, be described by a reduction of the transport coefficients: particle diffusivity, D , and heat conductivity χ . The exact mechanism reducing the anomalous transport coefficients is not yet known; however, some theories[10–12] and experiments[13, 14] suggest that flows in the plasma can tear apart turbulent eddies reducing the radial extent of the transported particles and heat. In the transport model used in this paper, only a mean flow due to $\mathbf{E} \times \mathbf{B}$ -drift is used, such that the transport coefficients become a direct function of the normalized radial electric field,

$$Z = \frac{\rho_p e E_r}{T_i}, \quad (4-34)$$

as is shown in Fig. 4.4.

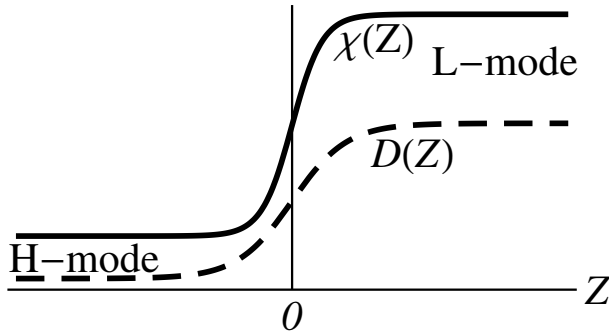


Figure 4.4: The dependence of the transport coefficients (particle diffusivity, D , and heat conductivity, χ) on the normalized radial electric field, Z . Neither the exact shape of the curve is important, nor the relative sizes of the minima and maxima as long as there is some significant difference between the minimum and maximum values, and the transition occurs for both transport coefficients around the same value of Z , which is chosen to be zero but can be shifted towards any other value.

To describe the dynamics during possible transitions of the transport, the evolution of the radial electric field [8, 15, 16] must be taken into account, via Ampères law which balances temporal changes of the radial electric field with the radial currents,

$$\varepsilon \frac{\partial Z}{\partial t} = \mu \frac{\partial^2 Z}{\partial r^2} + c_n \frac{T}{n^2} \frac{\partial n}{\partial r} + \frac{c_T}{n} \frac{\partial T}{\partial r} - G(Z), \quad (4-35)$$

where $\varepsilon = B_p^2/(B^2 \nu_i)$ is the dielectric constant of the polarized plasma. The radial currents are caused by the anomalous shear viscosity of the $\mathbf{E} \times \mathbf{B}$ -drift[17] (first term of right-hand side (RHS) where $\mu \sim \rho_p^2$ is the ratio of viscosity to collision frequency). The second and third terms are due to the bipolar part of the anomalous cross field flux, i.e., the excess flux of electrons relative to that of ions[18]. Furthermore, radial currents can be generated due to multiple different mechanisms[17, 18] which depend on the radial electric field itself, e.g., ion orbit losses, bulk viscosity (due to the inhomogeneity of the magnetic field), Reynolds stress, collisional processes (e.g., ripple diffusion, gyro viscosity), charge exchange, external current drive, etc., resulting in a function of the radial electric field with many terms. However, the cusp bifurcation of the radial electric field and the corresponding transi-

tion behavior in its neighborhood in parameter space can only occur around an inflection point of this function. Therefore, it is sufficient to Taylor expand this function of many terms around its inflection point, because the characteristic transition behavior described in Sec. 4.1 will occur right there. This leads to an effective description of the last term of the electric field evolution equation

$$G(Z) = a + bZ + Z^3. \quad (4-36)$$

This closed set of coupled partial differential equations [Eqs. (4-32a), (4-32b), and (4-35)] is evaluated on a spatial region which must be considerably larger than the size of the transport barrier to exclude boundary effects, but small enough that the core boundary stays away from the particle and heat sources in the core of the plasma. The outer edge of the plasma at the scrape-off layer (SOL) side is fixed at $r = 0$. The inner boundary of the considered spatial region is located at $r = -\infty$, this is allowed because compared to the size of the transport barrier the inner boundary is far enough away. Due to the absence of sources in the considered region, the total amount of particles and heat enters as a constant flux at this inner boundary

$$\begin{aligned} \Gamma(r = -\infty) &= \text{constant} = \Gamma_{-\infty}, \\ q(r = -\infty) &= \text{constant} = q_{-\infty}. \end{aligned} \quad (4-37)$$

At the other boundary of the system, i.e., the outer edge of the plasma, the temperature, and the density are forced to drop toward zero with a certain e-folding length into the scrape-off layer,

$$\frac{T'_e}{T_e} = \frac{-1}{\lambda_T} \quad \text{and} \quad \frac{n'_e}{n_e} = \frac{-1}{\lambda_n}, \quad (4-38)$$

with constant gradient lengths λ_T and λ_n , and where from now on the subscript "e" is used for SOL edge values and primes will denote total derivatives with respect to space. Due to the absence of sources, the continuity equations can be integrated such that the steady state particle- and heat- fluxes are constant over the entire spatial domain ($q' = 0$ and $\Gamma' = 0$, since we assume slab geometry) and can, therefore, be matched to the fluxes coming from the core,

$$\begin{aligned} 0 &= -\Gamma_{-\infty} - D(Z_0)n'_0, \\ 0 &= -q_{-\infty} - \chi(Z_0)n_0 T'_0 + \frac{T_0}{\gamma - 1}\Gamma_{-\infty}, \\ 0 &= -G(Z_0) + c_n \frac{T_0 n'_0}{n_0^2} + c_T \frac{T'_0}{n_0} + \mu Z''_0, \end{aligned} \quad (4-39)$$

where the steady state solutions are indicated with a subscript "0". Because it is not expected that the L-H transition behavior is initiated by some specific

difference between the transport coefficients, it is not necessary to keep track of them separately. So, without the loss of generality, it is allowed to make the following assumption on the transport coefficients:

$$\chi(Z) = \frac{D(Z)}{\zeta(\gamma - 1)}. \quad (4-40)$$

This assumption allows us to solve the steady state density and temperature profiles as a function of the particle diffusivity alone,

$$n'_0(r) = -\frac{\Gamma_{-\infty}}{D}, \quad (4-41a)$$

$$n_0(r) = n_{0e} - \Gamma_{-\infty} \int_0^r \frac{dr}{D}, \quad (4-41b)$$

$$T'_0(r) = \frac{\zeta D(Z_e)}{\lambda_n D} (T_{0e} - T_{-\infty}) \hat{n}^{-1-\zeta}, \quad (4-41c)$$

$$T_0(r) = T_{-\infty} + (T_{0e} - T_{-\infty}) \hat{n}^{-\zeta}, \quad (4-41d)$$

with

$$\begin{aligned} \hat{n} &\equiv \frac{n_0}{n_{0e}}, & n_{0e} &= \frac{\Gamma_{-\infty} \lambda_n}{D(Z_e)}, \\ T_{0e} &= \frac{T_{-\infty}}{1 + \frac{\lambda_n}{\zeta \lambda_T}}, & T_{-\infty} &= (\gamma - 1) \frac{q_{-\infty}}{\Gamma_{-\infty}}, \end{aligned} \quad (4-42)$$

where the functions of the radial electric field, like D and G , are always functions of the steady state profile, Z_0 , because deviations from steady state of those functions will always be written as a Taylor-expansion, e.g., $D(Z) \approx D(Z_0) + D_Z Z_1$. So, only the steady state profile of the radial electric field is needed, because the resulting diffusivity profile leads straightforwardly to the density and temperature profiles. Thus, consider the steady state equation for the radial electric field

$$\begin{aligned} 0 &= G - c_T \frac{T'_0}{n_0} - c_n \frac{T_0 n'_0}{n_0^2}, \\ &= G - \frac{T_{-\infty} n'_0}{n_0^2} (c_n + c_g \hat{n}^{-\zeta}), & c_g &\equiv \frac{\zeta c_T - c_n}{1 + \zeta \frac{\lambda_T}{\lambda_n}}, \end{aligned} \quad (4-43)$$

where the μ -term is neglected. This simplification is allowed by realizing that the radial electric field jumps from a L-mode value [positive root of Eq. (4-43)] at the core side to a H-mode value [negative root of Eq. (4-43)] inside the transport barrier. This instantaneous jump (for $\mu = 0$) is only smeared out due to this extra second derivative term (for $\mu \neq 0$) in a region of the order of $\mu \ll 1$. Thus, in the majority of the plasma, the value of the radial electric field is determined by the roots of Eq. (4-43) which are given by

$$-G(Z)D(Z) = \frac{T_{-\infty} D(Z_e)^2}{\Gamma_{-\infty} \lambda_n^2} (c_n \hat{n}^{-2} + c_g \hat{n}^{-\zeta-2}), \quad (4-44)$$

where the left-hand side (LHS) is a pure function of the radial electric field and the RHS is a pure function of the density, and the density is a smooth monotonic function of the radius starting from a constant n_{0e} at $r = 0$ and increasing to infinity at $r = -\infty$. Therefore the RHS of Eq. (4-44) (and therefore also the product $-GD$) is a smooth monotonic function of the radius too, growing from zero at the core boundary to a constant value at the edge given by

$$-G(Z_e)D(Z_e) = (c_n + c_g) \frac{(\gamma - 1)q_{-\infty}}{\Gamma_{-\infty}^2 \lambda_n^2} D(Z_e)^2. \quad (4-45)$$

This restriction of the edge radial electric field corresponds to the intersection of the tilted dashed line with the curved solid line plotted in Fig. 4.5.

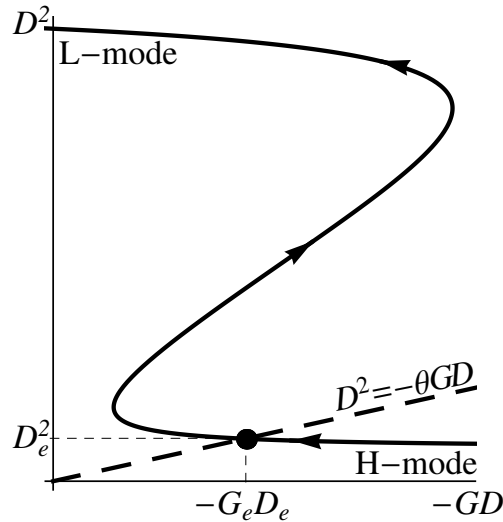


Figure 4.5: The steady state solution at the edge of the plasma, Z_e , is determined by the intersection of the solid curve (where the arrows indicate the monotonic increase of Z) with the tilted dashed line, as is dictated by Eq. (4-45).

From this figure, it can be clearly seen that the system can have high diffusivity (L-mode transport) or low diffusivity (H-mode transport) at the edge of the plasma depending on the slope of the tilted dashed line, θ ,

$$\theta = \frac{\Gamma_{-\infty}^2 \lambda_n^2}{q_{-\infty}(\gamma - 1)} \frac{1}{(c_n + c_g)}. \quad (4-46)$$

This parameter combines most of the control parameters which can move the system into and out of the H-mode. The intersection in Fig. 4.5 defined in Eq.

(4-45) determines the edge value of the radial electric field, Z_e . Combining this with the knowledge about the monotonic function of the radius $-GD$ gives the steady state profile for Z and, therefore, also for D such that we can use Eqs. (4-41b) and (4-41d) to produce the steady state profiles for the density and temperature of this system. As is already suspected from Fig. 4.5, there will be different types of solutions for different values of the parameter θ . To find the transition behavior and its threshold values, the bifurcation analysis of Sec. 4.2 is applied to this set of PDEs.

For the bifurcation analysis, it is necessary to Taylor expand the system to second order around the steady states which we just found. The linear operator becomes

$$M_1 = \frac{\partial \mathbf{f}}{\partial \mathbf{v}} = \begin{pmatrix} \nabla D \nabla & 0 & \nabla n'_0 D_Z \\ \nabla D T'_0 + \nabla D T_0 \nabla & \nabla D n'_0 + \nabla D n_0 \nabla & \nabla (n_0 T'_0 + n'_0 T_0) D_Z \\ -2c_n \frac{T_0 n'_0}{n_0^3} - c_T \frac{T'_0}{n_0^2} + \frac{c_T}{n_0^2} \nabla & c_n \frac{n'_0}{n_0^2} + \frac{c_T}{n_0} \nabla & -G_Z (+\mu \nabla^2) \end{pmatrix}, \quad (4-47)$$

with this it is possible to construct the eigenfunctions which satisfy $M_1 \mathbf{v}_1 = 0$ where $\mathbf{v}_1 = (v_n, v_T, v_Z)^T$ together with the co-eigenvector, $\mathbf{u}_1 = (u_n, u_T, u_Z)^T$, satisfying $\mathbf{u}_1^T M_1 = 0$ and therewith find the fold bifurcation of the system. Doing the whole analysis, it turns out that the existence condition for \mathbf{v}_1 and \mathbf{u}_1 reduces to a condition on the edge values. This reduction exists because the conservation laws for energy and density in steady state have a particle and heat flux which is constant over the whole radial domain, which are, therefore, equal to their boundary values. The perturbed system can also be integrated which leads to the integration constants, Γ_1 and q_1 ; however, if these would be nonzero, they would also add to the particle and heat flux at the edge, which is not allowed because these nonzero perturbations do not satisfy the boundary conditions. The perturbed system is, therefore, restricted to integration constants $\Gamma_1 = q_1 = 0$ such that the boundary values of the eigenfunctions, v_n , v_T , and v_Z , will restrict the eventual profile of the perturbation, similar to what was possible for the steady states. Eventually, it turns out that it is only possible to find the eigenfunctions with a vanishing eigenvalue if and only if

$$\frac{d}{dZ} \left(\frac{G}{D} \right) \Big|_e = 0. \quad (4-48)$$

This can indeed be recognized visually in the edge steady state condition for the radial electric field (plotted in Fig. 4.5), as is shown by the threshold values of θ in Fig. 4.6(a).

The cusp condition is defined as $\mathbf{u}_1^T (M_2 \mathbf{v}_1) \mathbf{v}_1 = 0$; the 3-tensor $M_2 = \partial M_1 / \partial \mathbf{v}_0$ can straightforwardly be found by differentiating the first order operator M_1 with respect to \mathbf{v} and then contracting it twice with the eigenvector

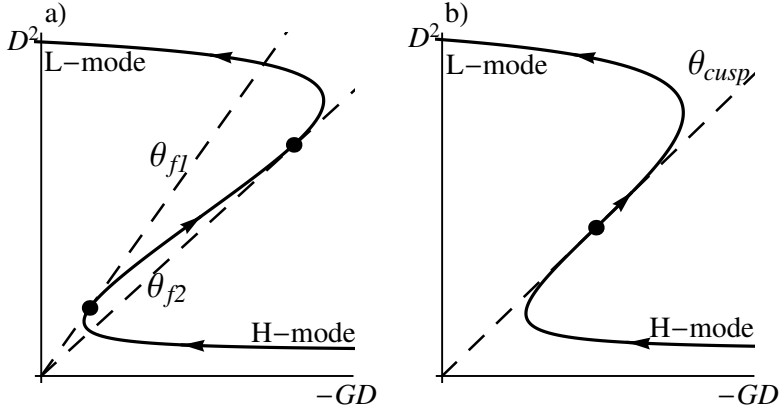


Figure 4.6: (a) The visual representation of the fold bifurcation, Eq. (4-48), giving the threshold values (θ_{f1} and θ_{f2}) of the control parameter. (b) The two fold bifurcations merge into a cusp bifurcation ($\theta_{f1} = \theta_{f2} = \theta_{cusp}$) by slight changes in the nonlinear function $G(Z)$ [e.g., the b -parameter of Eq. (4-36)] until the cusp condition is satisfied [see Eq. (4-49)].

v_1 after which the inner product must be taken with the co-eigenvector u_1 . This leads again to an expression of the radial electric field at the edge as is visualized in Fig. 4.6(b), at which the two fold bifurcations merge together,

$$\frac{d^2}{dZ^2} \left(\frac{G}{D} \right) \Big|_e = 0. \quad (4-49)$$

For the determination of the co-dimension 3 bifurcation, it is additionally necessary to find the Bogdanov-Takens bifurcation by checking for which parameters the following condition is satisfied:

$$\int_{-\infty}^0 (u_n v_n + u_T v_T + u_Z v_Z) dx = 0. \quad (4-50)$$

Combining the fold condition, the cusp condition, and the Bogdanov-Takens condition leads to the point in parameters space corresponding to the co-dimension 3 bifurcation

$$(a, b, \theta) = (0, 0, \infty). \quad (4-51)$$

Thus, it is now proven that this system contains all the transition dynamics which are related to this co-dimension 3 bifurcation, i.e., sharp, smooth and

oscillating transitions of the radial transport. It would also be very useful to be able to find the exact parameter space of where these different types of transitions may occur. For that it is necessary to find a separate condition for the Hopf bifurcations as was argued at the end of Sec. 4.2. Following the expression of Eq. (4-15), the generalized eigenvector \mathbf{v}_2 and generalized co-eigenvector \mathbf{u}_2 are needed. These can be found by solving Eq. (4-8). This system can be integrated leading to integration constants, Γ_2 and q_2 , which depend on the normal eigenfunctions v_n and v_T ,

$$\Gamma_2 = \int_{-\infty}^0 v_n dr, \quad (4-52a)$$

$$q_2 = \int_{-\infty}^0 \frac{T_0 v_n + n_0 v_T}{\gamma - 1} dr. \quad (4-52b)$$

For M_3 the linear operator M_1 needs to be perturbed in all its parameters leading to an enormous matrix which must be contracted multiple times with different eigenvectors to generate the right Hopf criterium. This is possible, however, the extensive algebra is omitted here and replaced by a less formal analysis of guessing when the steady state profiles will destabilize, eventually ending up with the same result. From the steady state restriction for the radial electric field of Eq. (4-44), it was already noted that the product of functions $-G(Z)D(Z)$ will always be a monotonic function of the radius. However, if the slope θ is decreased from L-mode values towards H-mode values, at a certain point just before reaching the fold bifurcation $-GD$ will change from increasing to decreasing at the edge. Because Z is a continuous function of the radius the profile of D^2 is found by following the solid curve along the direction of the arrows in Fig. 4.5. This means that for those values of θ also the function $-GD$ must first increase when going inwards before it will decrease again. However, this was not allowed because $-GD$ must be monotonous, which indicates that the steady state L-mode profile must turn unstable already before the fold bifurcation is reached at those points where

$$\left. \frac{d}{dZ} (GD) \right|_e = 0. \quad (4-53)$$

This indeed leads to the required Hopf bifurcation condition. The same reasoning can be applied for the back transition; both transitions are plotted in Fig. 4.7(a).

It can be noted from Fig. 4.7 that the eventual transition behavior does qualitatively change when the order changes in which the bifurcations are encountered when decreasing θ . For example, in Fig. 4.7(a) at θ_{H-L} , the H-mode becomes stable due to the Hopf bifurcation of that stationary state; so by the time θ_{L-H} is reached and the L-mode turns unstable, the system will

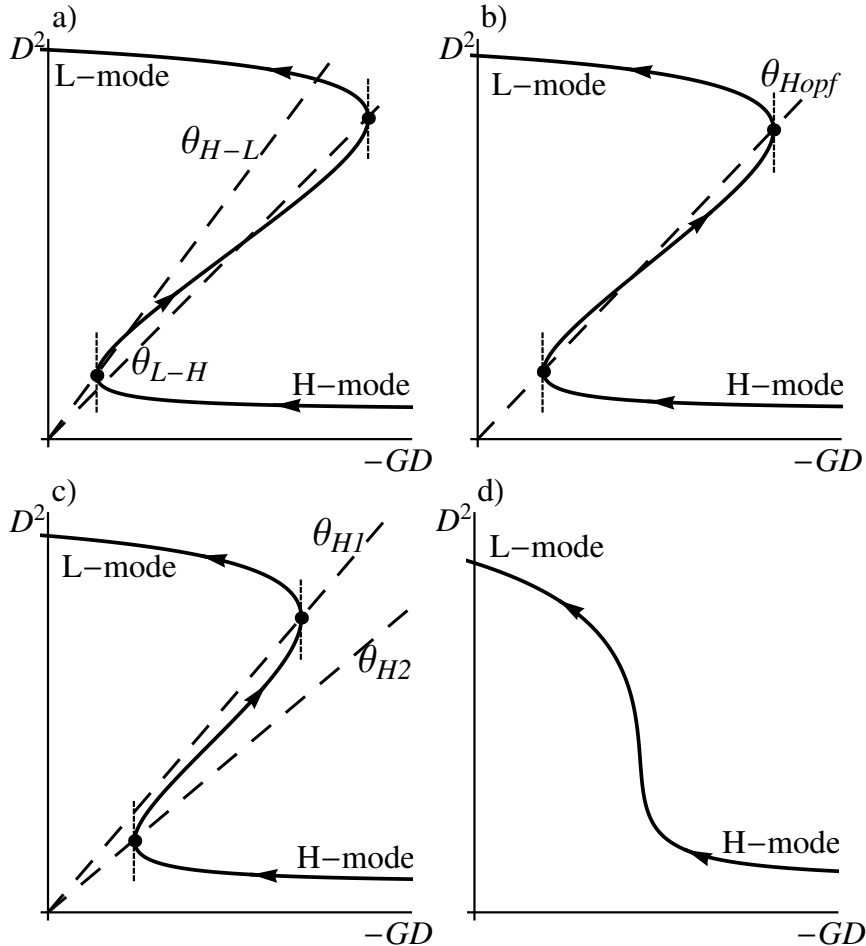


Figure 4.7: The Hopf bifurcations of the edge stationary states in four different cases.

rapidly transit to the stable H-mode. The opposite holds for the back transition, when increasing θ first, the L-mode becomes stable again, and when θ_{H-L} is reached, the system rapidly jumps towards the stable L-mode. Both transitions occur at different values of the control parameter θ leading to hysteresis behavior. If another type of parameter is changed the two Hopf bifurcations might change order, leading to Fig. 4.7(b) where there are still sharp transition only without the hysteresis. Until the Hopf bifurcations are ordered as in Fig. 4.7(c), where the L-mode already becomes unstable while

the H-mode is also unstable. At those points in parameter space where this holds, the edge stationary state cannot be on a stable fixed point but will be on a stable limit cycle solution of the system. So this will be the parameter regime of this model where the dithering solutions are situated. The same type of parameter can be changed even further such that both Hopf bifurcations merge and disappear such that there are only smooth transitions left as is indicated in Fig. 4.7(d). These four different types of transitions can be indicated in a complete parameter scan of this type of parameter (for this model for instance the b -parameter). As can be seen from Fig. 4.8, this parameter space is qualitatively similar to the parameter space of the FitzHugh-Nagumo model (see Fig. 4.3), which must be the case because they both have the same underlying bifurcation of co-dimension 3.

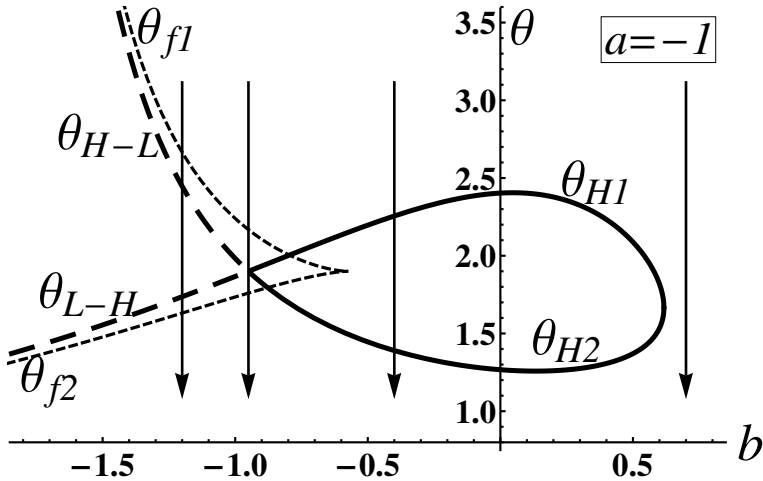


Figure 4.8: The control parameter space of the 1-D transport model, for fixed $a < 0$, describing L-H transitions by decreasing θ , e.g., the arrows corresponding to the edge steady states visualized in Fig. 4.7 [(a)-(d) is from left to right]. The short-dashed (cusp shaped) lines correspond to the two fold bifurcations which merge at the cusp bifurcation point (Fig. 4.6). The Hopf bifurcation curve consists of two parts; the dashed part corresponding to the sharp hysteresis like transitions and the solid curve surrounds the dither regime (Fig. 4.7).

4.5 Conclusion and discussion

In this paper, a general method has been introduced to find a certain bifurcation of co-dimension 3 in systems of both partial differential equations and ordinary differential equations. This is very useful to predict the complex nonlinear dynamical behavior of systems which describe spatial and temporal evolutions simultaneously. This can especially be exploited in systems which exhibit self generated transitions, such as the L-H transition in magnetically confined fusion plasmas. This co-dimension 3 bifurcation combines two different ways of controlling the existence and magnitude of the hysteresis in such systems. One is to merge the two separate fold bifurcations (which cause the separate L-H and H-L transitions), eventually leading to smooth transitions. The other way changes the two stable stationary states (L-mode and H-mode) into unstable stationary states leading to a stable limit cycle solution of the system, resulting in dithering-like transitions. Therefore, this bifurcation is particularly useful for L-H transition models, which must describe these observed transition phenomena. Thus, finding this bifurcation of co-dimension 3 in any dynamical system makes that system a candidate for a L-H transition model. The other way around if this bifurcation is not present in a model for the L-H transition, it is not capable of describing all transition phenomena.

Besides this global criterium for L-H transitions, additional threshold criteria for the L-H and H-L transitions follow directly from the bifurcation analysis in terms of all relevant parameters incorporated in the model. For the example of Zohm's model[8], this leads to the physical control parameters nicely combined in the single bifurcation parameter θ [defined in Eq. (4-46)]. So, as is expected, increasing the heating power will lead to increasing the heat flux coming from the core, $q_{-\infty}$, and with that it decreases θ towards its H-mode value. Remarkably, however, this model predicts that increasing the particle flux has the opposite effect of the heating power. This may be interpreted as just extra cooling of the plasma due to these extra particles. This is not observed probably because even in neutral beam heated plasmas, it is hard to increase the particle flux without heating the plasma, also the beneficial effect of extra momentum and flow due to these extra particles is not taken into account in this model. Furthermore, it is noted that many other parameters play a role in the L-H transition such as the edge gradient lengths determined by scrape-off layer physics. Additionally, the exact region of parameter space where dithering transitions are predicted is found due to the bifurcation analysis, as is plotted in Fig. 4.8.

The usefulness of this new method for future work, is that it is a tool which can be used to compare different L-H transition mechanisms with one another. This can be done in several ways, one is to do the bifurcation analysis on a completely different model and see which other parameters will lead to

the different transitions. The other is to incorporate new mechanisms into the transport model of Zohm and see how these influence the bifurcating behavior of the model. For instance, a more physics based description of the diffusivity and conductivity can be incorporated, if this mechanism would, for instance, pull the fold bifurcations further apart, then it will probably be a lot easier to go deep into H-mode. The size of the transport barrier and its parametric dependencies can also be determined, because this 1-D system also describes spatial transitions from the L-mode core to the H-mode edge in the region where multiple stationary states are allowed. Another possibility is to see how several mechanisms (as discussed in Sec. 4.4) influence the parameters of the function $G(Z)$. The entire system can also be extended to incorporate extra dynamical degrees of freedom, such as, for instance, the evolution of the turbulence level in combination with the zonal flows[19–21] and/or geodesic acoustic modes[22, 23].

Acknowledgements

This work, supported by the European Communities under the contract of Association between EURATOM/FOM, was carried out within the framework of the European Fusion Programme with financial support from NWO. The views and opinions expressed herein do not necessarily reflect those of the European Commission. This work is supported by NWO-RFBR Centre-of-Excellence on Fusion Physics and Technology (Grant nr. 047.018.002)

References

- [1] F. Wagner *et al.*, *Physical Review Letters* **49** (1982) 1408
- [2] F. Wagner, *Plasma Physics and Controlled Fusion* **49** (2007) B1
- [3] B. A. Carreras, P. H. Diamond, Y. M. Liangs, V. Lebedev and D. Newman, *Plasma Physics and Controlled Fusion* **36** (1994) A93, and references therein
- [4] T. Estrada, C. Hidalgo, T. Happel and P. H. Diamond, *Physical Review Letters* **107** (2011) 245004, and references therein
- [5] R. FitzHugh, *Biophysical Journal* **1** (1961) 445
- [6] J. Nagumo, *Proceedings of the Institute of Radio Engineers* **50** (1962) 2061
- [7] Y. A. Kuznetsov, *Elements of Applied Bifurcation Theory*, (Springer, New York 1998), 2nd ed.
- [8] H. Zohm, *Physical Review Letters* **72** (1994) 222
- [9] F. R. Gantmacher, *The theory of matrices*, vol. 1, (Chelsea Publishing Company, New York 1959)
- [10] K. H. Burrell, *Physics of Plasmas* **4** (1997) 1499
- [11] N. Chakrabarti and J. J. Rasmussen, *Physics of Plasmas* **6** (1999) 3047
- [12] P. H. Diamond, S.-I. Itoh, K. Itoh and T. S. Hahm, *Plasma Physics and Controlled Fusion* **47** (2005) R35
- [13] K. H. Burrell, *Physics of Plasmas* **6** (1999) 4418
- [14] G. S. Xu *et al.*, *Physical Review Letters* **107** (2011) 125001
- [15] S.-I. Itoh and K. Itoh, *Physical Review Letters* **60** (1988) 2276
- [16] S.-I. Itoh, K. Itoh, A. Fukuyama and Y. Miura, *Physical Review Letters* **67** (1991) 2485
- [17] K. Itoh, *Plasma Physics and Controlled Fusion* **36** (1994) A307
- [18] K. Itoh and S.-I. Itoh, *Plasma Physics and Controlled Fusion* **38** (1996) 1
- [19] D. del Castillo-Negrete, B. A. Carreras and V. E. Lynch, *Plasma Physics and Controlled Fusion* **46** (2004) A105

- [20] E. jin Kim and P. H. Diamond, *Physics of Plasmas* **10** (2003) 1698
- [21] M. A. Malkov and P. H. Diamond, *Physics of Plasmas* **16** (2009) 012504
- [22] G. D. Conway, C. Angioni, F. Ryter, P. Sauter and J. Vicente, *Physical Review Letters* **106** (2011) 065001
- [23] K. Miki and P. H. Diamond, *Physics of Plasmas* **17** (2010) 032309

Bifurcation theory of a one-dimensional transport model for the L-H transition

W. Weymiens, H.J. de Blank, and G.M.D. Hogeweij

FOM Institute DIFFER - Dutch Institute for Fundamental Energy Research,
Association EURATOM/FOM, Nieuwegein, the Netherlands

Abstract

Transitions between low and high-confinement (L-H transitions) in magnetically confined plasmas can appear as three qualitatively different types: sharp, smooth, and oscillatory. Bifurcation analysis unravels these possible transition types and how they are situated in parameter space. In this paper the bifurcation analysis is applied to a 1-dimensional model for the radial transport of energy and density near the edge of magnetically confined plasmas. This phenomenological L-H transition model describes the reduction of the turbulent transport by $E \times B$ -flow shear self-consistently with the evolution of the radial electric field. Therewith, the exact parameter space, including the threshold values of the control parameters, of the possible L-H transitions in the model is determined. Furthermore, a generalised equal area rule is derived to describe the evolution of the transport barrier in space and time self-consistently. Applying this newly developed rule to the model analysed in this paper reveals a naturally occurring transition to an extra wide transport barrier that may correspond to the improved confinement known as the very-high-confinement mode.

published in:
Physics of Plasmas **20**, 082306 (2013)

5.1 Introduction

In 1982 the ASDEX team discovered the so called "High confinement mode" or "H-mode"[1], in which the energy confinement of a magnetically confined fusion plasma becomes, typically, twice as good (compared to the standard "Low confinement mode" or "L-mode"). Although this very beneficial, L- to H-mode transition has been seen in most present day tokamaks, all physical mechanisms which are relevant to these transitions are still not fully identified[2].

Many different models have been introduced[3, 4] to explain the reduction of transport due to the L-H transition. Some models, based on sets of 0-dimensional dynamical equations, are well capable of qualitatively describing global temporal evolution behaviour around L-H transitions. However, they lack a description of the radial structure of the transport barrier. Since the improvements of diagnostic capabilities to observe highly spatially[2] and temporally[5, 6] resolved edge profiles, there is a growing need for L-H transition models capable of predicting such spatial and temporal observations together with their threshold parameters. These 1-dimensionally extended models exist (e.g., Refs. [7–9]). However, their analysis was restricted to simulations of different dynamical behaviors without the determination of their full parameter space and their corresponding threshold boundaries. Bifurcation analysis, however, will give the exact boundaries in parameter space between different states and the different types of transitions between them, and is therefore very useful in analysing L-H transition models.

The nonlinear dynamics observed during L-H transitions can be identified as certain fundamental bifurcations. These bifurcations nicely organise the parameter space in different regimes for the different types of transitions, such as the sharp L-H and H-L transitions exhibiting hysteresis, the smooth transitions, and the oscillating transitions (called dithering or I-phase). Reference [10] gives the bifurcation theory for 1-dimensionally extended models that allow the characterisation of these typical bifurcations in a basic model for the L-H transition based on partial differential equations (PDEs). In this paper an advanced phenomenological 1-dimensional transport model for the L-H transition is analysed on the basis of this extended bifurcation theory. The bifurcations of the steady state profiles are characterised together with their corresponding control parameters and threshold values, which illustrates the robustness of the bifurcation structure of these kinds of models under substantial modifications.

The considered model is based on the transport of particles and heat along the minor radius of a magnetically confined fusion plasma. The L-mode radial transport is assumed to be dominated by turbulence. The influence of flows on turbulence is widely viewed as a mechanism able to reduce radial transport. More specifically, it is expected that the $\mathbf{E} \times \mathbf{B}$ -flow, especially a shear in

the $\mathbf{E} \times \mathbf{B}$ -flow[11, 12], is capable of tearing apart turbulent eddies. So, to model this effect properly it is necessary to include the evolution of the radial electric field and the corresponding flow profile. The small scale behaviour of the tearing of turbulence, and the possible back reaction of turbulence generating zonal flows is not contained in this model. The effect of the large scale radial electric field gradient (mean flow shear) on the turbulence, is modeled by effective transport coefficients that directly depend on the radial electric field shear. This phenomenological description of transport reduction is used often in literature[13, 14], and has proven to be a useful simplification for H-mode modeling.

In general, nonlinear reaction diffusion systems can exhibit transition behavior. The spatial and temporal propagation of such transitions are analysed self-consistently, which leads to a generalised equal area rule. This newly developed rule could apply to all sorts of transition phenomena, such as flame front propagation or the propagation of signals in neurons. In this paper the generalised equal area rule is applied to the spatial and temporal evolution of the transport barrier[15, 16] as is described by the considered model. This analysis leads to the natural arising of two different types of barrier width scalings. Right after the L-H transition the barrier width is set by the viscosity of the plasma, corresponding to a width in the order of a few gyro-radii. If the heating power is raised sufficiently, the barrier can grow inward, the growing width being determined by the generalised equal area rule. This growth of a larger transport barrier may be a natural description of the occurrence of a very-high-confinement mode (VH-mode) as observed in DIII-D[17] and JET[18], and it could occur naturally in some reaction diffusion systems with a certain general structure, the so-called S-curve models[7, 13, 19].

This paper is organised as follows. First of all, the 1-dimensional L-H transition model is described in Sec. 5.2. In Sec. 5.3, the relevant bifurcations for the L-H transition are identified and compared to the original model introduced by Zohm[8]. In Sec. 5.5, a generalised equal area rule is introduced to describe the growth of the pedestal. In Sec. 5.5, this rule is applied to the considered model, and linked to the observation of VH-mode like states.

5.2 Transport model for the L-H transition

The degree of confinement is determined by the 1-dimensional transport in a tokamak along the minor radius of the torus, i.e., from the hot core of the toroidal plasma towards the colder edge. The radial transport of particles and heat is determined by the particle- and heat- fluxes, respectively, in the form of a continuity equation. We consider a layer near the edge of the plasma that is relatively thin compared to the plasma minor radius. We approximate this

layer, just for conciseness, with a slab geometry, such that these equations become

$$\frac{\partial n}{\partial t} = -\frac{\partial \Gamma}{\partial r}, \quad (5-1a)$$

$$\frac{\partial}{\partial t} \left(\frac{nT}{\gamma - 1} \right) = -\frac{\partial q}{\partial r}, \quad (5-1b)$$

where we assume equal temperatures of the ions and electrons, and the absence of particle and heat sources inside the layer. The particle and heat fluxes are given by

$$\Gamma = -D \frac{\partial n}{\partial r}, \quad (5-2a)$$

$$q = -\chi n \frac{\partial T}{\partial r} + \frac{\Gamma T}{\gamma - 1}. \quad (5-2b)$$

The particle flux, Γ , is governed by some effective particle diffusion due to the anomalous transport of electrons and ions. The heat flux, q , is a combination of some effective radial thermal conduction and heat advection due to the net mass-flow described by the particle flux, with γ the adiabatic index. A change from low confinement to high confinement can therefore be described by a change in the transport coefficients; particle diffusivity, D , and heat conductivity χ . In L-mode the transport is dominated by turbulence. A well known effect in turbulent fluid dynamics is the reduction of turbulence by the generation of sheared flows[2], these flows can be externally driven or generated from the turbulence itself via, e.g., Reynolds stress leading to zonal flows[20]. An analogous self organisation mechanism could be responsible for the formation of the self-sustained transport barrier in fusion plasmas[21]. The turbulence quenching sheared flows in a plasma are identified as the $\mathbf{E} \times \mathbf{B}$ -flows[22–24]. These flow shears are indeed observed as driven by Reynolds stress in the form of zonal flows[3, 25], and externally driven by probes generating a radial electric field[26], and by various other mechanisms. This quenching mechanism is frequently modelled[13, 14] as an effective diffusivity depending on the $\mathbf{E} \times \mathbf{B}$ -flow shear,

$$D = D_{min} + \frac{D_{max} - D_{min}}{1 + \tilde{\alpha}(V'_{\mathbf{E} \times \mathbf{B}})^2}, \quad (5-3)$$

where the prime denotes the radial derivative, and the square of the flow shear expresses the fact that both signs of the flow shear can suppress turbulence[27]. A similar expression is used for the thermal conductivity only with constants; χ_{min} and χ_{max} . Since the $\mathbf{E} \times \mathbf{B}$ -flow driven by a radial electric field can be approximated by, $V_{\mathbf{E} \times \mathbf{B}} \approx E_r/B$, the transport coefficients take

the form of

$$D = D_{min} + \frac{D_{max} - D_{min}}{1 + \alpha Z'^2}, \quad (5-4)$$

where Z is the normalised radial electric field,

$$Z = \frac{\rho_p e E_r}{T_i}, \quad \text{and} \quad \rho_p = \frac{mv_{th}}{qB_p}. \quad (5-5)$$

Furthermore, we do not expect the L-H transition to be initiated by some specific difference between the two transport coefficients. Such that we can make the following simplification: $\chi = D/\zeta(\gamma - 1)$, with ζ a proportionality factor, leading to the following transport equations:

$$\frac{\partial n}{\partial t} = \frac{\partial}{\partial r} \left(D \frac{\partial n}{\partial r} \right), \quad (5-6a)$$

$$\frac{\partial}{\partial t} (nT) = \frac{\partial}{\partial r} \left[D \left(\frac{n}{\zeta} \frac{\partial T}{\partial r} + T \frac{\partial n}{\partial r} \right) \right]. \quad (5-6b)$$

To model the evolution of the transport self-consistently it is necessary to include the evolution of the radial electric field explicitly[7, 8, 28]

$$\varepsilon \frac{\partial Z}{\partial t} = \mu \frac{\partial^2 Z}{\partial r^2} + c_n \frac{T}{n^2} \frac{\partial n}{\partial r} + \frac{c_T}{n} \frac{\partial T}{\partial r} - G(Z), \quad (5-6c)$$

where $\varepsilon = B_p^2/(B^2 \nu_i)$ is the dielectric constant of the polarised plasma. The radial currents are caused by the anomalous shear viscosity of the $\mathbf{E} \times \mathbf{B}$ -drift[29] (first term on the right-hand side (RHS) where $\mu \sim \rho_p^2$ is the ratio of viscosity to collision frequency). The second and third terms are due to the bipolar part of the anomalous cross field flux, i.e., the excess flux of electrons relative to that of ions[29]. Furthermore, additional radial current contributions may be generated due to a variety of mechanisms[13, 30] that depend on the radial electric field itself, e.g., ion orbit losses[31, 32], bulk viscosity[32, 33] (due to the inhomogeneity of the magnetic field), the anomalous cross field flux[28, 33], Reynolds stress, collisional processes (e.g., ripple diffusion, gyro viscosity), charge exchange[34, 35], external current drive, etc., resulting in a function of the radial electric field with many terms, $G(Z)$. However, general bifurcation theory implies that the dynamics corresponding to the L-H transition occurs in the neighborhood of the cusp bifurcation[10]. This cusp-bifurcation transition behaviour can only occur around an inflection point of this nonlinear function of the radial electric field. Therefore, to describe the transition behaviour it is sufficient to Taylor expand this function of many terms around its inflection point to be able to describe its L-H transition behavior. The Taylor expansion around an inflection point at $Z = Z_s$ is

$$G(Z) \approx a + b(Z - Z_s) + (Z - Z_s)^3. \quad (5-7)$$

This closed set of coupled PDEs (Eqs. (5-6a, b, c)) is evaluated on a spatial domain that must be considerably larger than the size of the transport barrier to exclude boundary effects, but small enough that the core boundary stays away from the particle and heat sources in the core of the plasma. The outer edge of the plasma at the scrape-off layer (SOL) side is fixed at $r = 0$. The inner boundary of the considered spatial domain is located at $r = -\infty$, this is allowed because compared to the size of the transport barrier the inner boundary is far enough away. At this inner boundary all the particles and heat enters the system (there are no additional sources within the domain). These influxes can be used as control parameters of the system

$$\begin{aligned}\Gamma(r = -\infty) &= \text{constant} = \Gamma_{-\infty} \\ q(r = -\infty) &= \text{constant} = q_{-\infty} \\ Z'(r = -\infty) &= 0.\end{aligned}\tag{5-8}$$

At the other boundary of the system, i.e., the outer edge of the plasma, the temperature, density, and radial electric field are forced to drop toward zero with a certain e-folding length into the scrape-off layer,

$$\frac{T'_e}{T_e} = \frac{-1}{\lambda_T}, \quad \frac{n'_e}{n_e} = \frac{-1}{\lambda_n}, \quad \frac{Z'_e}{Z_e} = \frac{-1}{\lambda_Z},\tag{5-9}$$

with constant gradient lengths λ_T , λ_n , and λ_Z of the same order of magnitude, and where from now on the subscript "e" is used for SOL edge values.

5.3 Bifurcation analysis

The closed set of three PDEs (Eqs. (5-6a)-(5-6c)) with the six boundary conditions (Eqs. (5-8) and (5-9)) is the complete L-H transition model considered in this paper. This model greatly resembles the model introduced by Zohm[8] to explain the dithering behaviour during L-H transitions, now often called the I-phase. The only difference between both models is the description of the effective diffusivity. In this paper the transport is reduced due to a shear in the $\mathbf{E} \times \mathbf{B}$ -flow (see Eq. (5-4)), in Zohm's model only the value of the radial electric field was taken into account (not its shear) in the following way:

$$D(Z) = \frac{D_{max} + D_{min}}{2} + \frac{D_{max} - D_{min}}{2} \tanh(Z).\tag{5-10}$$

The bifurcation analysis of Zohm's model was done in Ref. [10] and led to the following equation relating the steady state radial electric field profile to the

steady state density profile:

$$-G(Z)D(Z) = \frac{T_{-\infty} D(Z_e)^2}{\Gamma_{-\infty} \lambda_n^2} (c_n \hat{n}^{-2} + c_g \hat{n}^{-\zeta-2}), \quad (5-11)$$

where $\hat{n} = n_0/n_{0e}$, is the steady state density normalised to its edge value, $n_{0e} = \Gamma_{-\infty} \lambda_n / D(Z_e)$. $T_{-\infty} = (\gamma - 1)q_{-\infty}/\Gamma_{-\infty}$ is the core boundary value of the steady state temperature, and $c_g = (\zeta c_T - c_n) / (1 + \zeta \lambda_T / \lambda_n)$. The derivation of Eq. (5-11) did not rely on the fact the diffusivity explicitly depended on the value of the radial electric field and not its shear, therefore it is still valid when we plug in the diffusivity depending on the shear of the radial electric field. Nevertheless, the RHS of Eq. (5-11) only depends on the radius via the density profile, that is a monotonic increasing function of the radius (starting from n_{0e} at $r = 0$ and increasing to infinity at $r = -\infty$). Therefore, the profile of the product $-G(Z)D(Z')$ will be a smooth monotonic function of the radius too, growing from zero at the core boundary to a constant value at the edge given by

$$-G(Z_e)D(Z'_e) = (c_n + c_g) \frac{(\gamma - 1)q_{-\infty}}{\Gamma_{-\infty}^2 \lambda_n^2} D(Z'_e)^2. \quad (5-12)$$

Making use of the Robin boundary condition for the radial electric field, $Z'_e = -Z_e/\lambda_Z$, allows both sides of Eq. (5-12) to be parameterised by Z_e , as is shown in Fig. 5.1(a). The slope, θ , of the tilted dashed line is determined by a specific combination of the constant parameters of the system

$$\theta = \frac{\Gamma_{-\infty}^2 \lambda_n^2}{q_{-\infty}(\gamma - 1)} \frac{1}{c_n + c_g}. \quad (5-13)$$

This specific value will then determine at which point both sides of Eq. (5-12) are equal, i.e., both lines intersect, and therewith the value of the transport coefficients at the edge of the plasma. Obviously, high values of θ will correspond to L-mode transport and lower values of θ will correspond to H-mode transport. The L-H transition can thus be obtained by increasing, e.g., the heat flux coming from the core, $q_{-\infty}$, which is consistent with experiments. Additionally, other parameters can be used in this model to generate L-H transitions.

In Fig. 5.1(b) the possible edge states of the radial electric field for Zohm's model are reproduced from Ref. [10]. The structure of the solutions of both models is qualitatively the same, and therefore the same arguments can be applied to find the bifurcations of this new model. A set of two fold bifurcations are recognised at the values of θ bounding the region with three intersections (i.e., co-existence of L-mode and H-mode solutions). These two different fold bifurcations make sure there is hysteresis between the L-H transition and the H-L transition. The Hopf bifurcations change the stability of these

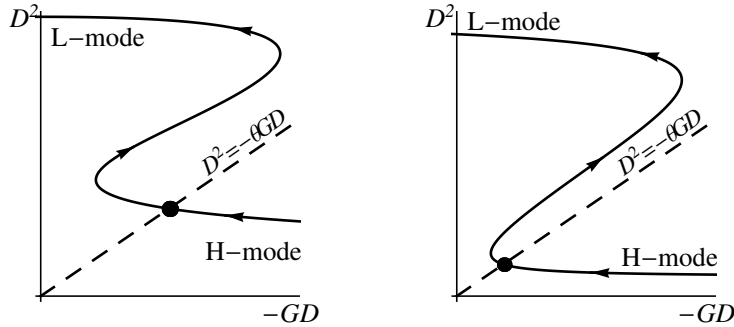


Figure 5.1: The steady state solution at the edge of the plasma, Z_e , is determined by the intersection of the solid curve (parameterised by increasing Z_e along the arrows) with the tilted dashed line, as is dictated by Eq. (5-12). (a) $E \times B$ -flow shear model of this paper, (b) Zohm's model for comparison[10].

stationary solutions. Right before the L-mode or H-mode solution disappears (at the fold bifurcation), it already becomes unstable (at the Hopf bifurcation, where the slope of the curved solid line is vertical). Thus, eventually the L-H transition will occur at the Hopf-bifurcation threshold for θ . However, if the H-mode is not yet stable (i.e., it did not have its Hopf-bifurcation yet) the system will not have a stable steady state solution and will start to oscillate.

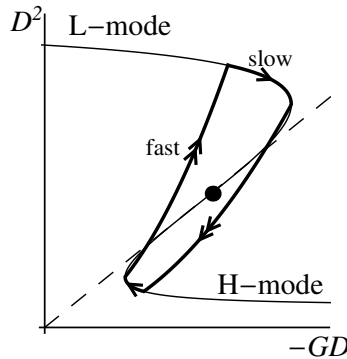


Figure 5.2: For this value of θ the intersection occurs in the regime without stable stationary states at the edge of the plasma. Without those the system will oscillate according to a stable limit cycle, as is created by the Hopf bifurcation.

This stable limit cycle, shown in Fig. 5.2, consists of a fast transition where the radial electric field changes on a timescale of $\mathcal{O}(\varepsilon)$. The system then tries to relax towards an H-mode profile on a diffusive timescale. However, it thus reaches the other Hopf bifurcation, where the radial electric field suddenly jumps back towards L-mode values, and subsequently the profiles adapt to these values on a diffusive timescale. Thus the whole period of the limit cycle consists of two diffusive parts and two fast jumps. The bifurcation boundaries in parameter space determine the exact thresholds between the different types of dynamics. In Fig. 5.3, the parameter space of both the $\mathbf{E} \times \mathbf{B}$ -flow shear model and Zohm's model is plotted, with the same values of the parameters. By comparing both parameter spaces of Fig. 5.3, one can immediately notice the different sizes of the limit cycle regions. So, in Zohm's model that describes only a flow (not the shear) the oscillations during an oscillatory L-H transition will last a lot longer than in the flow-shear model, when the heating power is ramped-up at the same rate. Beside this, the onset of the oscillatory behaviour in Fig. 5.3(b) is at values of the heating power at which the flow shear model would have past the oscillatory behaviour and went into H-mode already. Additionally, one can see that the values for θ_{L-H} are generally higher (i.e., lower heating power threshold) for the flow-shear model, consistent with the belief that sheared flow is more efficient in reducing turbulence than a flow without shear.

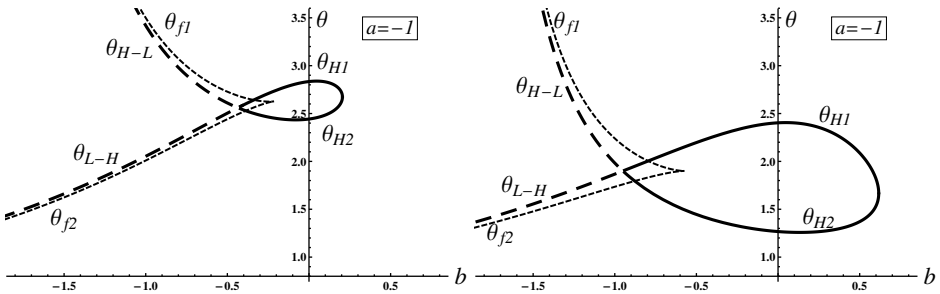


Figure 5.3: The (b, θ) -parameter space for fixed $a < 0$ of (a) $\mathbf{E} \times \mathbf{B}$ -flow shear model of this paper, and (b) Zohm's model[10]. The cusp-shaped short-dashed lines indicate the fold bifurcations (θ_{f1} and θ_{f2}). The Hopf bifurcations consist of two parts, the dashed lines (θ_{L-H} and θ_{H-L}) lead to the sharp L-H and H-L transitions. At θ_{H1} and θ_{H2} the Hopf bifurcations are in reversed order, such that in the region surrounded by the solid curve only limit cycle solutions are possible.

5.4 The transport barrier: space and time consistently

In this model the radial electric field is the main bifurcating variable of the model, that is similar to a three-component reaction diffusion system of the FitzHugh-Nagumo type. In general, these reaction diffusion systems have multiple stationary states and sharp transitions between them. These transitions can occur in time and space. The temporal transitions are regulated by a first order derivative, and the spatial transitions are regulated by a second order derivative,

$$-\varepsilon \frac{\partial X}{\partial t} + \mu \frac{\partial^2 X}{\partial r^2} = F(X) - c(r, t), \quad (5-14)$$

where $F(X)$ is a nonlinear function, such that the RHS can have up to three roots (X_- , X_0 , and X_+) depending on the value of the control parameter $c(r, t)$ that can be any continuous function of space and time. This form is generally valid for reaction diffusion systems of the FitzHugh-Nagumo type, however, in the following derivation the transitions between the roots are discussed in terms of the L-H transition to make the understanding of the applicability easier. Temporal transitions between the roots correspond to the sudden jumps from L-mode to H-mode and back, and the spatial transition occur when the core of the plasma exhibits L-mode like transport and the edge region exhibits H-mode like transport.

The limit of purely temporal transitions, and the limit of purely spatial transitions are well-known. In the limit of $\mu \rightarrow 0$ there is only a first order derivative of time, leading to a maximal hysteresis rule[16] for the temporal transition at threshold values of the control parameter c , at c_{L-H} and c_{H-L} , see Figs. 5.4(a) and 5.4(b). The other well known limit is $\varepsilon \rightarrow 0$, this limit describes with a second derivative in space how a high transport core can be connected to a low transport edge solution. In this time independent case the equation can be integrated over space once to give

$$\frac{dX}{dr} = \sqrt{\frac{2}{\mu} \int_{X_-}^X (F(X) - c) dX}, \quad (5-15)$$

which must vanish at X_+ , leading to the Maxwell's equal area (MEA) rule[13, 16],

$$\int_{X_-}^{X_+} (F(X) - c_{MEA}) dX = 0, \quad (5-16)$$

where c_{MEA} is defined to be that value such that the integral vanishes, as is shown in Fig. 5.4(c), note that X_- and X_+ depend on the value of the control parameter too. For the consideration of the entire system consistently we

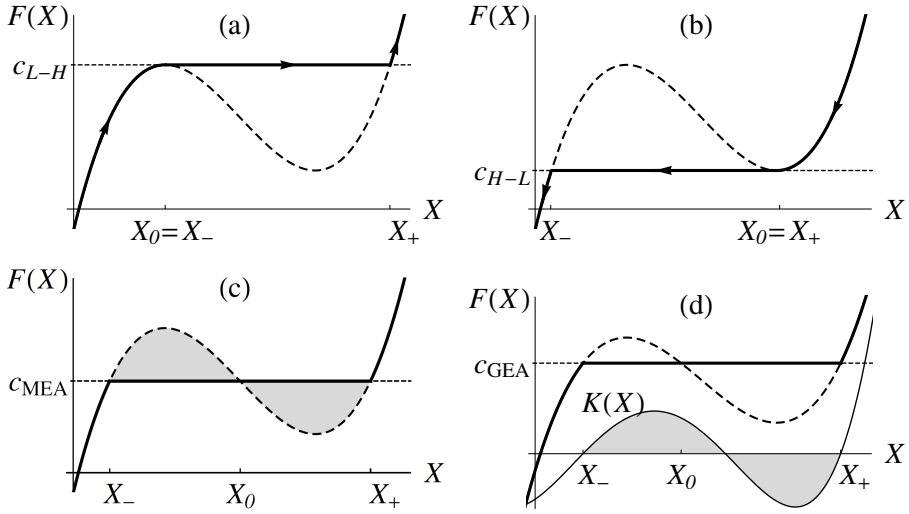


Figure 5.4: (a) Maximal Hysteresis ($\mu \rightarrow 0$): L-H transition. (b) Maximal hysteresis ($\mu \rightarrow 0$): H-L transition. (c) Maxwell's equal area rule ($\varepsilon \rightarrow 0$). (d) Generalised equal area rule ($\mu \ll 1, \varepsilon \ll 1$), where the relation between $K(X)$ and $F(X)$ is given in Eq. (5-18).

assumed that the jumps in time and in space are rapid (ε and μ are small), such that the transitions happen in an almost 1-dimensional zone in (r, t) -space, where the tangent to the zone is given by $dr/dt = -v$. This helps to treat both derivatives on the same footing: $d/dt \rightarrow v d/dr$, leading to the solution

$$\frac{dX}{dr} = \sqrt{\frac{2}{\mu} \int_{X_-}^X K(X) dX}, \quad (5-17)$$

where the new function $K(X)$ must satisfy:

$$K(X) - \varepsilon v \sqrt{\frac{2}{\mu} \int_{X_-}^X K(X) dX} = F(X) - c_{GEA}, \quad (5-18)$$

where c_{GEA} is defined such that the following integral vanishes,

$$\int_{X_-}^{X_+} K(X) dX = 0. \quad (5-19)$$

This is the generalised equal area (GEA) rule for the combined spatiotemporal transition from X_- to X_+ , that is visualised in Fig. 5.4(d). Note that $K(X_-) = K(X_+) = 0$ but $K(X_0) \neq 0$ differs from $F(X_0) = c_{GEA}$ by the square root of

its integral. The GEA rule determines the position in space and time of the transition between L-mode transport and H-mode transport corresponding to the temporal growth of the barrier region. In Fig. 5.5 the area in space and time which will exhibit H-mode behaviour, i.e., the edge transport barrier, is given as function of the control parameter $c(r, t)$. The black line surrounding the H-mode region is given by $c = c_{GEA}$ which depends on the local slope v . This nondecreasing function, $c_{GEA}(v)$, has special values $c_{GEA}(-\infty) = c_{H-L}$, $c_{GEA}(0) = c_{MEA}$, and $c_{GEA}(\infty) = c_{L-H}$.

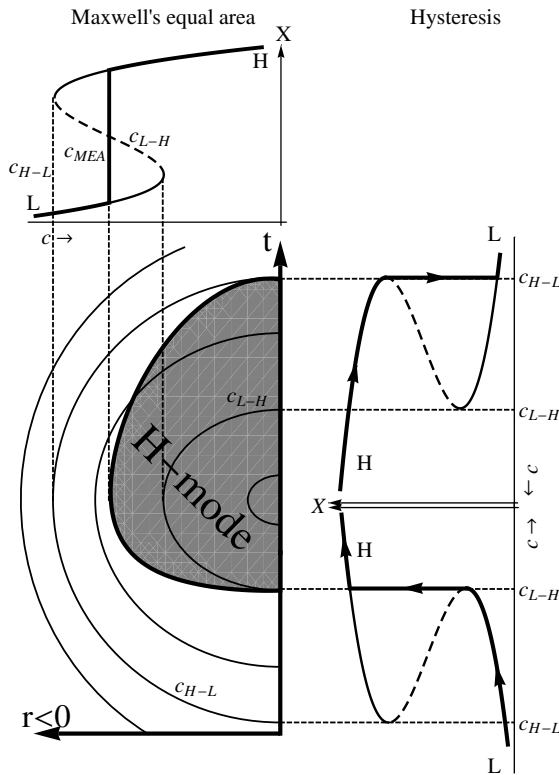


Figure 5.5: A contour plot of the control parameter $c(r, t)$ in space and time, in which the special contours $c = c_{L-H}$ and $c = c_{H-L}$ are indicated. The asymmetric thick contour corresponds to the generalised equal area rule, $c = c_{GEA}$ (Eq. (5-18)), bounding the region in (r, t) that exhibits H-mode transport. c_{GEA} depends on the local slope $v = -dr/dt$ and has special values: $c_{GEA}(v = \infty) = c_{L-H}$, $c_{GEA}(v = 0) = c_{MEA}$, and $c_{GEA}(v = -\infty) = c_{H-L}$.

5.5 Two different regimes in transport barrier sizes

In this section we apply the GEA rule to Zohm's model, because it is possible analytically, and it leads to specific diffusivity profiles as plotted in Figs. 5.6(b)-5.6(f), which may help the understanding. With the use of Eq. (5-11), we can rewrite the evolution equation of the radial electric field, Eq. (5-6c), in almost the same form as Eq. (5-14)

$$-\varepsilon \frac{\partial Z}{\partial t} + \mu \frac{\partial^2 Z}{\partial r^2} = G(Z) + \frac{f(\hat{n})}{D(Z)}, \quad (5-20)$$

where $f(\hat{n})$ is a pure function of the normalised steady state density, but more importantly is always independent of Z . The RHS of this equation is just slightly different than the RHS of Eq. (5-14), which makes it possible that this system can have two different regimes of transport barrier sizes as will become clear in this section. The MEA rule would dictate a transition from Z_- to Z_+ for such a value of $f(\hat{n})$ that the following integral vanishes:

$$\int_{Z_-}^{Z_+} G(Z) + \frac{f_{MEA}}{D(Z)} dZ = 0, \quad (5-21)$$

where Z_- and Z_+ are roots of the RHS of Eq. (5-20) with $f(\hat{n}) = f_{MEA}$ such that

$$-G(Z_-)D(Z_-) = -G(Z_+)D(Z_+) = f_{MEA}. \quad (5-22)$$

However, the GEA rule dictates a slightly different value of $f(\hat{n})$, namely, such a value that the solution of

$$K(Z) - \varepsilon v \sqrt{\frac{2}{\mu} \int_{Z_-}^Z K(Z) dZ} = G(Z) + \frac{f_{GEA}}{D(Z)}, \quad (5-23)$$

for $K(Z)$, has a vanishing integral

$$\int_{Z_-}^{Z_+} K(Z) dZ = 0, \quad (5-24)$$

where Z_- and Z_+ are roots of the RHS of Eq. (5-20) with $f(\hat{n}) = f_{GEA}$. This leads to a slightly different transition criterium,

$$-G(Z_-)D(Z_-) = -G(Z_+)D(Z_+) = f_{GEA}. \quad (5-25)$$

Thus, if Z_e passes a certain threshold value the GEA rule predicts that the transition moves inwards into the plasma starting out from the edge. It may

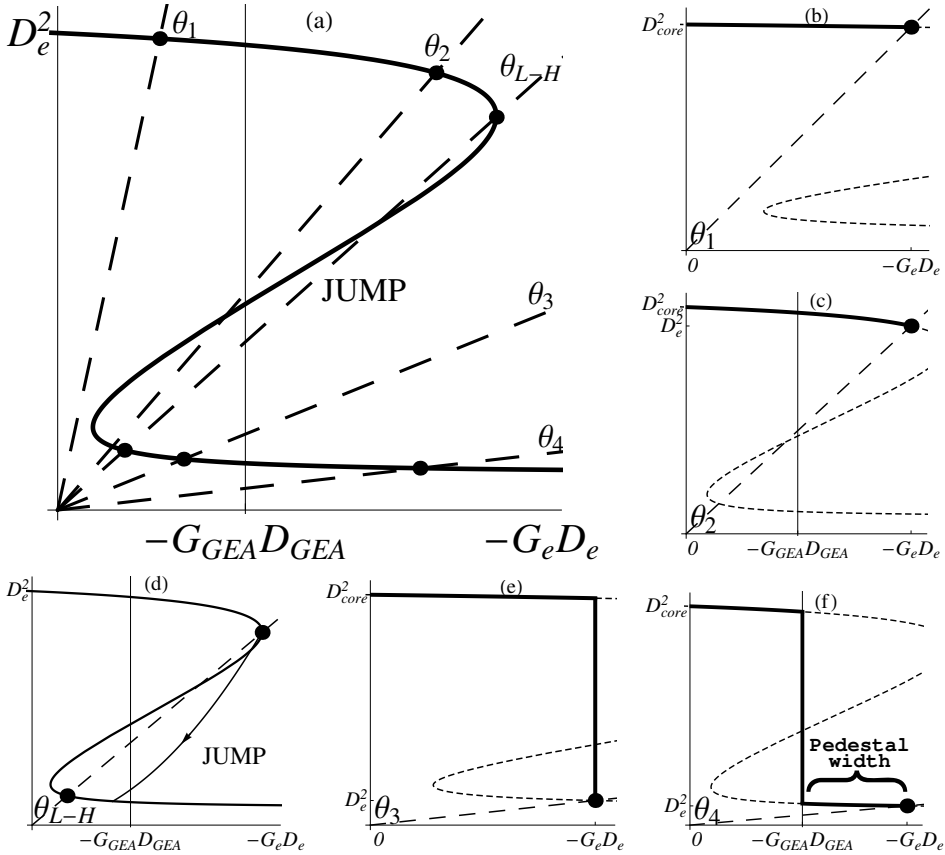


Figure 5.6: (a) The edge steady state solutions of Zohm's model for different values of the control parameter, θ . The profiles corresponding to these edge solutions are indicated in the surrounding graphs together with the jump trajectory during the L-H transition. The profiles are drawn from $r = -\infty$ (i.e., $-GD = 0$) with diffusivity D_{core} to the edge at $r = 0$ (i.e., $-GD = -G_e D_e$) with diffusivity D_e . (b) $\theta = \theta_1$, L-mode: The profile of the diffusivity squared which is almost constant over the entire spatial region. (c) $\theta = \theta_2$, L-mode: Approaching the L-H transition D_e will slightly drop. (d) $\theta = \theta_{L-H}$, The L-H transition: At the threshold value the Hopf bifurcation makes the L-mode unstable and the system jumps to the stable H-mode branch following the indicated trajectory; $G = \text{constant}$. (e) $\theta = \theta_3$, "thin-barrier H-mode:" The edge state did not yet exceed the GEA-threshold, Eq. (5-25). The barrier width is set by the viscosity, i.e., of the order of an ion gyro-radius. (f) $\theta = \theta_4$, "thick-barrier H-mode:" profile with an enlarged pedestal, whose width is set by the GEA rule.

occur that when this requirement is not yet fulfilled the intersection in Fig. 5.1 is already on the low diffusivity side, indicating that the edge state of the plasma has H-mode transport. This would lead to a profile of the radial electric field having an L-mode value in the entire spatial domain all the way up to the edge, where it jumps to an H-mode value only at this edge boundary. However, for finite viscosity, $\mu \neq 0$, this region is not infinitely thin, but of the order of the viscosity. Only when θ is decreased even further until the edge value of the radial electric field is such that the GEA requirement is fulfilled, then the transition starts to move inward towards a much wider transport barrier, as is shown in Fig. 5.5. In Fig. 5.6, an example is shown of such a transition, where the system has to go through a regime of a thin transport barrier set by the viscosity before the transport barrier can grow inwards according to the GEA rule. In panel (a) the decrease of the control parameter simulating an L-H transition is indicated with the sequence $\theta_1 \rightarrow \theta_2 \rightarrow \theta_3 \rightarrow \theta_4$. The corresponding steady state profiles of the diffusivity squared are shown in the surrounding panels, where the intersections (indicated with the black dots) determine the value of $-GD$ at the edge. In panels *b* and *c* the system is still in L-mode. When the threshold $\theta = \theta_{L-H}$ is met the Hopf bifurcation will make the L-mode solution unstable and the system will jump towards the only stable stationary state that is left. This very fast transition (of the order of ε) occurs along the lines of constant $G(Z)$ as is indicated by the arrow in panel (d). This is because on this very fast timescales the edge temperature and density cannot adapt, such that $G(Z)$ is not allowed to change too. However, the end point of the jump does not necessarily coincide with the edge stationary state dictated by the slope θ . Therefore, the system will evolve on a transport timescale until the new stationary state is reached. This new stationary state has an H-mode value at the edge, although the GEA condition, Eq. (5-25), is not yet fulfilled. The corresponding profile in this *thin-barrier H-mode* regime is plotted in panel (e). Only when θ is decreased so far that the intersection has crossed the GEA condition, then the transition moves into the plasma to build a *thick-barrier H-mode* as is shown in panel (f). So there are two different regimes of barrier thickness, the thick barrier has a width increasing with the input power, while the thin barrier has a constant width as function of the heating power. In the limit of small μ , we can assume that Z increases linearly from Z_- towards Z_+ , with $dZ/dr \propto (Z_+ - Z_-)/\sqrt{\mu}$. If we define the end of the barrier to be the point where the diffusivity is closer to L-mode values than to H-mode values ($Z = 0$ in the case of Zohm's model), then it leads to a barrier width proportional to $\sqrt{\mu} \frac{-Z_-}{(Z_+ - Z_-)}$.

5.6 Conclusion and discussion

Bifurcation analysis is a powerful tool to compare the qualitative transition behaviour of proposed L-H transition models. The model analysed in this paper is based on the reduction of transport due to $\mathbf{E} \times \mathbf{B}$ -flow shear combined with the transport equations for heat and particles, and the evolution of the radial electric field. The bifurcations found in this system of PDEs showed the organisation in parameter space of the three types of L-H transitions that are observed in magnetically confined fusion plasmas. Mostly observed in experiments is the sharp transition exhibiting hysteresis between the forward L-H transition and the backward H-L transition. Furthermore, there is the smooth transition from L-mode to H-mode and back. Additionally, a region in parameter space is identified with oscillatory transitions, like the dithering or I-phase. Since the qualitative bifurcation structure is the same as the one of Zohm's original model[8], it illustrates that this bifurcation structure is robust under substantial modifications. It would be interesting to further investigate how the bifurcation structure will or will not change with additional physics. The evolution of the turbulence itself and its interaction with zonal flows, like the 0-D variant introduced in Ref. [36], would be a relevant extension. Recently, a paper was published [37] which proposes such a combination of the 1-D transport equations with the evolution of the turbulence and zonal flows, and is probably suitable for investigation with our bifurcation analysis.

Furthermore, the full analysis of the spatial and temporal evolution of the transport barrier self consistently revealed a natural description of another type of transition. After the L-H transition a *thin-barrier H-mode* is created having a width of the order of the viscosity (approximately several gyro-radii). Thereafter, if the heating power is increased further, another threshold may be met, namely, GEA condition, Eq. (5-25). This GEA rule than describes the growth of an extra wide pedestal, the *thick-barrier H-mode*. This enlarged pedestal regime might be the mechanism responsible for the VH-mode observed in DIII-D[17] and JET[18]. This mechanism described in this paper is quite generally valid for bifurcating transport models (related to so-called S-curve models); however, a tokamak plasma might already reach some other limits (e.g., density limit, edge localized modes (ELMs) and disruptions) before the required heating power is reached. Since these effects are not incorporated in this model, we do not claim to have found a direct way to reach a VH-mode state.

Acknowledgements

This work, supported by the European Communities under the contract of Association between EURATOM/FOM, was carried out within the framework of the European Fusion Programme with financial support from NWO. The views and opinions expressed herein do not necessarily reflect those of the European Commission. This work is supported by NWO-RFBR Centre-of-Excellence on Fusion Physics and Technology (Grant nr. 047.018.002)

References

- [1] F. Wagner *et al.*, *Physical Review Letters* **49** (1982) 1408
- [2] F. Wagner, *Plasma Physics and Controlled Fusion* **49** (2007) B1
- [3] P. H. Diamond, A. Hasegawa and K. Mima, *Plasma Physics and Controlled Fusion* **53** (2011) 124001
- [4] P. W. Terry, *Reviews of Modern Physics* **72** (2000) 109
- [5] G. D. Conway, C. Angioni, F. Ryter, P. Sauter and J. Vicente, *Physical Review Letters* **106** (2011) 065001
- [6] T. Estrada, C. Hidalgo, T. Happel and P. H. Diamond, *Physical Review Letters* **107** (2011) 245004
- [7] S.-I. Itoh, K. Itoh, A. Fukuyama and Y. Miura, *Physical Review Letters* **67** (1991) 2485
- [8] H. Zohm, *Physical Review Letters* **72** (1994) 222
- [9] D. del Castillo-Negrete, B. A. Carreras and V. E. Lynch, *Plasma Physics and Controlled Fusion* **46** (2004) A105
- [10] W. Weymiens, H. J. de Blank, G. M. D. Hogeweij and J. C. de Valen  a, *Physics of Plasmas* **19** (2012) 072309
- [11] L. Schmitz *et al.*, *Physical Review Letters* **108** (2012) 155002
- [12] K. H. Burrell, *Physics of Plasmas* **4** (1997) 1499
- [13] J. W. Connor and H. R. Wilson, *Plasma Physics and Controlled Fusion* **42** (2000) R1
- [14] T. S. Hahm, *Plasma Physics and Controlled Fusion* **44** (2002) A87
- [15] P. H. Diamond, V. B. Lebedev, D. E. Newman and B. A. Carreras, *Physics of Plasmas* **2** (1995) 3685
- [16] V. B. Lebedev and P. H. Diamond, *Physics of Plasmas* **4** (1997) 1087
- [17] G. L. Jackson *et al.*, *Physical Review Letters* **67** (1991) 3098
- [18] C. M. Greenfield *et al.*, *Plasma Physics and Controlled Fusion* **35** (1993) B263
- [19] M. A. Malkov and P. H. Diamond, *Physics of Plasmas* **15** (2008) 122301

- [20] P. Shukla and L. Stenflo, *Physics Letters A* **307** (2003) 154
- [21] P. S. Marcus, T. Kundu and C. Lee, *Physics of Plasmas* **7** (2000) 1630
- [22] K. H. Burrell *et al.*, *Physics of Plasmas* **1** (1994) 1536
- [23] K. H. Burrell, *Physics of Plasmas* **6** (1999) 4418
- [24] H. Punzmann and M. G. Shats, *Physical Review Letters* **93** (2004) 125003
- [25] A. Fujisawa, *Nuclear Fusion* **49** (2009) 013001
- [26] R. J. Taylor *et al.*, *Physical Review Letters* **63** (1989) 2365
- [27] H. Biglari, P. H. Diamond and P. W. Terry, *Physics of Fluids B* **2** (1990) 1
- [28] S.-I. Itoh and K. Itoh, *Physical Review Letters* **60** (1988) 2276
- [29] K. Itoh and S.-I. Itoh, *Plasma Physics and Controlled Fusion* **38** (1996) 1
- [30] K. Itoh, *Plasma Physics and Controlled Fusion* **36** (1994) A307
- [31] F. Hinton and M. Chu, *Nuclear Fusion* **25** (1985) 345
- [32] K. C. Shaing and E. C. Crume, *Physical Review Letters* **63** (1989) 2369
- [33] A. B. Hassam, T. M. Antonsen, J. F. Drake and C. S. Liu, *Physical Review Letters* **66** (1991) 309
- [34] K. Itoh and S. I. Itoh, *Plasma Physics and Controlled Fusion* **37** (1995) 491
- [35] D. A. D'Ippolito and J. R. Myra, *Physics of Plasmas* **9** (2002) 853
- [36] E.-j. Kim and P. H. Diamond, *Physical Review Letters* **90** (2003) 185006
- [37] K. Miki, P. H. Diamond, Ö. D. Gürcan, G. R. Tynan, T. Estrada, L. Schmitz and G. S. Xu, *Physics of Plasmas* **19** (2012) 092306

6

Comparison of bifurcation dynamics of turbulent transport models for the L-H transition

W. Weymiens¹, S. Paquay², H.J. de Blank¹, and G.M.D. Hogeweij¹

¹ FOM Institute DIFFER - Dutch Institute for Fundamental Energy Research,
Association EURATOM/FOM, Nieuwegein, the Netherlands

² Eindhoven University of Technology, Department of Applied Physics,
PO Box 503, Eindhoven, The Netherlands

Abstract

In more than three decades a large amount of models and mechanisms have been proposed to describe a very beneficial feature of magnetically confined fusion plasmas: the L-H transition. Bifurcation theory can be used to compare these different models based on their dynamical transition structure. In this paper we employ bifurcation theory to distinguish two fundamentally different descriptions of the interaction between turbulence levels and sheared flows. The analytic bifurcation analysis characterises the parameter space structure of the transition dynamics. Herewith, in these models three dynamically different types of transitions are characterised, sharp transitions, oscillatory transitions and smooth transitions. One of the two models has a very robust transition structure and is therefore more likely to be more accurate for such a robust phenomenon as the L-H transition. The other model needs more fine-tuning to get non-oscillatory transitions. These conclusions from the analytic bifurcation analysis are confirmed by dedicated numerical simulations, with the newly developed code Bifurcator.

accepted by:
Physics of Plasmas

6.1 Introduction

In 1982 the ASDEX team discovered the so-called ‘High confinement mode’ or H-mode[1], in which the energy confinement of a magnetically confined fusion plasma becomes, typically, twice as good (compared to the standard ‘Low confinement mode’ or L-mode). This very beneficial, L- to H-mode transition has been seen in most present day tokamaks suggesting that the responsible mechanism is very robust. In the last three decades the variety of proposed L-H transition models has grown extensively. However, there is no consensus on the exact mechanism, or combination of mechanisms, responsible for this L-H transition[2].

Moreover, the type of dynamics during the transition is very characteristic. Therefore, the transition dynamics and the robustness of all proposed L-H transition models should be investigated. Bifurcation analysis[3] is a useful tool to check the possible transition dynamics within the model. Moreover, it characterizes the parameter space of these possible transition types, and therewith the sensitivity of the model to parameter changes, i.e., its robustness.

Although there may be different mechanisms determining the growth rate and the saturation mechanism of the turbulence, irrespective of the type of turbulence we restrict our description to the evolution of a radial profile of the turbulent fluctuation level, assuming some average over the fluctuations, consisting of a linear term describing the growth of the turbulence and a non-linear term describing the saturation mechanism, similar to Refs. [4–7]. I.e., the turbulence evolution can be described by a differential equation describing the magnitude of the turbulence level, containing two generic terms, one for linear growth rate and one for the non-linear saturation mechanism.

Presently, there is consensus about the influence of sheared $\mathbf{E} \times \mathbf{B}$ -flows on turbulence[8]. Microscale simulations show that sheared $\mathbf{E} \times \mathbf{B}$ -flows can tear apart the radial extent of turbulent eddies[9]. The $\mathbf{E} \times \mathbf{B}$ -flow shear reduction mechanism can then act either on the linear or the nonlinear term of the turbulence evolution equation. These two fundamentally different ways to model the interaction between sheared $\mathbf{E} \times \mathbf{B}$ -flows and turbulence are investigated in this paper with the use of bifurcation analysis.

Both descriptions do occur in literature. The investigation of the influence of sheared flows on turbulence was initiated by Biglari in 1990[10]. From here, the two separate directions where followed. Firstly, Carreras[11–14] and Diamond[4, 15] followed an analysis where the flow shear reduces the growth rate of the turbulence. In 2003 the zonal flows were added to this description[5, 6]. Recently, two complementary bifurcation analyses of this model were done by Dam[16] and Zhu[17]. Therefore, the influence of these small scale, spatial and temporal, fluctuations of the $\mathbf{E} \times \mathbf{B}$ -flow on the bifur-

cation structure is omitted in this paper.

The anomalous transport due to the turbulence increases linearly with the fluctuation level as suggested by Refs. [18–23]. According to the nonlinear description the anomalous transport is reduced by the flow shear $\propto (1 + \alpha\omega_s^2)^{-1}$ where ω_s is the shearing rate which was proposed by Hinton[24], and has been further investigated in Refs. [18, 19, 25] and used in the L-H transition models of Refs. [22, 26].

Recently, a different description of anomalous transport reduction was introduced by Miki[27], where the mean flow shear has a double effect on the transport. Firstly, it reduces the transport coefficient directly, and secondly it reduces the transport indirectly via the suppression of the growth rate of the turbulence. In this paper both effects are considered separately as two different descriptions of the same effect.

Thus, there is consensus that sheared $\mathbf{E} \times \mathbf{B}$ -flows reduce the anomalous transport, however there is no consensus yet about the way it should be modelled. Therefore, in this paper two different descriptions of the effects of sheared flows on the transport are compared on the basis of their bifurcation behaviour. In Sec. 6.2 the two transport models are introduced. In Sec. 6.3 the analytic bifurcation analysis is described. In Sec. 6.4 a numerical code is introduced specially designed for bifurcating systems, and the resulting numerical bifurcation analysis of the considered models is shown in Sec. 6.5.

6.2 Turbulent transport models for the L-H transition

The degree of confinement is determined by the 1-dimensional transport in a tokamak along the minor radius of the torus, i.e., from the hot core of the toroidal plasma towards the colder edge. The radial transport of particles and heat is determined by the particle- and heat- fluxes respectively, in the form of a continuity equation. We consider a layer near the edge of the plasma that is relatively thin compared to the plasma minor radius. We approximate this layer, just for conciseness, with a slab geometry, such that these equations become

$$\frac{\partial n}{\partial t} = -\frac{\partial \Gamma}{\partial r} \quad (6-1a)$$

$$\frac{\partial}{\partial t} \left(\frac{nT}{\gamma - 1} \right) = -\frac{\partial q}{\partial r} \quad (6-1b)$$

where we assume equal temperatures of the ions and electrons, the absence heat sources inside the layer, and that the combination of particle sources,

sinks and pinches inside this layer is not drastically changed by the L-H transition. Therefore, the particle and heat fluxes are given by

$$\Gamma = -D \frac{\partial n}{\partial r} \quad (6-2a)$$

$$q = -\chi n \frac{\partial T}{\partial r} + \frac{\Gamma T}{\gamma - 1} \quad (6-2b)$$

The particle flux, Γ , is governed by some effective particle diffusion due to the anomalous transport of electrons and ions. The heat flux, q , is a combination of some effective radial thermal conduction and heat advection due to the net mass-flow described by the particle flux, with γ the adiabatic index. A change from low confinement to high confinement can therefore be described by a change in the transport coefficients; particle diffusivity, D , and heat conductivity χ . The minimum amount of transport is determined by neoclassical effects, on top of that anomalous transport depends on the turbulence level. According to Refs. [18–23] the anomalous transport increases linearly with the turbulence level \mathcal{E} ,

$$D = D_{min} + (D_{max} - D_{min}) \frac{\mathcal{E}}{\mathcal{E}_{max}}, \quad (6-3)$$

where $\mathcal{E}_{max} = \gamma_L / \alpha_{sat}$ is the steady state turbulence level without any flow shear suppression. γ_L is the linear growth rate of the turbulence and α_{sat} depends on the saturation mechanism corresponding to that turbulence. Thus, in general the turbulence evolves according to

$$\frac{\partial \mathcal{E}}{\partial t} = \gamma_L \mathcal{E} - \alpha_{sat} \mathcal{E}^2, \quad (6-4)$$

where the time scale of the turbulence evolution is faster than the diffusive time scale. It is generally accepted[2] that the turbulence level is reduced by $\mathbf{E} \times \mathbf{B}$ -flow shear. This paper addresses the comparison between the two fundamental possibilities in reducing the turbulence. Either, the flow shear reduces the growth rate of the turbulence[4–6, 11, 13–15, 28],

$$\frac{\partial \mathcal{E}}{\partial t} = \gamma_L \left(1 - \tilde{\alpha} |V'_{\mathbf{E} \times \mathbf{B}}|^2 \right) \mathcal{E} - \alpha_{sat} \mathcal{E}^2, \quad (6-5)$$

which is named the linear model in this paper, or it enhances the saturation mechanism of the turbulence which is consistent with the descriptions in Refs. [18, 19, 22, 24–26],

$$\frac{\partial \mathcal{E}}{\partial t} = \gamma_L \mathcal{E} - \alpha_{sat} \left(1 + \tilde{\alpha} |V'_{\mathbf{E} \times \mathbf{B}}|^2 \right) \mathcal{E}^2. \quad (6-6)$$

which is named the nonlinear model in this paper. A radial electric field in a slab geometry causes a poloidal $\mathbf{E} \times \mathbf{B}$ -drift, $V_{\mathbf{E} \times \mathbf{B}} = E_r / B$, such that the

turbulence suppression term can be renormalised, $\tilde{\alpha}|V'_{\mathbf{E} \times \mathbf{B}}|^2 = \alpha Z'^2$, where Z is the normalised radial electric field,

$$Z = \frac{\rho_p e E_r}{T_i}, \quad \text{and} \quad \rho_p = \frac{mv_{th}}{qB_p}. \quad (6-7)$$

Since the L-H transition occurs on a very fast time scale, a proper model for the L-H transition should include the evolution of the flow on this fast time scale. The evolution of the radial electric field is determined by the sum of all possible radial currents in the edge of the plasma,

$$\varepsilon_0 \frac{\partial E_r}{\partial t} = - \sum J_r \quad (6-8)$$

An extensive list of all the possible mechanisms generating a radial current present in literature is given in Appendix 6.A. All these terms are summarised into an evolution equation for the normalised radial electric field,

$$\varepsilon \frac{\partial Z}{\partial t} = \mu \frac{\partial^2 Z}{\partial r^2} + c_n \frac{T}{n^2} \frac{\partial n}{\partial r} + \frac{c_T}{n} \frac{\partial T}{\partial r} - G(Z) \quad (6-9)$$

where the left-hand side (LHS) includes the polarisation current. The right-hand side (RHS) is arranged into a second derivative term, the terms depending on the profiles of density and temperature, and all the other terms are incorporated in the large polynomial $G(Z)$, as described in Appendix 6.A. For the description of the transition behaviour of this model it is only required that the function, $G(Z)$, has an inflection point. Since we are only interested in the transition behaviour of this model, we zoom in at this inflection point by taking only the Taylor expansion around this inflection point, $Z = Z_s$, into account,

$$G(Z) \approx a + b(Z - Z_s) + (Z - Z_s)^3. \quad (6-10)$$

The considered models now consist of a closed set of four coupled nonlinear equations, three partial differential equations (PDEs), Eqs. (6-1a), (6-1b) and (6-9), and one ordinary differential equation (ODE) for the turbulence, Eq. (6-5) or Eq. (6-6). The coordinate system in which the set of equations will be evaluated is chosen as follows: the outer edge of the plasma at the scrape-off layer (SOL) side is fixed at $x = 0$. The inner boundary of the considered spatial domain is located at $x = -\infty$, this is allowed because compared to the size of the transport barrier the inner boundary is far enough away. At this inner boundary all the particles and heat enters the system (there are no additional sources within the domain). These influxes can be used as control parameters of the system:

$$\begin{aligned} \Gamma(x = -\infty) &= \text{constant} = \Gamma_{-\infty} \\ q(x = -\infty) &= \text{constant} = q_{-\infty} \\ Z'(x = -\infty) &= 0 \end{aligned} \quad (6-11)$$

At the other boundary of the system, i.e., the outer edge of the plasma, the temperature, density and radial electric field are forced to drop toward zero with a certain e-folding length into the scrape-off layer,

$$\frac{T'_e}{T_e} = \frac{-1}{\lambda_T}, \quad \frac{n'_e}{n_e} = \frac{-1}{\lambda_n}, \quad \frac{Z'_e}{Z_e} = \frac{-1}{\lambda_Z}, \quad (6-12)$$

with constant gradient lengths λ_T , λ_n and λ_Z of the same order of magnitude, and where from now on the subscript "e" is used for SOL edge values. In the next section the possible transition types within these two models are analysed analytically, and confirmed by numerical bifurcation analysis in Sec. 6.5.

6.3 Bifurcation analysis

For the investigation of transition dynamics from one steady state to another it is necessary to characterise the possible steady states. Since the three PDEs of both models are the same, we start by analysing those steady state equations. First of all, we do not expect the L-H transition to be initiated by some specific difference between the two transport coefficients, D and χ . Therefore we can make the following simplification: $\chi = D/\zeta(\gamma - 1)$, with ζ a proportionality factor, leading to the following steady state transport equations:

$$-D(\mathcal{E}) \frac{\partial n}{\partial r} = \Gamma_{-\infty} \quad (6-13a)$$

$$-\frac{D(\mathcal{E})}{\gamma - 1} \left(\frac{n}{\zeta} \frac{\partial T}{\partial r} + T \frac{\partial n}{\partial r} \right) = q_{-\infty} \quad (6-13b)$$

The term proportional to μ in Eq. (6-9) smoothens the spatial jump between the L-mode core and the H-mode edge. Since clear identification of the pedestal region is desirable to discriminate L-mode from H-mode, the assumption that $\mu \rightarrow 0$ is used in this analytic bifurcation analysis. In the numerical bifurcation analysis of Sec. 6.5 the deviations for small μ are taken into account. Therefore the radial electric field steady state equation reduces to,

$$c_n \frac{T}{n^2} \frac{\partial n}{\partial r} + \frac{c_T}{n} \frac{\partial T}{\partial r} - G(Z) = 0 \quad (6-13c)$$

Combining[3] the above equations leads to,

$$-G(Z)D(\mathcal{E}) = \frac{T_{-\infty} D(\mathcal{E}_e)^2}{\Gamma_{-\infty} \lambda_n^2} (c_n \hat{n}^{-2} + c_g \hat{n}^{-\zeta-2}), \quad (6-14)$$

where $\hat{n} = n_0/n_{0e}$, is the steady state density normalised to its edge value, $n_{0e} = \Gamma_{-\infty} \lambda_n / D(Z_e)$. $T_{-\infty} = (\gamma - 1)q_{-\infty}/\Gamma_{-\infty}$ is the core boundary value of

the steady state temperature, and $c_g = (\zeta c_T - c_n) / (1 + \zeta \lambda_T / \lambda_n)$. The difference between the two models arises due to the turbulence level ODE. In case of the linear model the steady states are

$$\begin{cases} \mathcal{E} = 0, & \text{stable for } Z' \geq \sqrt{1/\alpha}, \\ \mathcal{E} = \frac{\gamma_L}{\alpha_{sat}} (1 - \alpha Z'^2), & \text{stable for } Z' < \sqrt{1/\alpha}. \end{cases} \quad (6-15)$$

For the nonlinear model the steady states are,

$$\begin{cases} \mathcal{E} = 0, & \text{always unstable,} \\ \mathcal{E} = \frac{\gamma_L}{\alpha_{sat}} \frac{1}{1 + \alpha Z'^2}, & \text{always stable.} \end{cases} \quad (6-16)$$

Using these expressions for the turbulence the resulting steady state diffusivities as function of Z' of both models can be compared, as is also shown in Fig. 6.1.

$$D^L(Z') = D_{min} + (D_{max} - D_{min})(1 - \alpha Z'^2), \quad (6-17)$$

$$D^{NL}(Z') = D_{min} + \frac{D_{max} - D_{min}}{1 + \alpha Z'^2}. \quad (6-18)$$

This nonlinear description of the transport reduction is exactly equivalent with what is proposed in Refs. [18, 19, 22, 24–26]. The bifurcation analysis of this non-dynamic transport reduction was done in Ref. [29]. Since the steady states of both those models are equal, the bifurcation dynamics of both models are expected to be qualitatively equivalent, as will be shown below.

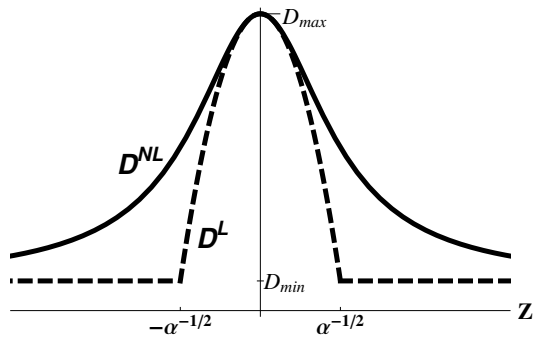


Figure 6.1: The transport coefficients as function of the radial electric field shear for the linear model (**L**), i.e., Eq. (6-17) for $|Z'| < \sqrt{1/\alpha}$, and the nonlinear model (**NL**), i.e., Eq. (6-18).

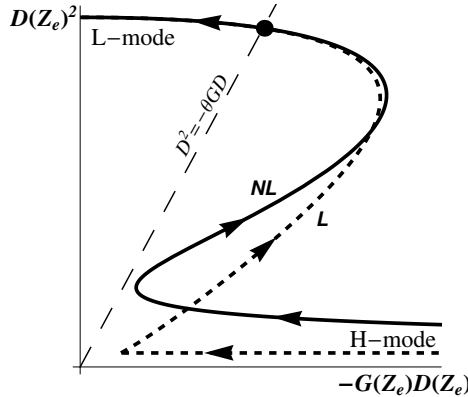


Figure 6.2: Both sides of the steady state Eq. (6-14) can be parameterised by Z_e . The RHS corresponds to the tilted dashed line. The LHS corresponds to the solid curve for the nonlinear model, and the dashed curve for the linear model, where the arrows indicate increasing Z_e , and $\alpha = 1.0$. The intersection, marked by the black dot, determines the edge steady state.

Evaluating Eq. (6-14) at the edge boundary, and using the Robin boundary conditions in Eqs. (6-17) and (6-18) leads to the following steady state criterion,

$$D(Z_e)^2 = -\frac{\Gamma_{-\infty}^2 \lambda_n^2}{q_{-\infty}(\gamma - 1)} \frac{1}{c_n + c_g} G(Z_e) D(Z_e), \quad (6-19)$$

such that both sides of the equation can be parameterised by Z_e as is shown in Fig. 6.2. The RHS corresponds to the tilted dashed line with a slope,

$$\theta = \frac{\Gamma_{-\infty}^2 \lambda_n^2}{q_{-\infty}(\gamma - 1)} \frac{1}{c_n + c_g}. \quad (6-20)$$

The LHS is slightly different for both models as is indicated by the two curves (**L** and **NL**). The intersection between the LHS-curve and the RHS-line indicated with the black dot determines the edge value of the radial electric field, Z_e , and therewith the transport coefficient at the edge of the plasma corresponding to either L-mode or H-mode. For large θ (as shown in Fig. 6.2) the intersection occurs for large diffusivity (squared) at the edge, i.e., L-mode, and for small values of θ the intersection occurs at small edge diffusivity, i.e., H-mode. The parameter θ is for instance controlled by the heat flux, $q_{-\infty}$, and is therefore consistent with experiments where an increasing heating power is used to bring the plasma from L-mode to H-mode.

The bifurcation theory introduced in Ref. [3] showed that the stability of the steady states changes at those values of the edge radial electric field where the slope of the curves, indicated with \mathbf{L} and \mathbf{NL} , are vertical, i.e., the Hopf bifurcation. Thus for decreasing θ the black dot of Fig. 6.2, i.e., the steady state Z_e solution, moves along the curve (either \mathbf{L} or \mathbf{NL}) until those curves have a vertical slope (as indicated in, e.g., Fig. 6.3(a) the right most point for the nonlinear model and Fig. 6.4(a) for the linear model). At that value of θ the Hopf bifurcation makes the L-mode unstable. Depending on the stability of the H-mode at that point, two things can happen. If the H-mode is stable, than the system quickly transits (on the time scale of ε) to the stable H-mode. If the H-mode is also unstable (as is shown in Fig. 6.3b), than the system will oscillate according to a stable limit cycle.

The different possibilities for the nonlinear model are shown in Fig. 6.3. In part a, the H-mode is stable at the Hopf bifurcation of the L-mode steady state, and therefore sharp transitions will occur. In panel b the H-mode is unstable and therefore the system will follow the limit cycle solution. In panel c the Hopf bifurcations disappeared and the stable L-mode smoothly transits to the stable H-mode. These three different types of transitions (sharp, oscillatory and smooth), are arranged by the parameter b of Eq. (6-10).

In contrast, for different values of b the transition dynamics (increasing and decreasing q_{∞}) of the linear model does not change. As is shown in Fig. 6.4 for the same range of values of b as for the nonlinear model, Fig. 6.3. In all three cases the H-mode is unstable at the point of the Hopf bifurcation of the L-mode, and therefore the system will always have an oscillatory phase during the transition from L-mode to H-mode and back.

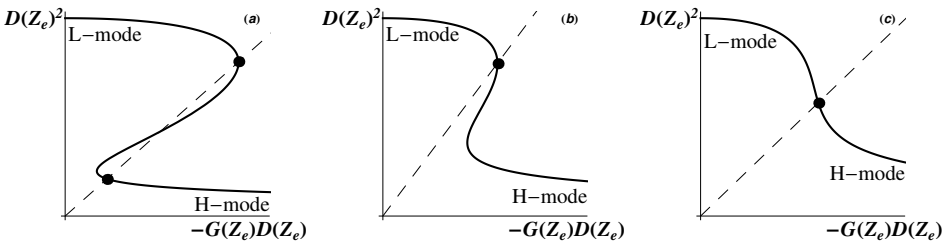


Figure 6.3: The edge steady state electric field of the nonlinear model with $\alpha = 1.0$ for three different values of b . (a) $b = -1.2$, sharp transition between the stable L-mode and the stable H-mode. (b) $b = -0.1$, limit cycle solutions where both L-mode and H-mode are unstable. (c) $b = 0.7$, The stable L-mode transits smoothly into a stable H-mode for increasing heat flux.

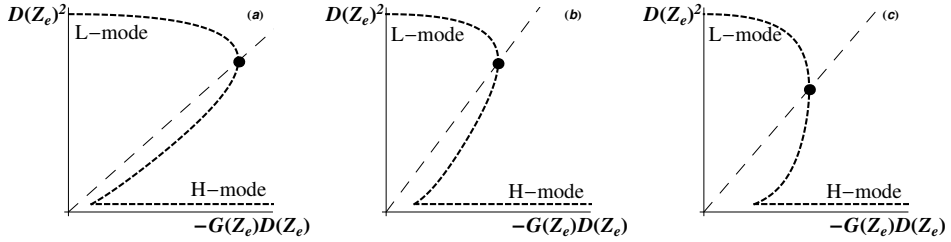


Figure 6.4: The edge steady state electric field of the linear model with $\alpha = 1.0$ for three different values of b . In all three panels there is a regime without stable solutions for decreasing θ in between the stable L-mode and stable H-mode leading to oscillatory transitions.

These observations about the possible transition dynamics are summarised in Fig. 6.5 where the parameter spaces $(b, q_{-\infty})$ of both models are shown with the Hopf bifurcation curves separating the L-mode, H-mode and oscillatory regimes. In Fig. 6.5(a) the parameter space of the nonlinear model is shown. In the middle region the oscillations separate the L-mode from the H-mode. To the left the Hopf bifurcations switch order and sharp transitions with hysteresis arise, because the Hopf bifurcation of the H-mode (i.e., H-L transition) occurs at lower threshold values of the heat flux than the L-H transition. To the right the Hopf bifurcations disappear and the region of L-modes is smoothly connected to the regime with H-modes. This bifurcation structure of the nonlinear model is very robust, i.e., no small changes in all the parameters considered in this model changes this picture qualitatively.

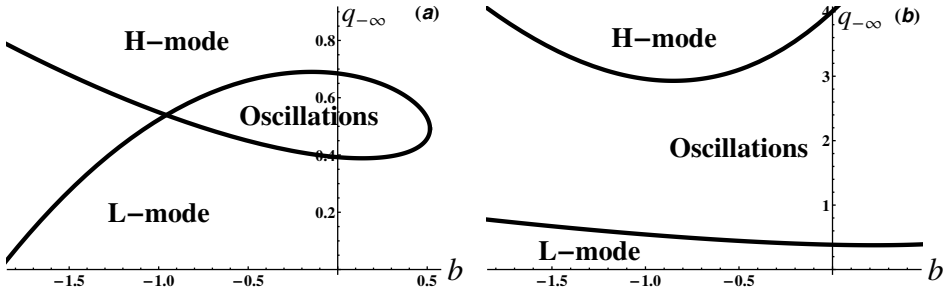


Figure 6.5: The Hopf bifurcations for $\alpha = 1.0$ in the $(b, q_{-\infty})$ parameter space, for (a) the nonlinear model and (b) the linear model.

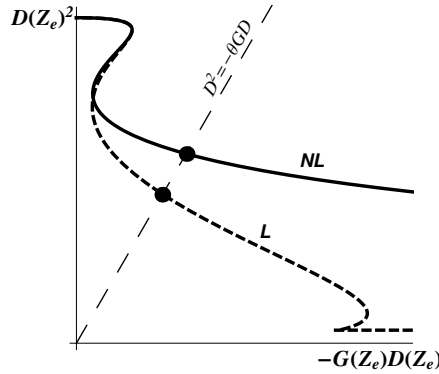


Figure 6.6: The radial electric field edge steady state condition for both models with $\alpha = 0.1$

Fig. 6.5(b) shows the parameter space of the linear model, and in this case the L-mode and H-mode are always separated by a regime of oscillations. However, the linear model is very sensitive to the parameter α . The bifurcation structure changes qualitatively when changing α , therefore the possible transition dynamics within this model changes. For $\alpha = 1.0$ only oscillatory transitions are possible as is shown in Fig. 6.5(b), however if α is reduced the $\mathcal{E} = 0$ (i.e., $D = D_{min}$) steady state moves further and further away towards higher values of the input heat flux (i.e., smaller θ), as is shown in Fig. 6.6 ($\alpha = 0.1$). Therefore, the characteristic bifurcation structure reappears again, such that for small α the three different types of transitions (sharp, oscillatory and smooth) are present in this model too, in the characteristic ordering of a co-dimension 3 bifurcation[3], as is shown in Fig. 6.7.

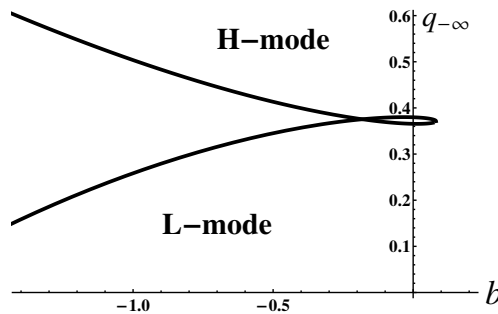


Figure 6.7: The bifurcation parameter space of the linear model with $\alpha = 0.1$

Thus similar transition dynamics can be found in both models. However, in the linear model bifurcation dynamics is very sensitive to α . In contrast the nonlinear model is very robust and shows qualitatively the same transition structure for all values of α .

To support the conclusions that can be drawn from the analytical bifurcation analysis a dedicated code has been created for the simulation of bifurcating systems of PDEs and/or ODEs, called *Bifurcator*. The next section gives a short summary of the design of Bifurcator and its capabilities.

6.4 Bifurcator

At its core, Bifurcator is a numerical solver for nonlinear ODEs, optimised to meet the accuracy and performance demands of studying bifurcating systems. Bifurcating systems of PDEs, like those describing the L-H transition in fusion plasmas, need to be discretised into a system of ODEs first. While this takes some effort, it allows the user to select the discretisation method most suitable for the problem at hand.

The time integration methods on the other hand are tailored for solving large stiff systems that typically arise from discretising diffusive transport equations like those describing the transport in tokamak edge plasmas. Specifically, Bifurcator employs various implicit Runge-Kutta (Radau, DIRK and Gauss) methods with an adaptive time stepping strategy to capture all physically relevant time-scales efficiently. Since these methods are implicit, the time integration does involve solving non-linear systems. This is done using Newton iteration and requires the user to also define the Jacobi-matrix of the discretised system of equations. The adaptive time step size is very helpful as the majority of the time the system evolves on a diffusive timescale, while the sudden transitions between metastable states occur in timescales orders of magnitude shorter.

Finally, a bifurcation detection scheme is implemented. In this scheme, Bifurcator obtains the steady state solution for a given set of parameters and varies one parameter over a given interval with some (user-defined) increment. By defining an appropriate “order” parameter for the model, Bifurcator can then detect transitions from one state to another (e.g., from L-mode to H-mode). Whenever such a jump is detected, Bifurcator backtracks to the last solution in the same state as the initial solution, reduces the parameter increment and then again solves the equations at the new parameter value. This allows Bifurcator to approach the critical value of the scanning parameter up to arbitrary accuracy.

All the features mentioned above are model-independent; the user only

needs to supply a discretisation of the equations to be analysed, and optionally an order parameter that describes the transition of interest for the bifurcation detection. At this moment, seven different bifurcating models are already implemented within Bifurcator. Bifurcator is configured through a combination of input files and command line arguments. These tell the program what model to analyse, which parameters and the time integration settings to use and optionally which parameter to perform a parameter scan in.

The features mentioned above make Bifurcator ideal for studying the models presented in this paper. In Sec. 6.5 the bifurcation detection scheme is used to analyse numerically the bifurcating behaviour of the models.

6.5 Numerical bifurcation analysis

Our numerical bifurcation analysis consists of many simulations of the considered models during which the heat flux parameter $q_{-\infty}$ is increased (for L-H transitions) or decreased (for H-L transitions) in small steps. It is important to simulate every step until the system is in steady state, so no ramping of the heat flux during the simulations, because that could cause additional dynamics. Since the systems are known to exhibit hysteresis it is important during a parameter scan to start every simulation from the steady state profiles of the previous step.

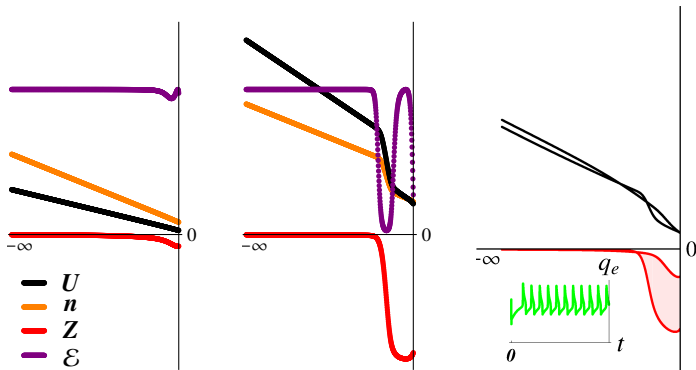


Figure 6.8: Three qualitatively different final states of the nonlinear model ($\alpha = 1.0$) i.e from left to right, L-mode, H-mode and the oscillatory phase. Four profiles, energy (black), density (orange), electric field (red), turbulence level (purple) and one time trace of the edge heat flux (green) are indicated.

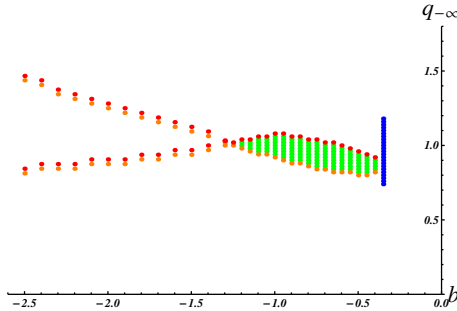


Figure 6.9: Simulated parameter space of the nonlinear model ($\alpha = 1.0$), where stable L-modes (orange) and stable H-modes (red) are either adjacent to each other (left part) indicating sharp transitions, separated by oscillatory phases (green region), or smoothly connected (blue trace). Note that on the left-hand side two branches of sharp transition occur, the upper branch corresponds to sharp L-H transitions and the lower one to H-L transitions indicating the hysteresis.

Simulations of the nonlinear model shows L-modes where the radial electric field profile is close to zero everywhere (LHS of Fig. 6.8) and the turbulence level stays close to \mathcal{E}_{max} , and H-modes where an electric field well is formed near the edge of the plasma (middle of Fig. 6.8) and locally the turbulence is greatly reduced. Increasing the heat flux, $q_{-\infty}$, in small steps results in L-H transitions that are either sharp (from one step to the next), smooth (slowly changing every step), or oscillatory. An example of these oscillations is shown on the RHS of Fig. 6.8, the radial electric field oscillates covering the shaded area and correspondingly the energy profiles ($U = nT/(\gamma - 1)$) oscillate leading to an oscillating outflux, $q_e(t)$, for a constant influx, $q_{-\infty}$, as is shown in the inset.

From the bifurcation analysis of the nonlinear model in Sec. 6.3 it resulted that the different types of L-H transitions (i.e., sharp, oscillatory and smooth) are ordered by the parameter b . This result is confirmed by the Bifurcator simulations shown in Fig. 6.9. On the right-hand side the series of blue points corresponds to a parameter scan of $q_{-\infty}$ in which the system smoothly went from L-mode profiles to H-mode profiles without any bifurcation. In the intermediate regime of b -values the system stays in L-mode up till the value of $q_{-\infty}$ marked by the orange points, increasing the heat flux one additional step and the system enters an oscillatory phase marked by the green points. The system keeps oscillating for increasing heat flux until it reaches a stationary

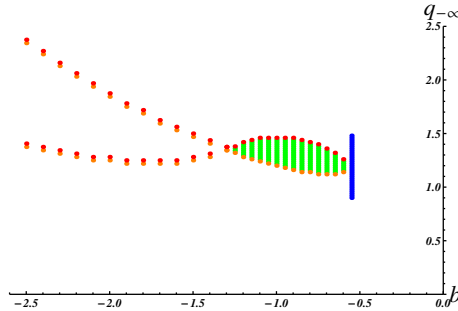


Figure 6.10: Numerical bifurcation structure of the flow shear model without turbulence level evolution[29], $\alpha = 1.0$

H-mode marked by the red points. In the left most part of the parameter space, the L-mode (orange) and the H-mode (red) are directly adjacent to each other indicating a sharp transition from an L-mode stationary state to an H-mode stationary state for a small increase of the heat flux. Since, in this b -parameter range, the back transitions from H-mode to L-mode occur at different values of the heat flux due to the hysteresis, these are separately indicated as the lower branch of red-orange points.

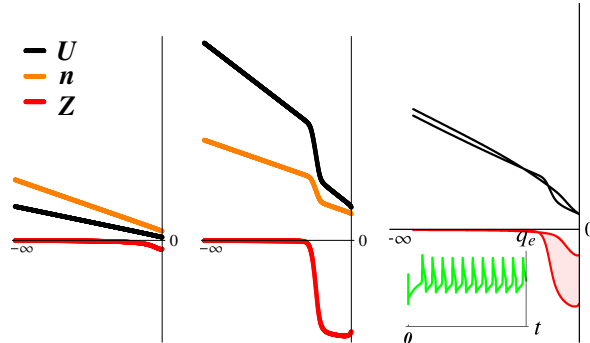


Figure 6.11: Three qualitatively different final states of the flow shear reference model without turbulence dynamics[29]. From left to right: L-mode, H-mode and the oscillatory phase. Three profiles, energy (black), density (orange), electric field (red) and one time trace of the edge heat flux (green) are indicated. ($\alpha = 1.0$)

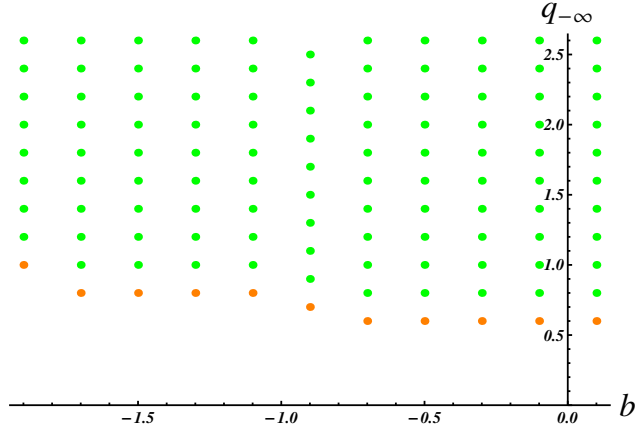


Figure 6.12: Numerical bifurcation structure of the linear model for $\alpha = 1.0$. Only transitions from L-modes into the oscillatory phase are observed for all values of b .

As was noted in Sec. 6.3 this nonlinear turbulence model is in steady state exactly the same as the flow shear model analysed in Ref. [3]. Although the dynamical equations are different the same bifurcation structure is therefore expected. Indeed, as is shown in Fig. 6.10, the bifurcation structure of this model is qualitatively the same. The exact values are somewhat shifted, however the robustness of the bifurcation structure is shown again. The three types of stationary state of this flow shear model without the turbulence dynamics are shown in Fig. 6.11.

The change from nonlinear reduction of the turbulence by sheared flows to the linear model, does change the bifurcation structure as was shown in Sec. 6.3. The region of oscillations opened up, to all values of b , such that only oscillatory transitions from L-mode to H-mode are possible. The numerical parameter scans in the heat flux do indeed show a transition from L-mode into the oscillatory phase for all values of b as is shown in Fig. 6.12. However, for very high values of the heat flux the profiles do settle in an H-mode steady state that is, however, not fully stationary and keeps oscillating a bit. Since in this part of parameter space we are far away from the organizing center of the co-dimension 3 bifurcation other bifurcations may become visible. Only when α is reduced such that the influence of the sheared flow becomes much less, then the original bifurcation structure corresponding to the co-dimension 3 bifurcation reappears as is shown in Fig. 6.13 for $\alpha = 0.1$. The corresponding profiles of the possible stationary states are shown in Fig. 6.14.

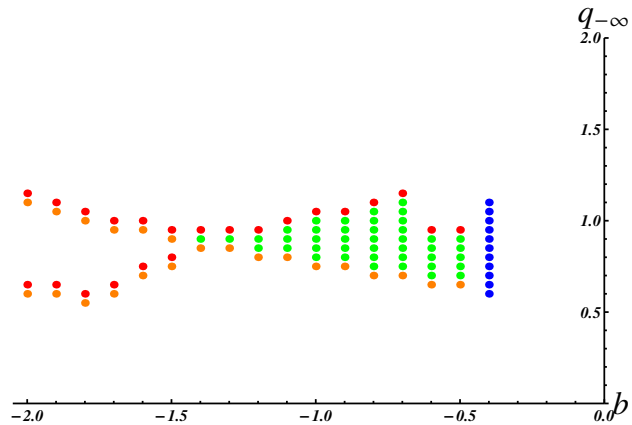


Figure 6.13: Numerical bifurcation structure of the linear model for $\alpha = 0.1$ corresponds to the characteristic co-dimension 3 bifurcation structure[3].

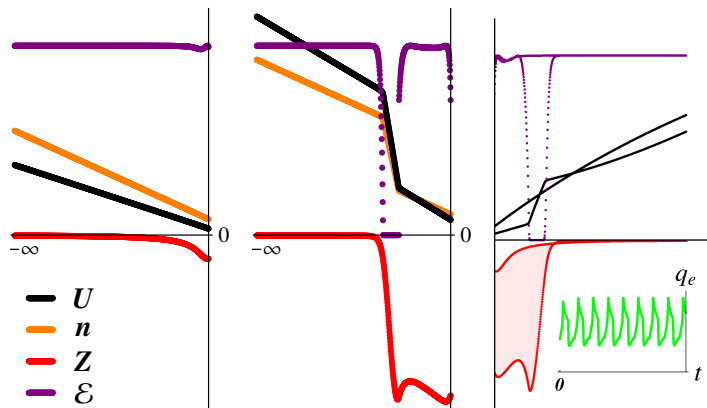


Figure 6.14: Three qualitatively different final states of the linear model with $\alpha = 0.1$. From left to right: L-mode, H-mode and the oscillatory phase. Four profiles, energy (black), density (orange), electric field (red), turbulence level (purple) and one time trace of the edge heat flux (green) are indicated.

Thus, the predictions from analytic bifurcation theory are confirmed by dedicated numerical simulations. The exact values of the transitions are slightly different in the numerical simulations than in the analytic analysis. This is mainly due to the assumption of $\mu = 0$ in the bifurcation analysis, and the finite value of $\mu = 0.05$ in the simulations, because this term directly enters in the equation determining the steady state, Eq. (6-14). However, the bifurcation structure is very robust and is therefore still intact.

6.6 Conclusion and discussion

Two fundamentally different descriptions of the turbulence reduction by sheared $\mathbf{E} \times \mathbf{B}$ -flows are compared on the basis of their bifurcation structure. The first description reduces the growth rate of the turbulence, and the second description enhances the saturation effect of the turbulence. These two descriptions are incorporated into a transport model evolving the energy, density and radial electric field (and therewith the $\mathbf{E} \times \mathbf{B}$ -flow).

On the basis of (analytical and numerical) bifurcation analysis the influence of both turbulence descriptions on L-H transition dynamics are compared. The nonlinear model has a very robust bifurcation structure in which three different types of transition dynamics can be identified, i.e., sharp, oscillatory and smooth transitions. In contrast, the linear model is sensitive to variations in α (the parameter indicating the effectiveness of the turbulence suppression by sheared flows). Only if this parameter is fine-tuned towards low values the same three types of transition dynamics can be identified. For large values of α the numerical analysis shows only transitions from L-mode to an oscillatory phase. Since the L-H transition is a very robust phenomenon observed in many magnetically confined fusion devices, it is expected that the underlying model is also very robust, which makes the nonlinear model more likely to be the better description.

Another reason why the analysis of transition dynamics is important, is because different types of transition dynamics are observed in experiments, as Carlstrom nicely notes in his review[30]. Most often the transition occurs spontaneously when increasing the heating power, but in low-density discharges at JT-60U[31] and DIII-D so-called 'transitionless H-modes' were observed. These smooth transitions from L-mode to H-mode without clear bifurcation are also seen in low-density discharges at JET[32-34], and also 'smoother' transitions are observed at ASDEX Upgrade[35]. Additionally, Carlstrom points out the 'dithering' transitions observed at ASDEX Upgrade [36], however nowadays there is lots of investigation into all types of oscillatory transitions, at DIII-D[37], ASDEX Upgrade[38, 39], EAST[40, 41], JET[42], TJ-II[43] and HL-2A[44]. Most probably some of these oscillations

are caused by the same mechanism, but there could also be multiple mechanisms at play leading to oscillatory behaviour around the L-H transition. Lately, the predator-prey type of oscillations between turbulence and zonal flows is used frequently to describe oscillatory behaviour, as in the papers of Miki[27, 45–48] these type of oscillations are embedded into a similar transport model as discussed in this paper. However, this paper shows that without the zonal flow interaction there are also oscillations inside this model, therefore Miki’s model probably has multiple types of oscillations depending on their parameter setting. Therefore, it is essential to do the bifurcation analysis of that model too. As is true for all proposed L-H transition models.

6.A Appendix: Radial currents

The evolution of the radial electric field has been subject to debate since the discovery of the H-mode. A large variety of physical mechanisms possibly influencing the radial electric field in magnetically confined plasmas are described in literature. Not one of them has been appointed to be the initiator of the L-H transition. Their relative importance to one another is still under discussion. In this appendix a number of radial current drive effects is listed.

$$\varepsilon_0 \frac{\partial E_r}{\partial t} = - \sum J_r = e \sum (\Gamma_e - \Gamma_i) \quad (6-21)$$

Since, only the dependence on the normalised radial electric field is important for this analysis, we copied the expressions from the relevant literature directly and only indicate the dependence on Z . First of all, a changing electric field in time causes the generation of a **neoclassical polarisation current**,

$$J_{pol} = \frac{\rho c^2}{B_\theta} \frac{\partial E_r}{\partial t}, \quad (6-22)$$

i.e., Eq. (3) of Ref. [49], and simulated by Refs. [50, 51]. Usually, this term is moved to the LHS of Eq. 6-21 and combined into the term $\varepsilon \partial Z / \partial t$ of Eq. (6-9). Furthermore, there are three types of viscosities driving current. Firstly, the **shear viscosity**,

$$J_{visc} = -\varepsilon_0 \varepsilon_\perp \nabla \cdot \mu_i \nabla E_r \quad (6-23)$$

i.e., Eq. (3) of Ref. [52], which leads to the term $\mu \partial^2 Z / \partial r^2$ in Eq. (6-9). This term is also discussed in Ref. [53] and reviewed in Ref. [54]. Secondly, the **bulk viscosity** generates a radial current, due to the inhomogeneity of the magnetic field,

$$\Gamma_i^{bv} = f_{bv} \nu_i \rho_p n_i \frac{Z - Z_0}{1 + Z^2} \quad (6-24)$$

i.e., Eq. (2.44) from review [55] and similar to Refs. [54, 56]. Initially investigated in Refs. [57–59]. And thirdly, the **gyroviscosity** generates a radial current according to reviews [54, 56]. However, no expression for this effect is given.

Moreover, the **anomalous cross field flux** has a bipolar part leading to a radial current,

$$\Gamma_e^{anom} = -D_e n \left(\frac{n'}{n} + \alpha \frac{T'}{T} + \frac{Z}{\rho_p} \right) \quad (6-25)$$

i.e., Eq. (3) of Ref. [60], which initially investigated this effect for the L-H transition. Later it was also used by Ref. [59], and reviewed in Refs. [54–56]. The first two terms are directly influenced by the density and temperature profiles and are therefore explicitly taken into account in the considered models, see Eq. (6-9). The third term is absorbed into the function $G(Z)$. A similar expression of current generation is due to the collisional process of **ripple diffusion**, described in Eq. (19) of Ref. [54],

$$\begin{aligned} \Gamma_i^{NC} \simeq -\varepsilon^2 \sqrt{\varepsilon_h} n v_D^2 \int_0^\infty dw \frac{w^{5/2} e^{-w} \nu(w)}{\nu^2 + \frac{3}{2} \sqrt{\frac{\varepsilon}{\varepsilon_h}} w_{rot}^2} \times \\ \left(\frac{n'}{n} + (w - 3/2) \frac{T'}{T} - \frac{Z}{\rho_p} \right). \end{aligned} \quad (6-26)$$

Another often proposed radial current generation mechanism is the **ion orbit losses** or loss cone losses, initially described in Eq. (2) of Ref. [53],

$$\Gamma_i^{lc} = \frac{1}{\sqrt{\varepsilon}} \frac{n_i}{\tau_{ii}} \rho_p \hat{F} e^{-Z^2}. \quad (6-27)$$

and similar expressions are reviewed in Refs. [54–56]. A more general expression for the ion orbit loss rate depending on the collisionality is first given in Ref. [61], and later used in Eq. (1) of Ref. [59],

$$\Gamma_i^{lc} = \frac{n_i \nu \sqrt{\varepsilon} \rho_{pi}}{\sqrt{\nu_{*i} + Z^4}} e^{-\sqrt{\nu_{*i} + Z^4}} \quad (6-28)$$

In the limit of $\nu_{*i} \rightarrow 0$ Eq. (6-27) is recovered. Furthermore, Reynolds stresses can cause a radial flux of ions, $\Gamma_i^{v\nabla v}$, as explained in Ref. [54]. This effect is employed for the L-H transition by Ref. [62], and reviewed by [55, 56]. Moreover, the influx of neutrals and their **charge exchange** reactions leads to a difference in radial flux of ions compared to electrons, as is firstly used in Ref. [63], and extensively investigated in Ref. [64], and reviewed in Ref. [54] in Eq. (52d),

$$\Gamma_i^{cx} = -n_0 \langle \sigma_{cx} v \rangle n_i \rho_p (Z_0 + Z - qV_p / \varepsilon v_{th}). \quad (6-29)$$

Finally, the radial electric field can be manipulated by biasing the plasma with a external voltage[52, 65],

$$J_{ext} = \text{constant} \quad (6-30)$$

Altogether, this leads to Eq. (6-9) where the sum of Eqs. (6-24)-(6-30) is represented by $G(Z)$. For this model to describe L-H transition physics it is necessary that this long polynomial has an inflection point somewhere, and that in the neighbourhood of this point the transport coefficients do vary. Therefore, it is sufficient to take into account only the Taylor expansion around the inflection point to be able to describe L-H transition physics, $G(Z) \approx a + b(Z - Z_s) + (Z - Z_s)^3$, similar to Refs. [66, 67]. The coefficients a , b and Z_s of this Taylor expansion depend, via the different contributions to Eq. (6-21) discussed in this Appendix, on a large number of quantities that can in principle be determined experimentally, albeit with varying accuracy. Additionally, the influence on the L-H transition by global changes to the plasma, such as triangularity and the direction of the single-null divertor, could also be understood as changes to some of the contributions to Eq. (6-21). To determine which parameters can be used as experimental control parameters for the L-H transition, the relative importance of all these effects need to be determined at the edge of the plasma. Since many terms described in this appendix scale with the density, an educated guess could be that the density may be used to control the type of L-H transition.

Acknowledgements

This work, supported by the European Communities under the contract of Association between EURATOM/FOM, was carried out within the framework of the European Fusion Programme with financial support from NWO. The views and opinions expressed herein do not necessarily reflect those of the European Commission. This work is supported by NWO-RFBR Centre-of-Excellence on Fusion Physics and Technology (Grant nr. 047.018.002)

References

- [1] F. Wagner *et al.*, *Physical Review Letters* **49** (1982) 1408
- [2] F. Wagner, *Plasma Physics and Controlled Fusion* **49** (2007) B1
- [3] W. Weymiens, H. J. de Blank, G. M. D. Hogeweij and J. C. de Valen  a, *Physics of Plasmas* **19** (2012) 072309
- [4] P. H. Diamond, Y.-M. Liang, B. A. Carreras and P. W. Terry, *Physical Review Letters* **72** (1994) 2565
- [5] E.-j. Kim and P. H. Diamond, *Physical Review Letters* **90** (2003) 185006
- [6] E. jin Kim and P. H. Diamond, *Physics of Plasmas* **10** (2003) 1698
- [7] Z. Wang, P. Diamond,   . G  rcan, X. Garbet and X. Wang, *Nuclear Fusion* **51** (2011) 073009
- [8] K. H. Burrell, *Physics of Plasmas* **6** (1999) 4418
- [9] K. H. Burrell, *Physics of Plasmas* **4** (1997) 1499
- [10] H. Biglari, P. H. Diamond and P. W. Terry, *Physics of Fluids B* **2** (1990) 1
- [11] B. A. Carreras, V. E. Lynch, L. Garcia and P. H. Diamond, *Physics of Fluids B: Plasma Physics* **5** (1993) 1491
- [12] B. A. Carreras, P. H. Diamond, Y. M. Liangs, V. Lebedev and D. Newman, *Plasma Physics and Controlled Fusion* **36** (1994) A93
- [13] B. A. Carreras, D. Newman, P. H. Diamond and Y.-M. Liang, *Physics of Plasmas* **1** (1994) 4014
- [14] B. A. Carreras, V. E. Lynch, L. Garcia and P. H. Diamond, *Physics of Plasmas* **2** (1995) 2744
- [15] P. H. Diamond *et al.*, *Plasma Physics and Controlled Nuclear Fusion Research* **2** (1992) 97
- [16] M. Dam, M. Br  ns, J. Juul Rasmussen, V. Naulin and G. Xu, *Physics of Plasmas* **20** (2013) 102302
- [17] H. Zhu, S. C. Chapman and R. O. Dendy, *Physics of Plasmas* **20** (2013) 042302
- [18] T. S. Hahm, *Physics of Plasmas* **1** (1994) 2940
- [19] T. S. Hahm and K. H. Burrell, *Physics of Plasmas* **2** (1995) 1648

-
- [20] P. H. Diamond, V. B. Lebedev, D. E. Newman and B. A. Carreras, *Physics of Plasmas* **2** (1995) 3685
 - [21] D. del Castillo-Negrete, B. A. Carreras and V. E. Lynch, *Plasma Physics and Controlled Fusion* **46** (2004) A105
 - [22] Ö. D. Gürcan, P. H. Diamond, T. S. Hahm and R. Singh, *Physics of Plasmas* **14** (2007) 042306
 - [23] I. Calvo and B. A. Carreras, *Physics of Plasmas* **14** (2007) 102507
 - [24] F. L. Hinton, *Physics of Fluids B: Plasma Physics* **3** (1991) 696
 - [25] Y. Z. Zhang and S. M. Mahajan, *Physics of Fluids B: Plasma Physics* **4** (1992) 1385
 - [26] F. L. Hinton, G. M. Staebler and Y. B. Kim, *Plasma Physics and Controlled Fusion* **36** (1994) A273
 - [27] K. Miki, P. H. Diamond, Ö. D. Gürcan, G. R. Tynan, T. Estrada, L. Schmitz and G. S. Xu, *Physics of Plasmas* **19** (2012) 092306
 - [28] B. A. Carreras, P. H. Diamond, Y. M. Liangs, V. Lebedev and D. Newman, *Plasma Physics and Controlled Fusion* **36** (1994) A93, and references therein
 - [29] W. Weymiens, H. J. de Blank and G. M. D. Hogeweij, *Physics of Plasmas* **20** (2013) 082306
 - [30] T. N. Carlstrom, *Plasma Physics and Controlled Fusion* **38** (1996) 1149
 - [31] M. Mori, *Plasma Physics and Controlled Fusion* **36** (1994) A39
 - [32] L. D. Horton *et al.*, *26th EPS Conf. on Plasma Physics* **23J** (1999) 193
 - [33] Y. Andrew *et al.*, *Plasma Physics and Controlled Fusion* **48** (2006) 479
 - [34] C. Maggi *et al.*, *Nuclear Fusion* **54** (2014) 023007
 - [35] F. Ryter *et al.*, *Plasma Physics and Controlled Fusion* **40** (1998) 725
 - [36] H. Zohm *et al.*, *Plasma Physics and Controlled Fusion* **37** (1995) 437
 - [37] L. Schmitz *et al.*, *Physical Review Letters* **108** (2012) 155002
 - [38] G. D. Conway, C. Angioni, F. Ryter, P. Sauter and J. Vicente, *Physical Review Letters* **106** (2011) 065001
 - [39] F. Ryter *et al.*, *Nuclear Fusion* **53** (2013) 113003

- [40] G. S. Xu *et al.*, *Physical Review Letters* **107** (2011) 125001
- [41] H. Wang *et al.*, *Nuclear Fusion* **52** (2012) 123011
- [42] A. Loarte, R. D. Monk, A. S. Kukushkin, E. Righi, D. J. Campbell, G. D. Conway and C. F. Maggi, *Physical Review Letters* **83** (1999) 3657
- [43] T. Estrada, C. Hidalgo, T. Happel and P. H. Diamond, *Physical Review Letters* **107** (2011) 245004
- [44] J. Cheng *et al.*, *Physical Review Letters* **110** (2013) 265002
- [45] K. Miki, P. H. Diamond, L. Schmitz, D. C. McDonald, T. Estrada, Ö. D. Gürcan and G. R. Tynan, *Physics of Plasmas* **20** (2013) 062304
- [46] K. Miki *et al.*, *Nuclear Fusion* **53** (2013) 073044
- [47] K. Miki, P. H. Diamond, S. H. Hahn, W. W. Xiao, Ö. D. Gürcan and G. R. Tynan, *Physical Review Letters* **110** (2013) 195002
- [48] K. Miki, P. H. Diamond, S.-H. Hahn, W. W. Xiao, Ö. D. Gürcan and G. R. Tynan, *Physics of Plasmas* **20** (2013) 082304
- [49] F. L. Hinton and J. A. Robertson, *Physics of Fluids* **27** (1984) 1243
- [50] R. V. Shurygin and R. L. Dewar, *Plasma Physics and Controlled Fusion* **37** (1995) 1311
- [51] T. P. Kiviniemi *et al.*, *Physics of Plasmas* **10** (2003) 2604
- [52] N. Kasuya, K. Itoh and Y. Takase, *Nuclear Fusion* **43** (2003) 244
- [53] K. Itoh, S.-I. Itoh, M. Yagi and A. Fukuyama, *Physics of Plasmas* **5** (1998) 4121
- [54] K. Itoh and S.-I. Itoh, *Plasma Physics and Controlled Fusion* **38** (1996) 1
- [55] J. W. Connor and H. R. Wilson, *Plasma Physics and Controlled Fusion* **42** (2000) R1
- [56] K. Itoh, *Plasma Physics and Controlled Fusion* **36** (1994) A307
- [57] K. C. Shaing and E. C. Crume, *Physical Review Letters* **63** (1989) 2369
- [58] K. Itoh and S.-I. Itoh, *Nuclear Fusion* **32** (1992) 2243
- [59] S. Toda, S.-I. Itoh, M. Yagi, A. Fukuyama and K. Itoh, *Plasma Physics and Controlled Fusion* **38** (1996) 1337

- [60] S.-I. Itoh and K. Itoh, *Physical Review Letters* **60** (1988) 2276
- [61] K. C. Shaing, J. E. C. Crume and W. A. Houlberg, *Physics of Fluids B: Plasma Physics* **2** (1990) 1492
- [62] A. B. Hassam, T. M. Antonsen, J. F. Drake and C. S. Liu, *Physical Review Letters* **66** (1991) 309
- [63] S.-I. Itoh and K. Itoh, *Nuclear Fusion* **29** (1989) 1031
- [64] D. A. D'Ippolito and J. R. Myra, *Physics of Plasmas* **9** (2002) 853
- [65] J. Cornelis, R. Sporken, G. van Oost and R. Weynants, *Nuclear Fusion* **34** (1994) 171
- [66] S.-I. Itoh, K. Itoh, A. Fukuyama and Y. Miura, *Physical Review Letters* **67** (1991) 2485
- [67] H. Zohm, *Physical Review Letters* **72** (1994) 222

7

Evaluation and future prospects

In this chapter we revisit the research questions posed in chapter 1, and discuss the conclusions drawn from the answers to these questions. Furthermore, the future line of research necessary to conclusively determine the L-H transition mechanism, is discussed.

7.1 Conclusions and discussion

The main question that motivates the research in this thesis is:

How can we employ bifurcation theory to unravel the L-H transition mechanism?

To answer this important question for the control of fusion energy plasmas, first of all the link between L-H transition dynamics and certain bifurcations is investigated.

What bifurcation structure can be recognised in L-H transition dynamics?

The three different types of dynamics observed during L-H transitions are sharp transitions, smooth transitions and oscillatory transitions. In chapter 3 it is shown that these types of transitions occur around a co-dimension 3 bifurcation that combines two fold bifurcations with a Hopf bifurcation, known as a degenerate Bogdanov-Takens bifurcation. The dynamics in the neighbourhood of this co-dimension 3 bifurcation is organised in such a way that the oscillatory transitions are in parameter space always in between the smooth transitions and the sharp transitions as is depicted in Fig. 3.4. Note that dynamical systems that exhibit the three types of transition dynamics without the co-dimension 3 bifurcation do exist. However, the fact that such a model shows for instance oscillatory behaviour around the transition from one state to the other is merely a coincidence. An example of such a model is analysed by Ball[1], and it shows indeed that some parameters need to be fine-tuned to get the oscillatory behaviour near the transition. In contrast,

the co-dimension 3 bifurcation robustly connects the three types of transition behaviour. Therefore, the identification of the co-dimension 3 bifurcation in proposed L-H transition models directly proves that the characteristic transition behaviour is robustly present in the model. Although systematic analysis of the normal form on center manifolds at the degenerate Bogdanov-Takens bifurcation in the literature [2] reveals that the most general unfolding has four parameters, the FitzHugh-Nagumo form relevant for edge transport barriers has only three. Therefore, to tackle the 1-dimensional problem of the formation of the edge transport barrier we asked the following question.

How can we identify the co-dimension 3 bifurcation in 1-dimensional models?

First of all, it is noted, in chapter 4, that the bifurcation analysis is a local analysis around the steady state solution, such that a Taylor expansion of the system can be considered. Secondly, two eigenvectors with vanishing eigenvalues of the linear operator of the system need to be found for the fold bifurcations. At the cusp bifurcation additionally the second term in the Taylor expansion evaluated in the same direction as the fold bifurcation must vanish. The third condition, needed to pinpoint the co-dimension 3 bifurcation, is given by a vanishing inner product of the two eigenvectors. These conditions are summarised in Eq. (4-11). A separate description of the Hopf bifurcation away from the co-dimension 3 bifurcation is given in Eq. (4-15), determining the region of oscillations in the analysed model. This general bifurcation analysis is applied to the well known 0-dimensional FitzHugh-Nagumo model to show its validity. However, in 1-dimensional systems much more can be learned about the spatial behaviour of the transition physics. Therefore, in chapter 5 the following question is investigated.

How do these 1-dimensional bifurcating models combine transitions in time and in space?

A general nonlinear partial differential equation for the description of a reaction diffusion system of the FitzHugh-Nagumo type is investigated. Its terms are a first order derivative to time, a second order derivative to space, a non-monotonic function and a control parameter, i.e., Eq. (5-14). Investigating this general system lead to the formulation of a generalised equal area rule for simultaneous transitions in space and time. This generalised equal area rule is applicable to moving sharp transition fronts described by this partial differential equation, such as flame front propagation, propagation of signals in neural cells and the growth of the pedestal during an L-H transition. The two limits of purely temporal transitions and purely spatial transitions correspond to the well known transition rules of maximal hysteresis and the Maxwell equal area rule, respectively.

With this mathematical framework in place we firstly analysed a known bifurcating transport model, introduced by Zohm[3] in 1994 to describe oscillatory behaviour near the plasma edge.

What is the bifurcation structure of the model proposed by Zohm?

The analysis of this 1-dimensional model, done in chapter 4, showed that the state of the plasma profiles could be determined by the edge value of the radial electric field. The oscillatory transitions from one state to the other simulated by Zohm[3] are confirmed with our bifurcation analysis. However, it turned out that this model additionally contains sharp as well as smooth transitions both without any oscillation. Altogether it is shown that this model does contain the co-dimension 3 bifurcation discussed above. Although the co-dimension 3 bifurcation point in parameter space lies at infinity ($\theta = \infty$), the unfolding of this bifurcation, opening up the oscillatory domain, is in the physically accessible part of its parameter space. Therefore, all three types of L-H transitions are contained within the model. Furthermore, the generalised equal area rule is applied to this model uncovering a remarkable feature. In chapter 5 it is shown that for Zohm's model there are two different regimes of transport barrier widths, because it is possible in this model to have an edge state that is in H-mode, without the satisfaction of the generalised equal area rule. This leads to the realisation that right after the L-H transition the system first exhibits a so-called thin-barrier H-mode. Thereafter, when the heat flux is increased such that the generalised equal area rule is satisfied, the barrier will grow inward into a so-called thick-barrier H-mode, as is shown in Fig. 5.6.

Since some intuition about the occurrence of bifurcations in 1-dimensional systems is gained, the next step is to investigate how different physics descriptions influence the bifurcating behaviour, meanwhile building step by step a very robust transition model containing all the relevant physics. This is addressed by following two research questions.

Firstly, the direct transport reduction mechanism is changed. From a bifurcation theory point of view this is interesting to investigate, because it changes the essential coupling between the nonlinear bifurcating variable and the passive diffusive equations, due to which oscillatory behaviour is possible.

How does the bifurcation structure change when changing the transport reduction mechanism?

From a physics point of view this is an interesting question, because it is expected that a shear in the $E \times B$ -flow is more effective in reducing the turbulence than the $E \times B$ -flow itself. Microscopic turbulence considerations showed that models based on the $E \times B$ -shearing give indeed a more accurate

description of the transport reduction[4–7]. In chapter 5 both mechanisms are compared on the basis of their influence on the bifurcation dynamics. Both models contain the co-dimension 3 bifurcation and therefore show qualitatively the same transition behaviour. One of the benefits of bifurcation theory is that this qualitative behaviour can quantitatively be compared. The main conclusion that can be drawn from this comparison, is that in the flow shear model all the transitions occur at lower values of the heat flux, and therefore the flow shear mechanism is more efficient in reducing the transport and triggering the L-H transition.

Secondly, a different extension of the considered transport model is the implementation of a separate equation governing the evolution of the turbulence level itself. From a physics point of view this is a very relevant extension, because the $\mathbf{E} \times \mathbf{B}$ -flows actually quench the turbulence, and more as a side-effect of that, the transport is reduced.

How does the bifurcation structure change when adding an extra dynamical equation for the turbulence?

From a bifurcation point of view this is even more drastic than the previous change, because due to this additional dynamical equation the coupling between the nonlinear bifurcating variable and the passive diffusive variables became indirect, possibly adding more dynamics to the system. Even more additional dynamics could be generated if the turbulence generate flows by themselves. These additional small scale flows, i.e., zonal flows, are recently more and more investigated in context of the L-H transition, e.g., [8, 9]. As this additional interaction between turbulence and zonal flows could cause oscillations by itself it is important to separate the different effects and investigate them separately, otherwise it may become unclear what causes which type of oscillations. Therefore, the first step is to implement the equation governing the growth and saturation of the turbulence and the reducing effect of the, larger scale, sheared mean $\mathbf{E} \times \mathbf{B}$ -flows.

What is the best dynamical description of the turbulence reduction by sheared $\mathbf{E} \times \mathbf{B}$ -flows?

Chapter 6 discusses two fundamentally different possibilities for the turbulence reduction mechanisms by sheared mean $\mathbf{E} \times \mathbf{B}$ -flows. Either it is implemented as a reduction of the growth rate (linear term), or it is implemented as an enhancement of the saturation mechanism (nonlinear term). Therewith are the transport coefficients directly determined as a linearly increasing function of the turbulence level. The enhanced saturation description is essentially equivalent with the flow shear model investigated in chapter 5, because its steady state corresponds exactly with the non-dynamic description of the $\mathbf{E} \times \mathbf{B}$ -flow shear reduction of the transport. Still it is partly surprising that the bifurcation structure of this dynamically extended model shows

again the co-dimension 3 structure, showing again the robustness of this bifurcation. In case of the growth rate reduction, however, the co-dimension 3 bifurcation structure is broken. Only when the effectiveness (parameterised by α , see, e.g., Eq. (6-15)) of the growth rate reduction is small, then the co-dimension 3 structure reappears again with the three different types of transitions. Otherwise (for larger α), only oscillatory transitions are possible in this model. Therefore, this model is sensitive to fine-tuning of the parameter α , which makes it a less robust model. It does not make it false yet, but it makes it less likely to be correct, at least.

Thus, all in all the mathematical basis for the employment of bifurcation theory is given. Thereafter, the proof of principle for L-H transition models is given. And discriminating conclusions are drawn for possible physically relevant model extensions based on their bifurcation dynamics. What is left to do is to continue this line of research to finally unravel the L-H transition mechanism.

7.2 Outlook

The first steps in unravelling the L-H transition mechanism with the use of bifurcation theory are taken in this thesis. The extensive amount of proposed L-H transition models, all with their own specific combination of mechanisms, can now be judged and compared on the basis of their bifurcation behaviour. This is essential to further understand the L-H transition, because there is a serious lack of discussion on how different proposed models relate to one another.

In order to convince the H-mode community (which are mainly experimentalists) about this new theoretical approach, it is necessary to map out the experimental bifurcating behaviour. If it is shown how the different types of transition dynamics are organised in the experimental parameter space, then immediately a tool to control the L-H transition is given, that is directly applicable. This does not necessarily have to be the co-dimension 3 bifurcation structure, although everything points to it. If the experimental bifurcation ordering is different, then different bifurcations need to be investigated in the proposed L-H transition models, but still the bifurcation analysis is very useful. The first hints of the experimental bifurcation structure have been encountered during this research. At JET, the transitions from a state that is clearly L-mode to one that is clearly H-mode occur gradually for increasing heating power for very low density plasmas[10, 11]. Thus, at JET the density can be used to force the L-H transition (and maybe the H-L transition) to be smooth. Much more common are the sharp L-H transitions, that are thoroughly investigated to build the scaling laws used for the extrapolation

to future devices[12]. These scaling laws, however, are only applicable in a (small) part of experimental parameter space, therefore it is unlikely that they are still correct when extrapolated out of their regime of validity, especially for such a nonlinear plasma phenomenon as the L-H transition. For instance, it is well known that towards low densities the scaling laws start to fail. Instead of a decreasing power threshold for decreasing density, as predicted by the scaling law, the power threshold starts to increase again below a certain density. This effect is called the 'roll over of the power threshold'. Many dedicated experiments are done to understand this roll over effect, and it appears, especially at ASDEX-Upgrade[13], that for densities near this roll over point oscillatory transitions (called I-phase at ASDEX-Upgrade) are observed. Since there are many types of oscillations observed at different tokamaks it is not possible yet to determine the density regime in which they all (or a physically related subset) occur. However, it can strongly be concluded that there are smooth transitions at very low densities, there are oscillatory transitions for densities around the roll over and there are sharp transitions for high densities. However, dedicated investigations are necessary to determine that the density may be used to control the dynamics during the L-H and H-L transitions.

One should be aware of the fact that this density ordering may also be just a side effect of the underlying physical mechanism, for instance the penetration of neutrals is strongly dependent on the density, and those neutrals cause friction on the flows in the plasma. So it is reasonable to believe that it may be the neutral friction that causes the change in dynamics, and that the density dependence is just one of the observable effects. This is one of the many examples of the encountered complexity in fusion plasma physics.

Besides showing the usefulness of bifurcation analysis for experiments it is necessary to continue the investigation from the theoretical perspective. There are several physically relevant extensions of the considered models that can be proposed at this point. However, in the future other mechanisms may turn out to be essential for the L-H transition. One of the most obvious suggestions is the formation of flows driven by the turbulence itself. This well known effect of zonal flow generation in fluid dynamics is proposed several times for the L-H transition. There is, however, no clear picture yet on whether the turbulence can generate mass flows just as in fluid dynamics or that it generates $\mathbf{E} \times \mathbf{B}$ -flows directly. If the latter is true then interaction terms should be added to the existing equations of both the turbulence level and the radial electric field. In this case it could be such that the original part of the model describes the large mean $\mathbf{E} \times \mathbf{B}$ -flows and that this additional interaction can only add small scale fluctuations to it, very similar to the zonal flow description in models of Diamond and coworkers. Thus, a proper bifur-

cation analysis comparison should be done between a model describing one radial electric field with fluctuations and a model describing separately the mean flows and the zonal flows.

However, with such extensions of the models, one should be aware of the possibility of multiple types of oscillations. From bifurcation theory we learned that for a model to contain oscillatory transition behaviour it is sufficient to have a bifurcating variable with multiple stationary states, that is coupled to a passive damped equation. Therefore, adding the mutual interaction between turbulence and zonal flows that can oscillate by themselves, could cause interfering oscillations. Thus, it is important to characterise where in parameter space both type of oscillations are dominant and how they interact.

Furthermore, it should also be checked that the addition of source terms in the continuity equations do not alter the bifurcation structure. This is a necessary addition if the model will be compared quantitatively to the experiments.

References

- [1] R. Ball and R. L. Dewar, *journal of plasma and fusion research series* **4** (2001) 266
- [2] Y. A. Kuznetsov, *International Journal of Bifurcation and Chaos* **15** (2005) 3535
- [3] H. Zohm, *Physical Review Letters* **72** (1994) 222
- [4] Y. Z. Zhang and S. M. Mahajan, *Physics of Fluids B: Plasma Physics* **4** (1992) 1385
- [5] T. S. Hahm, *Physics of Plasmas* **1** (1994) 2940
- [6] T. S. Hahm and K. H. Burrell, *Physics of Plasmas* **2** (1995) 1648
- [7] J. W. Connor and H. R. Wilson, *Plasma Physics and Controlled Fusion* **42** (2000) R1
- [8] E.-j. Kim and P. H. Diamond, *Physical Review Letters* **90** (2003) 185006
- [9] K. Miki, P. H. Diamond, Ö. D. Gürcan, G. R. Tynan, T. Estrada, L. Schmitz and G. S. Xu, *Physics of Plasmas* **19** (2012) 092306
- [10] L. D. Horton *et al.*, *26th EPS Conf. on Plasma Physics* **23J** (1999) 193
- [11] C. Maggi *et al.*, *Nuclear Fusion* **54** (2014) 023007
- [12] F. Ryter and the H-mode Threshold Database Group, *Plasma Physics and Controlled Fusion* **44** (2002) A415
- [13] G. D. Conway, C. Angioni, F. Ryter, P. Sauter and J. Vicente, *Physical Review Letters* **106** (2011) 065001

Summary

This thesis contributes to the research done to better understand the complex dynamics of fusion plasmas, particularly the magnetically confined fusion plasmas here on earth. This better understanding is essential to be able to control the fusion energy production and stability of these plasmas. An extraordinary, but very beneficial, feature is the spontaneous formation of a transport barrier, called the *H-mode*, which is the topic of this thesis. This barrier reduces the transport of particles and energy out of the plasma, such that the temperature and density in the core of the plasma can rise, leading to increased fusion power.

After more than three decades of research into the H-mode transport barrier it is still not fully understood which physical mechanism is responsible for this spontaneous phenomenon in the plasma. Therefore, we investigated a new analysis technique, based on the mathematical field of *bifurcation theory*, to analyse the possible dynamics within proposed models. The dynamics during the transition from the initial L-mode (low-confinement mode, without transport barrier) to the H-mode (high-confinement mode) is very characteristic, and definitely not all models are capable of describing such transition dynamics.

The transport of particles and heat out of the plasma is adequately described as a 1-dimensional system. Therefore, we extended the bifurcation theory to be applicable to 1-dimensional systems, especially aimed at the detection of a specific bifurcation, known as the *co-dimension 3 bifurcation*. This particular bifurcation organises three different types of transition dynamics, namely, (i) sharp transitions, during which the system suddenly jumps from one state to the next; (ii) smooth transitions, where the transition is not suddenly but more gradual; (iii) and oscillatory transitions, where the system first oscillates before it settles in the new state. These three types of transitions agree with observations of the L-H transitions. One conclusion is that a full model for the L-H transition should contain this co-dimension 3 bifurcation.

The investigation of bifurcating 1-dimensional models leads to a self-consistent description of the spatial growth of a transport barrier in time. For this a *generalised equal area rule* is introduced by us which is widely applicable, for instance, for the propagation of flame fronts or the propagation of signals in neural cells.

With all this mathematics in place, the bifurcation structure of four different models for the L-H transition is investigated. The basics of these models are all the same; two equations describe the transport of particles and heat,

and one equation describes the evolution of the radial electric field. This electric field is known to be able to reduce the transport, especially turbulent transport. Turbulence in fusion plasmas dominates the transport in L-mode, thus, a local reduction of this turbulence may explain the formation of a transport barrier. The manner in which the radial electric field interacts with the turbulence and what the effect is on the transport, is not fully understood. Therefore, four different descriptions for the reduction of the transport due to the radial electric field are investigated based on their influence on the transition dynamics, i.e., their bifurcation structure.

Two of the models have transport coefficients directly related to the radial electric field. In the first model the transport coefficients depend on the electric field, in the second model on its gradient. The dynamics during transitions from large to reduced values of the transport coefficients in both models are shown to exhibit the characteristic co-dimension 3 bifurcation structure. This shows the robustness of this bifurcation to substantial changes of the model. The robustness of the bifurcation structure is very important, since the L-H transition is seen in all present-day magnetically confined fusion devices, indicating that the underlying mechanism must be very robust. Another benefit of bifurcation analysis is that qualitatively similar structures of both models can be quantitatively compared. Such comparison confirmed the conjecture that the electric field shear is better in reducing transport than the magnitude of the electric field.

The other two models differ fundamentally, since an additional equation that dynamically describes the evolution of the turbulence is added. Thus, the transport coefficients are explicit functions of the turbulence level. The effect of the radial electric field shear is to reduce the turbulence level, and not directly the transport coefficients. This influence of the radial electric field on the turbulence level can be modelled in two fundamentally different ways. One is that the radial electric field shear reduces the growth rate of the turbulence (third model) and the other is that the radial electric field shear enhances the saturation mechanism of the turbulence (fourth model). Due to this additional dynamic equation more dynamics may be expected. However, the bifurcation analysis shows that in the enhanced saturation model the co-dimension 3 bifurcation is still robustly present. In contrast, the reduced growth rate model shows mainly oscillatory transitions, and only with fine-tuning of the parameters the sharp and smooth transitions can occur within this model. Thus, this model is less robust in its transition dynamics, and is therefore less likely to be a proper description of the L-H transition mechanism compared to the enhanced saturation mechanism.

Thus, it is shown in this thesis that bifurcation theory is an essential tool to unravel the physical mechanism behind the L-H transition.

Samenvatting

Dit proefschrift draagt bij aan het onderzoek tot een beter begrip van de complexe dynamica van fusieplasma's, en dan voornamelijk de fusieplasma's die we hier op aarde met magneetvelden proberen op te sluiten. Dit voortschrijdend inzicht is essentieel voor het onder controle kunnen houden van de fusie-energie productie en de stabiliteit van deze plasma's. Een bijzonder, en heel voordelig, fenomeen in fusieplasma's is de spontane vorming van een transportbarrière, genaamd de *H-mode*, wat het onderwerp is van dit proefschrift. Deze barrière reduceert het transport van deeltjes en energie die het plasma uitstromen, zodat de temperatuur en dichtheid in de kern van het plasma kan stijgen, wat tot verbeterd fusievermogen leidt.

Na meer dan drie decennia van onderzoek naar deze H-mode transportbarrière is het nog steeds niet volledig begrepen welk fysisch mechanisme verantwoordelijk is voor dit spontane fenomeen. Daarom onderzoeken we een nieuwe analyse techniek, gebaseerd op de wiskundige kennis van de *bifurcatie theorie*, voor het bepalen van mogelijke dynamica in potentiële modellen. De dynamica gedurende de transitie vanaf de L-mode (lage-energie toestand) naar de H-mode (hoge-energie toestand) is namelijk heel karakteristiek, en lang niet alle modellen kunnen deze specifieke transitie-dynamica verklaren.

Het transport van warmte en deeltjes uit het plasma kan bij benadering beschreven worden als een 1-dimensionaal systeem (de andere twee richtingen kunnen we dus even vergeten). Daarom hebben we ook de bifurcatie theorie toepasbaar gemaakt voor 1-dimensionale systemen, en dan voornamelijk gericht op het detecteren van een specifieke bifurcatie, genaamd de *co-dimensie 3 bifurcatie*. Deze specifieke bifurcatie organiseert drie verschillende soorten transities, namelijk, (i) scherpe transities, waarbij het systeem plotseling springt van de ene toestand naar de andere; (ii) gladde transities, waarbij de transitie niet plotseling is maar meer geleidelijk; (iii) en oscillerende transities, waarbij het systeem eerst oscilleert voordat het in de nieuwe toestand eindigt. Deze drie soorten transities komen overeen met de observaties van verschillende L-H transities. Waaruit we concluderen dat een volledig model van de L-H transitie deze co-dimensie 3 bifurcatie moet bevatten.

Het onderzoek naar bifurcaties in 1-dimensionale modellen leidt tot een consistente beschrijving van de ruimtelijke groei van de transportbarrière in tijd. Hiervoor is door ons een *gegeneraliseerde gelijke-oppervlakken-regel* geïntroduceerd, welke breed toepasbaar is, bijvoorbeeld voor propagatie van vlamfronten of signalen in zenuwcellen.

Met de hiervoor beschreven wiskundige technieken is de bifurcatie struc-

tuur van vier verschillende modellen voor de L-H transitie onderzocht. De basis van deze vier modellen is hetzelfde; twee vergelijkingen voor de beschrijving van het transport van warmte en deeltjes, en een vergelijking die de evolutie van het radieel elektrisch veld beschrijft. Het is bekend dat dit elektrisch veld in staat is om het transport te reduceren, en dan voornamelijk het turbulente transport. Turbulentie in fusieplasma's domineert het transport in L-mode, een lokale reductie van de turbulentie kan daarom mogelijk de vorming van een transportbarrière verklaren. De manier waarop het elektrisch veld interageert met de turbulentie en wat daarvan het effect is op het transport is niet volledig begrepen. Daarom zijn vier verschillende beschrijvingen voor de reductie van het transport door middel van een radieel elektrisch veld onderzocht op basis van hun invloed op de transitie-dynamica, dat wil zeggen hun bifurcatiestructuur.

Twee van de modellen hebben transportcoëfficiënten direct afhankelijk van het elektrisch veld. In het eerste model hangen de transport coëfficiënten af van de grootte van het elektrisch veld, en in het tweede model van de gradiënt van het elektrisch veld. Het is aangetoond dat de dynamica van beide modellen tijdens de transitie van grote tot gereduceerde waardes van het transport correspondeert met de karakteristieke co-dimensie 3 bifurcatiestructuur. Dit laat mooi de robuustheid zien van deze bifurcatie onder substantiële veranderingen van het model. De robuustheid van de bifurcatiestructuur is heel belangrijk, omdat de L-H transitie in alle huidige magnetische fusiemachines is gezien, wat impliceert dat het onderliggend fysisch mechanisme ook heel robuust moet zijn. Een ander voordeel van bifurcatie analyse is dat kwalitatief transitie gedrag van beide modellen op een kwantitatieve manier vergeleken kan worden. Hiermee is het vermoeden bevestigd dat de gradiënt van het elektrisch veld inderdaad beter is in het reduceren van het transport dan de absolute waarde van het elektrisch veld.

De andere twee modellen zijn wezenlijk anders omdat er een extra vergelijking aan toegevoegd is die de dynamische evolutie van de turbulentie beschrijft, zodat de transportcoëfficiënten expliciete functies van het turbulentieniveau zijn. De elektrisch veld gradiënt beïnvloedt de turbulentie en zo dus indirect de transportcoëfficiënten. De invloed van het elektrisch veld op het turbulentieniveau kan op twee fundamenteel verschillende manieren beschreven worden. Bij de ene manier reduceert de gradiënt van het elektrisch veld de groeisnelheid van de turbulentie (derde model) en bij de andere manier versterkt de gradiënt van het elektrisch veld de verzadiging van de turbulentie (vierde model). Vanwege deze extra dynamische vergelijking zou meer dynamisch gedrag verwacht kunnen worden. Echter, de bifurcatie analyse laat zien dat in het versterkte-verzadiging model de co-dimensie 3 bifurcatie nog steeds robuust aanwezig is. In tegenstelling tot het gereduceerde-

groeisnelheid model die voornamelijk oscillerende transities bevat, en alleen door de parameters heel precies af te stemmen kunnen ook scherpe en gladde transities in het model voorkomen. Dus dit model is veel minder robuust in zijn transitie dynamica en is daarom waarschijnlijk een minder goede beschrijving van het L-H transitie mechanisme vergeleken met het versterkte-verzadiging mechanisme.

Dus dit proefschrift laat zien dat de bifurcatie theorie een essentieel hulpmiddel is voor het ontwarren van het fysisch mechanisme achter de L-H transitie.

Acknowledgement

Vier jaar werken bij een instituut dat zo divers en gezellig is als Rijnhuizen/DIFFER dan leer je veel mensen kennen. En het zijn al die mensen die er voor hebben gezorgd dat ik echt een hele fijne tijd heb gehad, en wil hen daarom erg bedanken.

Laten we beginnen bij het begin, want zonder mijn studiegenoot en goede vriend, Joeri, was ik hier nooit terecht gekomen. Dus heel veel dank gaat uit naar hem, ook zeker voor zijn hulp met de beginselen van de bifurcatie theorie. Daarnaast vergeet ik nooit mijn tweede en derde werkdag, de plasma conferentie in Lunteren, tot diep in de nacht doorgegaan met biljarten in de kelder op een hele gare tafel met mijn promotor Tony. Dat noem ik nu eens goed kennis maken met de baas. En de dag er na natuurlijk net zo gaar als de biljarttafel weer naar de presentaties luisteren. Verder wil ik Tony ook zeker bedanken voor de vele leuke gesprekken en interesse in mijn werk.

Wat betreft mijn onderzoekswerk beschreven in dit proefschrift heb ik ongelofelijk veel te danken aan mijn beide dagelijks begeleiders, Hugo en Dick. Zij namen hun taak als *dagelijks* begeleiders heel serieus, en ik kon ze dan ook dagelijks storen met alle soorten vragen, het maakte niet uit waarover. En dat heb ik dan ook met veel plezier gedaan, ze stonden altijd open voor een goede/lange inhoudelijke discussie en kwamen altijd met nieuwe inzichten en ideeën. Dankzij hen is dit proefschrift tot stand gekomen, daarvoor (en voor nog veel meer) dus heel veel dank.

Ook Egbert was altijd erg geïnteresseerd en betrokken bij ons werk, en is een duidelijke en georganiseerde groepsleider van CPP-HT, waarvoor dank. Ook alle andere groepsleden (Hans, Fabien, Bircan, Bram, Delyan, Jens, Jane, Hugo vdB, Willem, Diego, Nicola, Jan-Willem, Jacco, Jeroen, John) wil ik bedanken voor vele interessante presentaties, en ook het aanhoren van en feedback geven op mijn presentaties. En in het bijzonder wil ik Jonathan bedanken voor het zijn van een hele fijne collega en goede vriend. En ook Stefan, want buiten dat we altijd fijn konden samenwerken, heb jij met het bouwen van Bifurcator een hele grote bijdrage geleverd aan dit proefschrift. Geen vraag of verzoek was te gek, jij kreeg alles voor elkaar, en ben nog steeds onder de

indruck van jouw computer kennis.

Een enthousiasmeboost kreeg ik elke keer weer van Marco en Menno, bedankt voor jullie aanstekelijke enthousiasme voor mijn onderzoek. Verder zijn er heel wat anderen met wie ik interessante discussies en leuke tijd heb gehad tijdens zomerscholen, conferenties en/of andere meetings, daarvoor dank aan: Athina, Ephrem, Merlijn, Ivo, Jurrian, Peter, Dima, Roger, Greg en Thijs.

Buiten al deze onderzoeksgerelateerde collega's heb ik ook heel wat andere collega's leren kennen. Zo raakte ik betrokken bij de Rijnhuizen Wiki toen Rob mij vroeg om Oli (de andere initiator van de Wiki) op te volgen in de *Wiki Board of Editors*. Het was altijd weer leuk om samen met Rob bierflesjes te beplakken en uit te reiken tijdens het praatje van de maand, opdat niemand de Wiki zou vergeten. Voor het vertrek van Rob werd ook John toegevoegd aan de Wiki Board, en nu is het de tijd voor Hugo om mijn stokje over te nemen. Bedankt aan allen die aan de Rijnhuizen Wiki hebben meegewerkten. Als lid van de Wiki Board nam ik ook plaats in de webredactie. Elke maand weer ging ik met veel plezier naar het (steeds voller wordend) Aquarium voor de webredactievergadering. Het bleef ook leuk omdat we elke keer weer erg constructief bezig waren om de interne en externe communicatiemiddelen te optimaliseren. Daarvoor dank aan Arian, Gieljan, Wim, Gerben, Martijn, Serge, Adelbert, Marja, Santi, Britta, Hugo, Jacqueline en Erik.

Een ander belangrijk onderdeel van werken bij Rijnhuizen/DIFFER is natuurlijk *koffie drinken*. Ik wil mijn lieve buren, Rianne, Miranda, Gieljan en Arian, erg bedanken voor de continue stroom aan cafeïne richting onze hoek van het gebouw. Dat ik 's ochtends als de telefoon ging alleen maar hoefde op te nemen met 'ja lekker' en meteen weer kon ophangen was een teken dat er goed voor me gezorgd werd. Ook de hartelijke *Goedemorgen!* van Kees hoorde bij het ochtendritueel, net zoals de altijd super vriendelijke Fatna die hard haar best deed om van de puinhopen op mijn bureau wat te maken. Dank jullie beiden.

En er werd natuurlijk nog veel meer koffie gedronken. En wil dan ook vele bedanken voor de gezellige uurtjes tijdens de koffiepauzes, onder andere natuurlijk, Pieter Willem, Bob, Han, Andries, Richard Al, Hennie, Thomas, Irem, Alberto, Niek, Gijs, Wim G, Dirk, Stein, Gerard, Noortje, Marc, Pedro, Ogé, Rob P, Waldo en één ieder die al vaker genoemd is in dit dankwoord. De altijd vrolijke dames die al deze koffie voorzien hebben, en ook vele tosti's voor mij gebakken hebben, verdienen een bedankje. Dus Joke, Petra, Carolien, Jannie, Ricksha en Nisha, bedankt. Ook de opgewekte goedemorgens van José, An en Loes horen bij een dagje Rijnhuizen. Verder wil ik zeker nog Sander bedanken die mij enorm geholpen heeft tijdens de voorbereiding op mijn bruiloft hier bij Rijnhuizen. Ook stonden de helpdeskmannen Jan-Willem,

Robbert en voorheen Edwin altijd met een glimlach voor je klaar om je te helpen waar ze konden, dank daarvoor.

Daarnaast zorgde Rijnhuizen ook voor de nodige ontspanning. Zo zal ik de wandelingen door het park en de vele potjes Mölkky niet snel vergeten. Dank voor het lang in stand houden van deze traditie: Lenze, Hugo vdB, Gido en Gydo. Maar bovenal zal ik de partijtjes voetbal op dinsdag en donderdag heel erg gaan missen. Anton, Toon, Dick, Frank, Hans, Kirill, Erik, Rianne, Sébastien, Teo, Wei, Sebastiaan, Dam, Gijs, Damien, en ook de vele oud-spelers, Aad, Kees vdG, Oli, Nicola, Tim, Robin, Joost, Joeri, Jonathan, Steven, Rolf, Stefan, Sam, Timon, Tomas, Reinier, Thijs, Jimmy, Oscar, Charlie, Jarno, Ralph, Bas, Vincent en Jeroen, ontzettend bedankt voor al die vele verloren (en af en toe ook wel eens gewonnen) wedstrijden.

Een andere vorm van ontspanning was het Sinterklaascabaret. Deze onvergetelijke mooie tijd is geheel en alleen mogelijk gemaakt door een groep kanjers, Aron, Miranda, Irene, Rolf, Peter en Gieljan: Ontzettend bedankt voor de leuke tijd! Natuurlijk ook Joke bedankt voor al je steun, Miranda voor alle uren die je aan de filmpjes hebt besteed, Bram voor het maken van de mooie opname en zeker ook de technische ondersteuning van Paul, Alex, Fred en Jan. Allemaal heel erg bedankt. De daarop volgende vrijdagmiddagen waren ook zeker erg gezellig mede dankzij het CrisisTeam in combinatie met Anton, Jan, Ed, Wim H, Frits, Ronald, Ben, Eric, Albert, Willem en Leon.

En als laatste wil ik nog één collega in het bijzonder heel erg bedanken voor de ontzettend leuke tijd: Rianne, heel erg mega bedankt!! Dankzij jou was geen enkele dag saai, wat hebben we veel gekletst, gediscussieerd, geklaagd en gelachen. Het was altijd leuk, en ik zal je daarom erg gaan missen.

Naast al deze fantastisch collega's van de afgelopen vier jaar, is er nog iemand die mij al meer dan tien jaar erg gelukkig maakt. Lieve Lotte, jij ook heel erg bedankt voor simpelweg alles, en in het bijzonder de afgelopen vier jaar waarin voor ons ook heel wat is veranderd. We begonnen met samenwoonen, enkele jaren later trouwden we, en onlangs natuurlijk de geboorte van onze zoon, Jesse. Voornamelijk dankzij jou heb ik op een relaxte manier dit proefschrift op tijd af kunnen hebben.

Curriculum vitae

- 24-06-1986 Born in Leiderdorp, the Netherlands
- 1998 – 2004 Preparatory Science Education (VWO)
Rijnlands Lyceum, Oegstgeest
- 2004 – 2007 Bachelor of Science in Physics & Astronomy with Honours certificate
University of Amsterdam
- 2007 – 2009 Master of Science in Theoretical Physics
University of Amsterdam and VU University of Amsterdam
- 2010 – 2014 Ph.D. candidate in Fusion Physics
FOM Institute DIFFER
Dutch Institute for Fundamental Energy Research